SENSITIZATION OF LANTHANIDE IONS BY TRIARYLBORON FUNCTIONALIZED B-DIKETONES

by

Larissa Frances Smith

A thesis submitted to the Department of Chemistry

In conformity with the requirements for

the degree of Master of Science

Queen's University

Kingston, Ontario, Canada

(September, 2014)

Abstract

This work concerns the development of two classes of triarylboron functionalized β-diketone ligands. In the first class, the boron unit is conjugated with a phenyl linker and the diketone backbone. In the second class, the boron unit, the aryl linker, and the diketone backbone are non-conjugated with a mutual orthogonal arrangement. To understand the impact of the location of the triarylboron unit on the electronic and photophysical properties of the β-diketone ligands, difluoroboron chelate complexes were synthesized and characterized. The complexes were studied computationally to determine the singlet and triplet transitions, along with their major contributing orbitals. They were then studied for their photophysical properties. The first class of ligands displayed a concentration dependent excimer emission. Finally, they were studied for their ability to sense fluoride and the binding constants of the fluoride-boron interaction were estimated.

The four ligands were also investigated for their use in selective sensitization of Tb(III) and Eu(III). The four Ln(III) complexes were characterized and their photophysical properties were investigated. The first class of ligands were found to be effective in activating Eu(III) emission while the second class is effective in activating Tb(III) emission. The Eu(III) complexes were found to have a low quantum efficiency, but can it can be greatly enhanced by the addition of fluoride ions. In contrast, the Tb(III) complexes have moderate quantum efficiencies that are quenched upon the addition of fluoride. The selective sensitization of Eu(III) and Tb(III) and the luminescent response towards fluoride is caused by the distinct intra-ligand charge transfer transitions of the two classes of ligands and the triarylboron unit.

Acknowledgements

First and foremost, I would like to thank my supervisor, Dr. Suning Wang, for her endless patience, guidance, and mentorship. She has pushed me to always try to be better. I am deeply grateful for the amount of time she has spent with me developing my skills as a chemist, a researcher, and a writer.

I am thankful to the many professors and staff at Queen's University who have taught my graduate courses and have always been available to help me academically and personally. I would like to extend special thanks to my committee members, Dr. Donal Macartney and Dr. Jean-Michel Nunzi, for taking the time to consider my work, as well as their continued advice and support. Additionally, I would like to thank Dr. Francoise Sauriol for her help with NMR, Hartmut Schmider for his help with HPCVL, and Dr. Ian Wyman for his help with binding constants.

The past and current Wang group members have been invaluable to my experience at Queen's and I appreciate their friendship, assistance, and support. I wish to thank Maria Varlan and Dr. Barry Blight for helping me to start this work and teaching me many synthetic chemistry techniques. Dr. Hee Jun Park assisted me during synthesis, for which I am grateful. Dr. Allison Brazeau, Yingli Rao, Yufei Li, and Soren Mellerup have helped me maintain my sanity during the last two years. I would especially like to thank Sean M^{c}Donald. He has encouraged and motivated me when I needed it the most. He has listened to endless rants about my unsuccessful reactions, has read countless versions of this thesis, and has been a source of unyielding support for the last two years.

Last but not least, I am very fortunate to have my family, friends, and colleagues who have enriched my time at Queen's. My family has always believed in me and has fostered my curiosity and excitement for science. Dean Smith and Marie Barnes have given their encouragement, friendship, and shoulders to lean on. They reminded me that quitting was not an option. Kathy Launier and Bryan Launier have given me an outlet for my creativity and have been amazingly understanding and supportive housemates. Mita Dasog inspired me to go to graduate school and to aim for excellence. Throughout this process, she has given me valuable advice and encouragement.

Table of Contents

List of Figures

List of Tables

List of Abbreviations and Symbols

2-Me-THF	2-methyl tetrahydrofuran
A	absorbance
Å	angstrom
acac	acetylacetonate
AETE	absorption-energy transfer-emission
Anal. Calc.	elemental analysis calculated
B3LYP	Becke 3-Parameter Exchange, Lee, Yang, and Parr
c	concentration, speed of light
℃	degrees Celsius
CD_2Cl_2	deuterated methylene chloride
$CDCl_3$	deuterated chloroform
cm^{-1}	wavenumbers
CT	charge transfer
d	doublet
dbm	dibenzoylmethane
dd	doublet of doublets
DFT	density functional theory
DMF	dimethylformamide
E	energy
EA	elemental analysis
EPA	United States Environmental Protection Agency
eq.	equivalents
ET	energy transfer
F	structure factor
g	gram
h	Planck's Constant
HOMO	highest occupied molecular orbital
hz	Hertz
I	intensity, integration of the emission peak
IC	internal conversion
IR	infrared
ISC	intersystem crossing
J	coupling constant, Joules
K	Kelvin
K	binding constant
k	rate, rate constant
l	path length
LHMDS	lithium hexamethyldisilazide
LMCT	ligand to metal charge transfer
LUMO	lowest unoccupied molecular orbital

M	molar
m	meter
mes	mesityl (2,4,6-trimethylphenyl)
mg	milligram
MHz	megahertz
min	minute
mL	milliliter
MLCT	metal to ligand charge transfer
mmol	millimole
MO	molecular orbital
n	refractive index
nm	nanometer
nmr	Nuclear Magnetic Resonance
ns	nanoseconds
OLED	organic light emitting diode
ph	phenyl
phen	1,10-phenanthroline
PMMA	poly(methyl methacrylate)
ppb	parts per billion
ppm	parts per million
ppy	2-phenylpyridine
s	seconds
S_0	singlet ground state
S_1	singlet excited state
T_1	triplet excited state
TBAF	tetrabutylammonium fluoride
TD-DFT	time dependent density functional theory
THF	tetrahydrofuran
TOPO	trioctylphosphine oxide
UV	ultraviolet
UV-Vis	ultraviolet-visible
°	degrees
δ	chemical shift
Δ	change
ε	molar absorptivity coefficient
λ	wavelength
μM	micromolarity
μs	microsecond
Φ	quantum efficiency
τ	lifetime
Σ	sum

Chapter 1

Introduction

Recently, research interest into organic luminescent materials has gained increasing attention due to their potential applications in non-linear optics,[1] sensing,[2] and display technologies.[3] Within these compounds, triarylboron compounds have emerged as an important class of materials. The empty p_π orbital on boron is able to promote charge-transfer luminescence[4] and act as a Lewis acid to sense small anions.[5] Meanwhile, using bulky aryl groups helps to protect the boron center from nucleophilic attack, making these complexes highly stable.[6] Since the position of the triarylboron moiety in these molecules has been found to affect the absorption and emission of the molecule,[7] they are highly tunable, which makes them highly attractive as optoelectronic materials.[8]

Another highly tunable class of luminescent organic molecules is the β-diketones. This class of compound has three positions for varied functionality, leading to many specifically designed molecules.[9] Typically, they are designed to chelate a metal ion for either acting as an ancillary ligand[10] or enhancing emission intensity.[11] Lanthanide β-diketonate complexes have been thoroughly investigated for their photophysical properties and many unique β-diketones have been synthesized for this purpose.[12] Alternatively, a β-diketone can coordinate to difluoroboron instead. This has found to improve the molar absorptivity and quantum yield of the parent molecule.[13] Due to this, many difluoroboron β-diketonate complexes have been synthesized and studied for a wide variety of applications including white-light emission,[14] mechanochromism,[15] and organic light emitting diodes (OLEDs).[16]

By combining a β-diketone with a triarylboron on different positions on the backbone, the photophysical properties could be further tuned. These new triarylboron functionalized β-diketone ligands can then be used for both β-diketonate main-group chelate complexes and metal ion complexation. The boron difluoride chelate complexes will allow for intense study of the ligand properties, while also being useful for small anion sensing. Due to the enhanced charge-transfer from a triarylboron unit, the β-diketonate

complexes can also be used to sensitize lanthanide metal ions. The resulting lanthanide complexes could also be used for small anion sensing.

This chapter will begin with a general overview of photophysical processes. It will then give a literature review of triarylboron complexes and their photophysical properties. The ability of these molecules to act as luminescent sensors for small anions will be discussed. A review of β-diketones chelating both metal ions and difluoroboron follows. Finally, the intriguing photophysical properties of the lanthanide metal ions will be discussed. The chelation of the lanthanide metal ions by β-diketones for various applications will be introduced and the fluoride sensing applications of lanthanide metal ions will be introduced. Representative examples of each class of compounds will be presented.

1.1 Photo-excitation

The first law of thermodynamics states that energy cannot be created or destroyed—only converted to a different form.[17] Some forms include kinetic, electrical, thermal, chemical, and electromagnetic radiation (light). The amount of energy associated with a photon can be determined by its wavelength using the Planck relation[17] (Equation 1.1), where E represents the energy in Joules, h is Planck's constant, c is the speed of light in a vacuum and λ is the wavelength in meters. This inverse relationship of energy and wavelength leads to the conclusion that long wavelengths of light are low in energy (such as radio waves or microwaves) and short wavelengths of light are high in energy (such as gamma rays or X-rays).

$$E = \frac{hc}{\lambda} \qquad \text{Equation 1.1}$$

Transitions between different electronic states in molecules can be achieved through photo-excitation. When the excited molecule returns to the ground state, it may release the energy as a photon, or light, which is known as the phenomenon of luminescence.

1.2 Luminescence

The term "luminescence" was coined in 1888 by Eilhard Wiedemann from the Latin, lumen.[18] It is presently defined as the phenomenon when light is spontaneously emitted from an electronically excited

species without being stimulated by heat, which is known as iridescence.[19] There are many subcategories of luminescence, but in all cases the light that is generated is from an electronically excited state relaxing to the ground state, releasing the excess energy as light. In this way, the difference in molecular electronic states can be known because the wavelength of the light is proportional to the difference in energy. Some of the different types of luminescence include electroluminescence, chemiluminescence, mechanoluminescence, or photoluminescence.[20] In this thesis, only photoluminescence will be discussed.

1.2.1 Photoluminescence

Photoluminescence is defined as the emission of light from an excited state following the excitation of an electron from a higher energy source of light.[19] It can be further sub-divided into fluorescence or phosphorescence, depending on the mechanism of emission, which is illustrated in the Jablonski diagram, Figure 1.1.

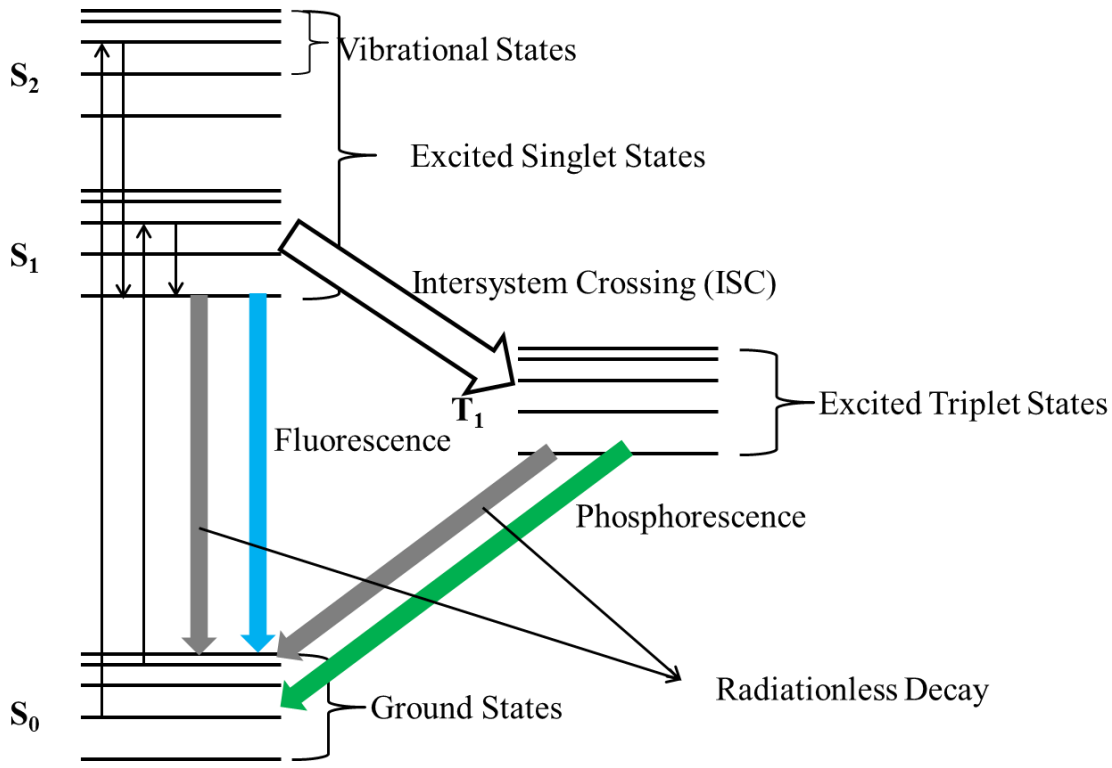

Figure 1.1 A Jablonski energy diagram showing the possible pathways of the excited state relaxation.

Every electronic energy state can be further divided into smaller vibrational and rotational energy states. In the ground state, the highest occupied molecular orbital is usually occupied by two electrons that have opposing spins. This state is commonly referred to as the singlet ground state. When a molecule in the ground state is photo-irradiated, an electron is excited into a higher energy state (S_1, S_2, etc) and maintains its spin and parity to the remaining electron. From this excited state, the electron will relax to the bottom of the S_1 state *via* internal conversion (IC). This is known as Kasha's rule.[21] Once in the excited state, the electron can do one of three things. First, it can relax to the ground state through non-radiative decay. Second, it can relax to the ground state and lose the excess energy as a photon: fluorescence. For fluorescent systems, the amount of time that the electron spends in the excited state, the lifetime (τ), is on the order of nanoseconds and the emission intensity is not very sensitive to the presence of oxygen.[22] Finally, it can flip its spin through an intersystem crossing (ISC) to an excited triplet state. Transitions from this energy level to the ground state are now forbidden by spin. This leads to a much longer excited state lifetime (μs or longer) and greater oxygen sensitivity of the state. Once the electron does relax, the energy can be released as a photon (phosphorescence) or non-radiatively. Typically, the photoluminescence wavelength of light emitted is longer than the initial wavelength absorbed. This difference is known as the Stoke's shift.[23] Phosphorescence has a larger Stoke's shift than fluorescence because of the triplet energy level being lower than the singlet energy level. The presence of a heavy atom can cause mixing of the singlet and triplet state through spin-orbit coupling and allow a rapid intersystem crossing to occur.

Other mechanisms of photoluminescence can occur when metal d or f orbitals are involved. These mechanisms include ligand-to-metal charge transfer (LMCT), metal-to-ligand charge transfer (MLCT), and absorption-energy transfer-emission (AETE). In the scope of this thesis, only AETE will be considered in depth.

1.2.2 Quantum Yield

An important value in the comparison of luminescent materials is the quantum yield (Φ). This is a measurement of the number of photons emitted relative to the number of photons absorbed (Equation 1.2), and therefore, measures the efficiency of the conversion from the excited state into luminescence.

$$\Phi = \frac{number\ of\ photons\ emitted}{number\ of\ photons\ absorbed} \qquad \text{Equation 1.2}$$

From this equation, the maximum quantum yield possible is 1.0; however, this is usually not the case due to the presence of non-radiative decay processes. Since the number of photons is challenging to measure experimentally, two methods have emerged to measure this quantum yield. The first method is by using a calibrated integration sphere, where the sample is placed inside a sphere that is assumed to have 100% reflectivity.[24] The amount of transmitted light can be related to the number of photons absorbed and the emission intensity can be measured and related to the amount of photons emitted. This method is more commonly used for solid samples. The second method, and the most common for samples in solution, compares the absorption and emission values to that of an appropriate (matching absorption and emission wavelengths) standard whose quantum yield is known. Typical standards for organic molecules have quantum yields near 1.0 and include 9, 10-diphenylanthracene and quinine sulfate.[25]

In the second method, the absorption profiles of the sample and standard must be similar in order to use an intersecting point as the excitation wavelength for both samples. The concentration of the sample is important to avoid deviations from the Beer-Lambert Law (Equation 1.3). Where A is the absorbance value, l is the path length of the cuvette, c is the concentration of the molecule, and ϵ is the molar absorptivity.

$$A = \epsilon l c \qquad \text{Equation 1.3}$$

At higher concentrations errors from aggregation and an uneven distribution of the excited species can cause scattering losses.[26] To avoid this, it is suggested that the absorbance maxima of the sample and standard at the excitation wavelength be $A < 0.1$. When measuring the emission, the emission wavelength must be similar such that the integration of each emission curve can be taken over the same range. Once

these factors have been accounted for, the quantum yield of each sample can be calculated by using Equation 1.4.

$$\phi_{sample} = \phi_{std} \left(\frac{A_{std)}}{A_{sample}}\right)\left(\frac{I_{sample}}{I_{std}}\right)\left(\frac{n_{sample}}{n_{std}}\right)^2 \quad \text{Equation 1.4}$$

Where A is absorbance, I is the integration of the emission peak and *n* is the refractive index of the solvent. This correction factor implies that the solvent choice does not have to be matched in order to take the measurement. Quantum yield can also be related to the lifetime of the excited state by Equation 1.5.[26]

$$\phi = k_r \tau \quad \text{Equation 1.5}$$

Where k_r is the rate of radiative decay and τ is the lifetime of the excited state, which is inversely proportional to the rate of radiative and non-radiative decay. This implies that the lifetime and the quantum yield share a linear relationship and some prediction can be made about the quantum yield if the lifetime of the excited state is known.

1.3 Organoboron Compounds

Organoboron compounds are organic compounds that contain a boron moiety. These compounds have many applications including photoswitchable materials,[27] dyes,[28] Suzuki-Miyura crosscoupling,[29] frustrated Lewis pairs,[30] OLEDs,[31] and small anion sensors.[5] Only triarylboron compounds, namely three-coordinate boron compounds in which each substituent is an aryl ring, will be discussed in this work.

1.3.1 Triarylboron Compounds

Three coordinate boron centers are trigonal planar around the boron center with an empty p_z orbital in the perpendicular plane (Figure 1.2). The empty orbital makes the boron center Lewis acidic, making it susceptible to nucleophilic attack. In order to prevent this, bulky aryl substituents such as anthryl or mesityl are required to protect the boron center. These protected compounds are typically stable under ambient conditions.[6] The empty orbital is the key to the photophysical properties because it acts as an electron acceptor in the charge transfer process. This leads the triarylboron compounds to have tunable

emission colors for many applications. Due to the steric protection provided by the aryl groups, the Lewis acidic boron is selective for binding by small anions, which will be discussed in **1.3.3.**

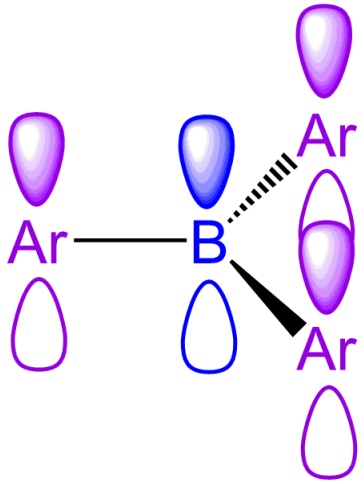

Figure 1.2 The structure of an sp^2 hybridized triarylborane (Ar = Aryl).

1.3.2 Photophysical Properties of Triarylboron Compounds

The empty p_π orbital on boron makes it ideal for accepting an electronic charge transfer from an electron donor, such as an amine, leading to either fluorescence or phosphorescence. With the HOMO located on the donor group and the LUMO located on the boron, the molecule can undergo intramolecular charge transfer resulting in a highly polarized excited state. This leads to well-documented solvatochromic effects where the emission wavelength of the molecule red-shifts as the polarity of the solvent increases.[32] In 2003, Doi *et al*. studied the distance dependence of charge transfer fluorescence between the donor and the boron center.[33] They found that as the distance is increased, the charge transfer efficiency is decreased and, therefore, the emission is red-shifted and the quantum efficiency decreases. Further experimental and DFT calculations by Hudson *et al*. showed that functionalization with a triarylborane in locations where the HOMO has large atomic orbital contribution lowers the energy of the HOMO and results in blue-shifted emission.[7]

Finally, the charge transfer process in organoboron compounds does not necessarily need conjugated pathways, and could also occur through space. In 2006, Liu *et al*. found that linearly conjugated molecules have through bond charge transfer and that both U- and V-shaped bonding motifs show weak through space charge transfer (Figure 1.3).[34] The U- and V-shaped molecules have low emission quantum yields compared to linearly conjugated ones and those that have shorter side arms, hence shorter donor-acceptor separation distances are more luminescent than the ones that have longer arms.

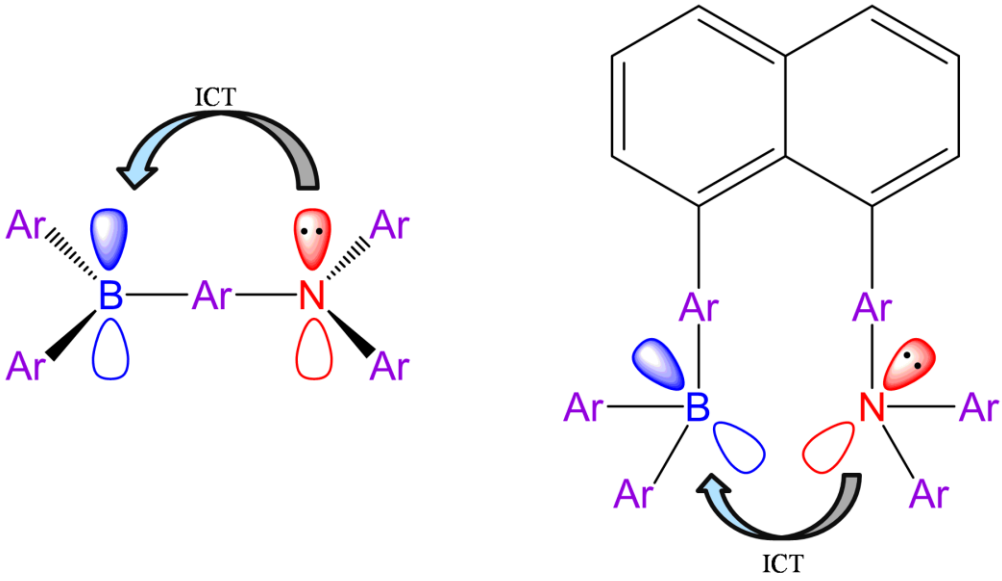

Figure 1.3 A diagram showing the two different charge transfer pathways in donor-acceptor boron compounds with a linear geometry and a U-shaped geometry.

1.3.3 Triarylboron Compounds in Anion Sensing

One of the most important applications for triarylboron compounds, which is a significant driving force behind their research, is their use as luminescent sensors for small anions such as F^- and CN^-. In low concentrations (0.7-1.2 ppm), fluoride has been shown to have positive effects on dental health, especially reducing the rate of tooth decay and osteoporosis.[35] For these reasons, many municipalities in North America add fluoride to their water systems. However, in higher concentrations fluoride has a negative impact on human health and can cause stomach ulcers, stress fractures, or even hypocalcemia.[36] To

prevent these negative effects, the US Environmental Protection Agency (EPA) recommends no more than 4 ppm in drinking water, and strongly recommends less than 2 ppm is best.[37] Fluoride can also be found in aerosols, such as sarin gas, which releases F^- upon hydrolysis.[38]

The detection of fluoride in water is challenging due to the high hydration enthalpy (-504 kJ/mol).[39] With a detection limit of 20 ppb, the analytical method of choice for measuring fluoride in water is the ion selective electrode.[40] The electrode for fluoride consists of a lanthanum fluoride crystal which has a similar selectivity for hydroxide and so the experiments must be done in acidic conditions.[41] Recent research has focused on synthesizing molecular sensors for fluoride where reversible binding can occur. This can be followed by the absorption or luminescence spectra of the molecule because they are easy to measure and highly sensitive to structural changes. Sensors can be "turn-on", where the absorption or emission peak intensifies or changes energy, or "turn off", where the absorption or emission peak is quenched.

Triarylboron compounds have emerged as a class of compounds that could be used to sense F^- and CN^-. The boron center is protected from nucleophilic attack of large anions by using sterically hindering aromatic groups. They are also attractive sensors because the LUMO contains substantial boron *p*-character. Once a fluoride is bound to the p_z orbital on the boron center, the conjugation of the molecule is disrupted, which produces an absorption or fluorescence response that can be measured using spectrometers.

The first triarylborane fluoride sensor was demonstrated in 2001 by Yamaguchi *et al*.[42] As shown in Figure 1.4, when a 10 μM sample of tris(9-trianthryl)borane, in THF, was titrated with tetrabutylammonium fluoride (TBAF) there was a rapid colour change of the solution from orange to clear. This change was also followed by UV-visible spectroscopy and the binding constant of fluoride to boron was determined to be 2.8 (± 0.3) x 10^5 M^{-1}. The compound showed only a small response to AcO^- and OH^- (K = ~10^3 M^{-1}) and no response to anions such as Cl^-, Br^-, I^-, ClO_4^-, or BF_4^- due to their larger size. In 2003, the same group reported that by using a triarylboron-functionalized porphyrin system, the

same binding event could be followed by emission spectroscopy.[43] This system also showed a rapid color change; however, the fluoride was easily removed upon the addition of water.

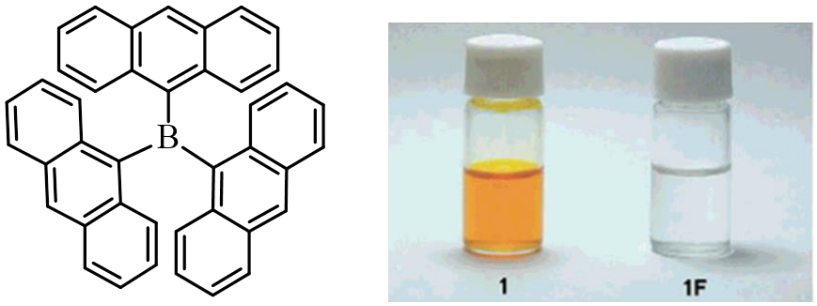

Figure 1.4 Left: A triarylboron compound for sensing fluoride. Right: The photographs showing the color change of the boron compound after the addition of fluoride ions.[42]

Gabbai and coworkers have worked extensively to overcome this limitation and synthesized molecules that are able to sense fluoride in the presence of water.[44] In order to overcome the large hydration enthalpy, the Lewis acidity of the boron center needs to be increased either by introducing electron withdrawing groups, increasing the π- conjugation, or by adding a peripheral cationic substituent. Early work showed that a chelating diborane on a 1,8-napthalane backbone (Figure 1.5) resulted in a much higher binding constant than previously seen (5 x 10^9 M^{-1})—approximately 1000 times that of $BMes_3$.[45] The addition of water did not lead to decomplexation, however, treatment of $B(C_6F_5)_3$ could remove the fluoride. This result implied that there was potential for an aqueous organoboron fluoride sensor.

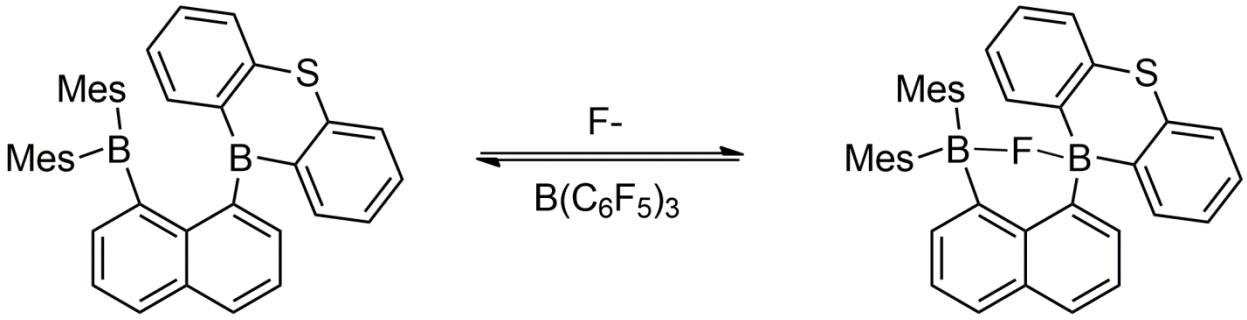

Figure 1.5 A chelating diborane is useful for fluoride sensing.

More recently, they combined the increased Lewis acidity effects with Coulombic effects and synthesized cationic boron compounds for sensing.[46] Triarylboranes with either ammonium or phosphonium groups has aided in the solubility of the sensors in both aqueous and biphasic solvent mixtures (Figure 1.6). In 2009, Gabbai and coworkers reported a cationic phosphonium triarylborane that was capable of sensing fluoride concentrations as low as 4 ppm in 9:1 H_2O:MeOH.[47] This was determined by the UV-visible spectral titration in a solution buffered to pH 4.9 to promote HF formation and reduce the competitive hydroxide species. Since the EPA standard for maximum contaminant level of fluoride is 4 ppm, this result is highly significant. Further success has been found recently with an aryl antimony compound able to sense the amount of fluoride in Texas A&M's tap water as 0.4 (± 0.05) ppm (compared to the documented 0.44 ppm in the most recent water quality tests).[48]

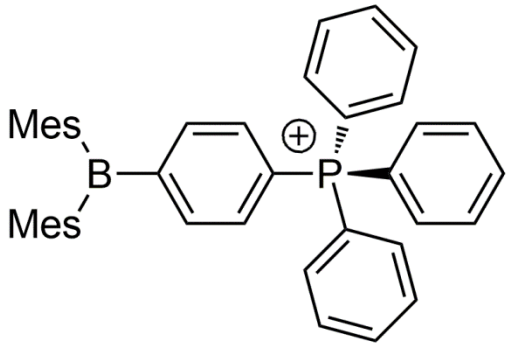

Figure 1.6 Structure of a phosphonium-borane capable of sensing fluoride in concentrations as low as 4 ppm in aqueous media.

1.4 β-Diketones

The β-diketones are organic molecules that have two carbonyl groups separated by one carbon atom.[49] This separator carbon is denoted as the α-carbon. Typically, the substituents on the α-carbon are hydrogen atoms. Due to the keto/enol tautomerization (Figure 1.7), these hydrogens are especially acidic and have a typical pKa of ~13 in DMSO.[50] The simplest β-diketone, acetylacetone (Hacac), is one that has methyl groups in the 1 and 3 positions. The substituents in these positions, and on the α-carbon, can influence

many factors about the molecules such as: the keto/enol equilibrium position, the amount of light absorbed, and the singlet and triplet energy levels.[51]

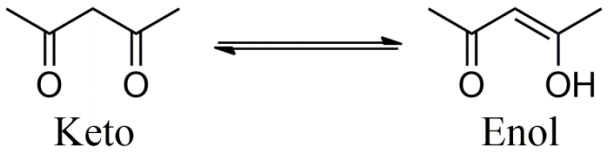

Figure 1.7 The keto and enol form of β-diketone occur through tautormization.

The β-diketones are easily synthesized through a Claisen condensation between a deprotonated methyl ketone and ethyl or methyl ester.[52] This ease of synthesis and the wide variety of possible substituents have led them to be widely used by organic chemists in malonic ester syntheses[53] and Michael additions,[54] whereas inorganic chemists have found them to be useful chelating ligands.[49] Many β-diketones are commercially available and inexpensive.

1.4.1 β-Diketonate Metal Complexes

The history of metal β-diketonate chelate complexes follows the development of inorganic chemistry. The first complex was synthesized in 1887 and several prominent studies followed to elucidate the nature of bonding and chelation in the complexes.[49] In 1945, Calvin and Wilson suggested that the six-membered chelate ring that was formed by bidentate chelation to a Cu^{2+} ion is aromatic.[55] Due to the strong bidentate chelation and complex solubility in organic solvents, the chelates were originally used for separating metal ion mixtures.[56] Since that time, there has been a wide variety of β-diketone architectures developed for many metal-β-diketonate complexes and applications including ancillary ligands or tuning photophysical properties.

Acetylacetone is often used as an ancillary ligand in catalysis because it aids in the solubility of the catalyst complex in non-polar solvents.[57] In phosphorescent Pt compounds, it provides good solubility and solid-state stability while the rigid structure and high triplet energy help to promote the phosphorescent

quantum yield.[11] This means that the β-diketonate has a direct impact on the photophysical properties of the complex. Mou *et al*.[58] studied the effect of changing the ligand to dibenzoylmethane (dbm) (Figure 1.8).

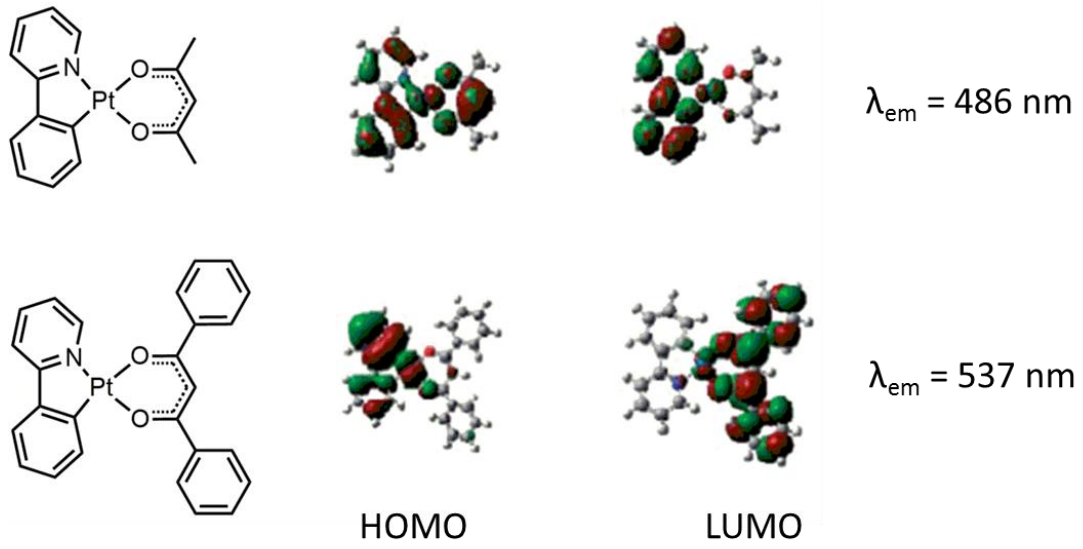

Figure 1.8 Impact of substituents on electronic structure and phosphorescence of β-diketonate Pt(II) complexes.[58]

They determined that compared to [Pt(ppy)(acac)] (where ppy= 2-phenylpyridine), [Pt(ppy)(dbm)] displayed more intense absorption bands. The emission wavelengths of the [Pt(ppy)(dbm)] complexes were also red-shifted 51 nm from [Pt(ppy)(acac)]. DFT data showed that while the [Pt(ppy)(acac)] HOMO was evenly distributed across the molecule, the LUMO was located on 2-phenylpyridine. For [Pt(ppy)(dbm)], the HOMO was located on the ppy and the Pt^{2+} center while the LUMO was located on the dbm moiety. This indicated that the β-diketonate has changed from being an ancillary ligand to actively participating in the phosphorescence of the compound, which provided a simple way to tune the emission color of the cyclometalated Pt^{2+} compounds. Tsujimoto *et al.* found that by using 1,3-bis(3,4-dibutoxyphenyl)propane-1,3-dione instead of dipivaloylmethane, higher quantum yields and shorter phosphorescent lifetimes could be achieved, which was favorable for OLED applications.[59] Finally,

Blight *et al.* found that by functionalizing dibenzoylmethane with a triarylboron moiety, the electron deficiency of the boron shifted the MLCT to the dbm ligand instead of to ppy.[60] DFT data demonstrated that the HOMO was located on the ppy and the Pt^{2+} center, whereas the LUMO was located on the dbm ligand with the empty boron orbital contributing ~20% to the LUMO (Figure 1.9).

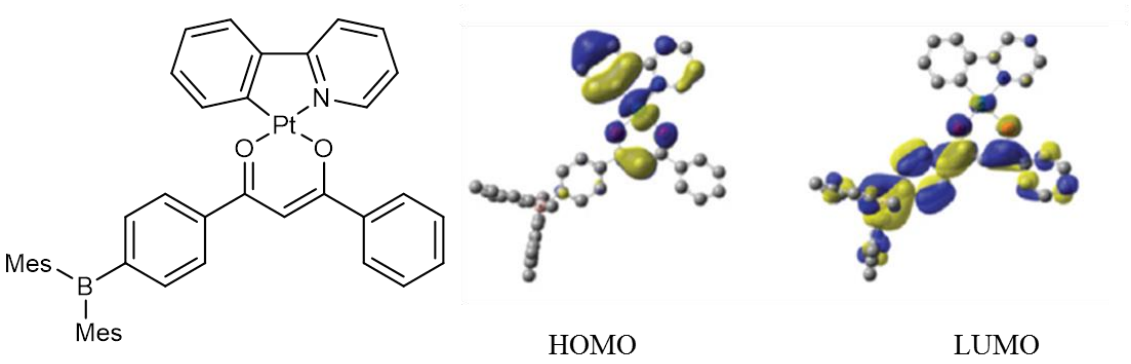

Figure 1.9 The HOMO and LUMO diagrams of the triarylboron functionalized dbm and ppy Pt complex.[60]

The compounds could also be used for fluoride sensing and upon the addition of fluoride, the emission colour changed from orange to yellow. It was found computationally that the addition of fluoride increased the energy of triplet state resulting in the blue-shifted emission color. This was the first example of Pt-β-diketonate complexes that were used for fluoride sensing.

1.4.2 Difluoroboron β-Diketonates

Instead of chelating a metal ion to a β-diketone, many main group elements can also be chelated. One of the moieties is difluoroboron. In 1924, Morgan and Tunstall reported that interactions between acac and boron trichloride formed unstable complexes and bisacetylacetone boronium salts were isolated instead. [61] They went on to report that boron trifluoride reacted energetically with both Hacac and Hdbm to form a difluoroboron chelate compound and hydrogen fluoride (Figure 1.10).

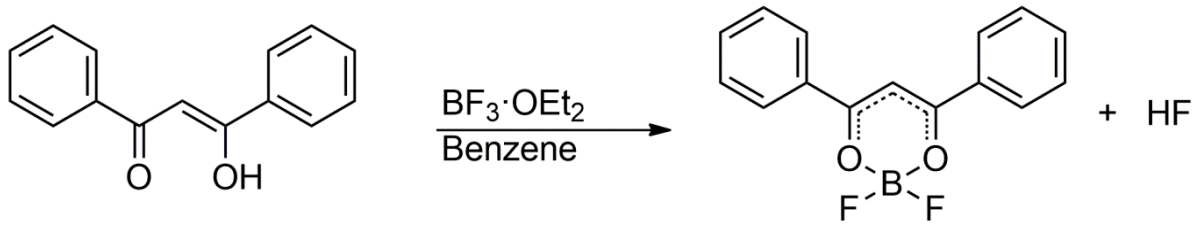

Figure 1.10 The synthesis of dbm-BF_2 as reported by Morgan and Tunstall.

The photophysical properties of the free ligands compared to the difluoroboron compounds were studied in 1996 by Chow *et al*.[13] They discovered that each chelate compound showed significant molar absorptivity enhancement and overall higher quantum yield, relative to the parent diketone. The authors rationalized that the chelate complex formation with boron utilized the non-bonding electrons on the carbonyl oxygen and the empty boron p-orbital to create a resonance-stabilized ring where the π orbital of the diketonate backbone becomes the HOMO. This implies that the HOMO-LUMO transition is $\pi \rightarrow \pi^*$ in the chelate compound and $n \rightarrow \pi^*$ in the parent. This is further supported by a hypsochromic shift from the parent molecule to the chelate complex in both absorption and emission. The Huckel Linear Combination of Atomic Orbitals (LCAO) model that the authors devised is shown in Figure 1.11 where the size of the orbital indicates the relative magnitude of the orbital coefficient. The boron bears no electron density in either diagram and the enhanced absorption and emission of the compounds seem to come from the rigid forced planarity of the diketonate as well as added conjugation. A computational study performed by the Fraser group[62] confirms that there is little electron density on the BF_2 moiety in difluoroboron β-diketonates.

HOMO LUMO

Figure 1.11 LCAO[13] (left) and DFT[62] (right) HOMO and LUMO diagrams of difluoroboron β-diketonates.

The Fraser group has done extensive work to expand the applications of difluoroboron β-diketonate compounds. They have shown that long-lived room temperature phosphorescence can occur when dbm-BF_2 is derivatized to have a poly(lactic acid) tail.[63] However, the phosphorescence is quenched in the presence of oxygen. With the help of collaborators, they have used this system to test for hypoxia, which is an indicator of cancer in human cells.[64] They have also shown that these compounds can be mechanochromic in the solid state by changing from blue to yellow with changes in pressure. [65] Over time, the scratched surface recovers the initial blue emission showing a "self-healing" optical material (Figure 1.12).

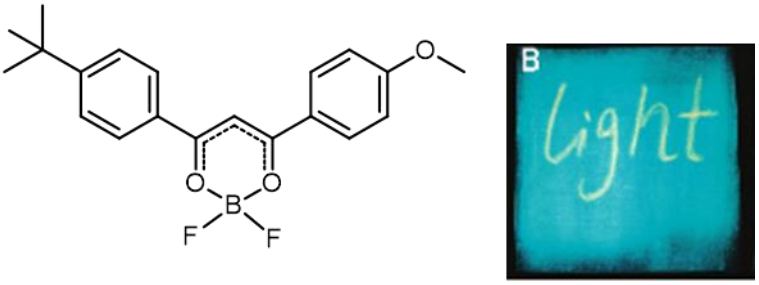

Figure 1.12 A mechanochromic difluoroboron β-diketonate that shows yellow emission after pressure is applied.[65]

A later study concluded that in amorphous solids mechanical stimuli can cause the formation of dimers or aggregates that face each other and have a low lying emission band that causes the yellow emission colour. [66]

Ikeda and coworkers have studied dbm-BF_2 and its 4,4'-isopropyl derivative and observed the yellow emission colour in solution.[67] At low concentrations ($<10^{-3}$ M) both complexes have a blue emission colour (~400 nm). However, when the concentration of the sample is increased, a yellow emission band ~550 nm arises (Figure 1.13). This has been attributed to excimer formation: where at high concentrations an excited molecule and a non-excited molecule form a dimer and a fluorescent charge transfer can occur. Being able to tune the emission color by controlling the concentration caused the authors to postulate that these systems could be used for white light applications.

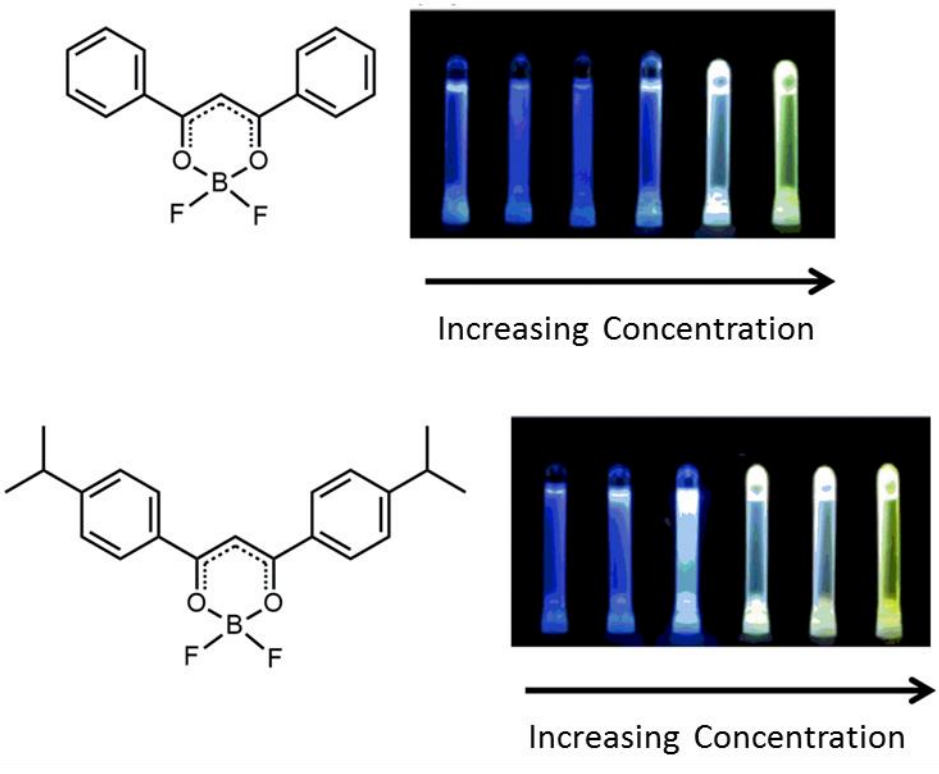

Figure 1.13 The fluorescence color change of difluoroboron β-diketonates in CH_2Cl_2 with increasing concentration.[67]

1.5 Lanthanides

The lanthanide elements consist of 15 members that span from lanthanum to lutetium that fill the 4f shell. The lanthanides were first discovered in 1787 by Carl Arrhenius in a single mineral deposit near the town of Ytterby, Sweden.[68] It was not until 1907, however, that all of the naturally occurring lanthanides would be isolated. While they are part of the rare earth elements, they are by no means rare. Even the least abundant lanthanide, thulium, is more abundant than iodine.[68] The electronic configuration of the lanthanide elements follows the pattern $[Xe]4f^n5d^16s^2$ where $0 \leq n \leq 14$. Upon ionization, the lanthanides typically exist in their trivalent state due to the stabilization experienced by the 4f, 5d, and 6s orbitals leading to electron configurations of the type $[Xe]4f^n$. The large radial expansion of the $5s^2$ and $5p^6$ in the xenon core makes the 4f orbitals "inner orbitals" within the trivalent specices.[69] Consequently, the Ln(III) ions display very similar chemical properties. Due to the shielding of the 5s and 5p orbitals, bonds between lanthanides and ligands are mainly ionic with at most 5-7% covalencey.[68] The Ln(III) ions are hard Lewis acids that form complexes with high coordination numbers, often eight or nine coordinate, with a preference for hard donors, such as anionic oxygen donors. Complexation with monodentate ligands is unfavorable because it is difficult to displace water molecules due to the high hydration enthalpies.[70] The shielding of the 4f shell results in well-defined and stable f-energy levels that do not show much variation with coordinating ligands or solvent. This leads to many intriguing spectroscopic and magnetic properties that are characteristic of the lanthanide ions and not the complex. Discussion of the spectroscopic properties of Ln(III) complexes is presented below.

1.5.1 Photophysical Properties of Lanthanide(III) Metal Ions

Interest into the photophysical properties of Ln(III) ions began in the 1880's when Crookes[71] (and later Urbain)[72] used flame emission spectroscopy to determine the purity of newly discovered lanthanides. Later, they were used in luminescent glasses,[73] lamps, and lasers.[74] The $4f^n$ electronic configuration generates multiple electronic energy levels whose energies are well-defined and characteristic for each element. As a result of the shielding from the more outer orbitals, these electronic states are insensitive to

the chemical environment. Therefore, the f→f emission from the Ln(III) ions displays a narrow range of wavelengths. The emissions range from the ultraviolet (not shown) to the near infrared regions (Figure 1.14).[75]

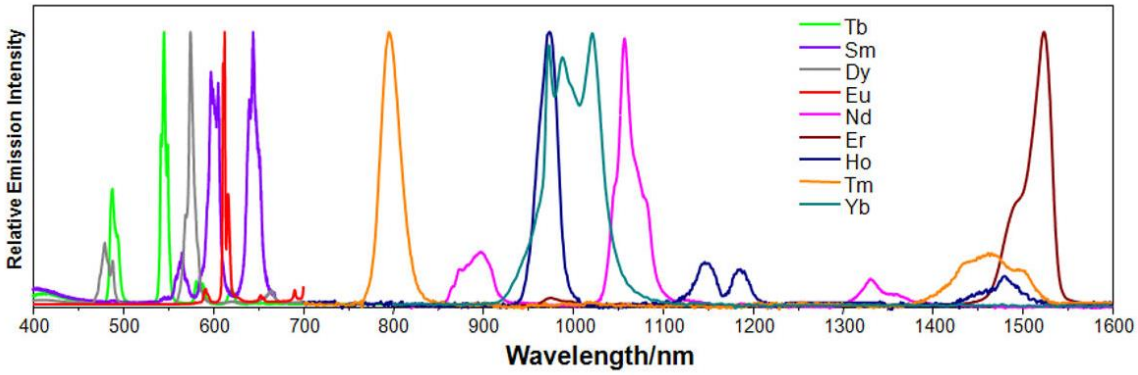

Figure 1.14 The emission of the Ln(III) ions ranges from the UV (not shown) to the near IR region.[75]

Unfortunately, due to the Laporte forbidden nature of the f→f transition, the molar absorptivity is small, which limits the emission intensity. In the 1940's Weissman reported that organic ligands (typically with hard oxygen donors) bound to the Eu(III) ion could absorb UV light and transfer the energy to the lanthanide causing an increase in europium emission intensity.[76] In the 1960's Crosby determined that the sensitization occurs from the ligand triplet state.[77] Since then, the mechanism of sensitization of lanthanide emission has been determined to be the absorption-energy transfer-emission mechanism (AETE).[78] This means that the ligand in the ground state (S_0) absorbs incoming photons and becomes excited into the singlet state (S_1). The excited molecule then undergoes an intersystem crossing to the lowest energy triplet state (T_1). From here, the energy transfers to the lanthanide cation causing an excitation of the f→f transition on the lanthanide center. When relaxing from the f→f excited state, the typical lanthanide emission occurs. This mechanism is illustrated in a Jablonski-like diagram shown in Figure 1.15.

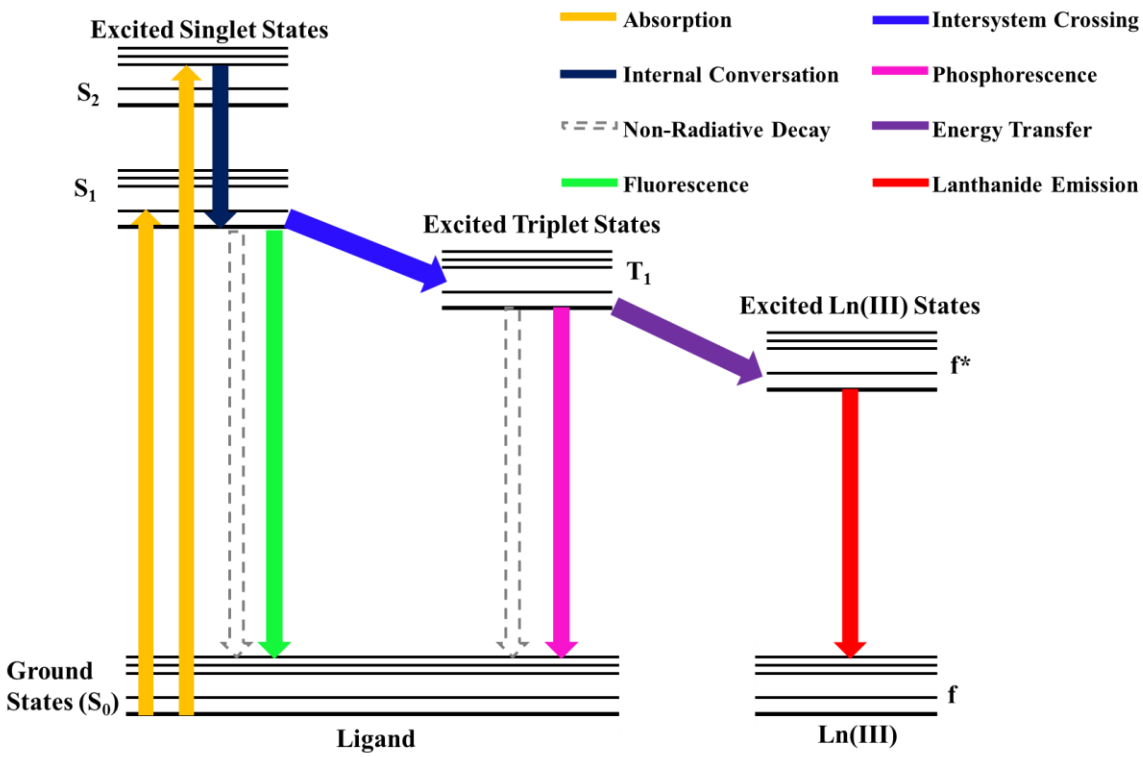

Figure 1.15 A Jablonski diagram illustrating the AETE mechanism of Ln(III) emission.

The mechanism is optimized if it occurs as described above. However, energy can be lost through many other pathways such as ligand fluorescence, ligand phosphorescence, or non-radiative decay. Additionally, the energy matching between the ligand triplet energy level and the energy accepting state of the lanthanide are of vital importance for optimizing sensitization. If the ligand's triplet state is too low, no sensitization will occur. However, if the triplet state is too high it is possible that another energy state could be accessed and another decay pathway to dominate. The lanthanide ions that are common for organic ligands to sensitize are Eu(III) and Tb(III) which both emit in the visible region ($^5D_0 \rightarrow {}^7F_2$: 612 nm and $^5D_4 \rightarrow {}^7F_5$: 546 nm, respectively). Their energy levels and major transitions are shown in Figure 1.16. Sm(III) and Dy(III) also emit in the visible region and can be used in sensitization studies, although they suffer from low quantum yields and are, therefore, less commonly investigated. The energy transfer mechanism implies that the initial absorption occurs on the organic ligand, resulting in large Stoke's

shifts. Due to the Laporte forbidden transitions, lanthanide emissions also have long excited state lifetimes. Coupled with the narrow emission bands, the photophysical properties of lanthanides make them useful for many applications including OLEDs[79] and cellular imaging.[80]

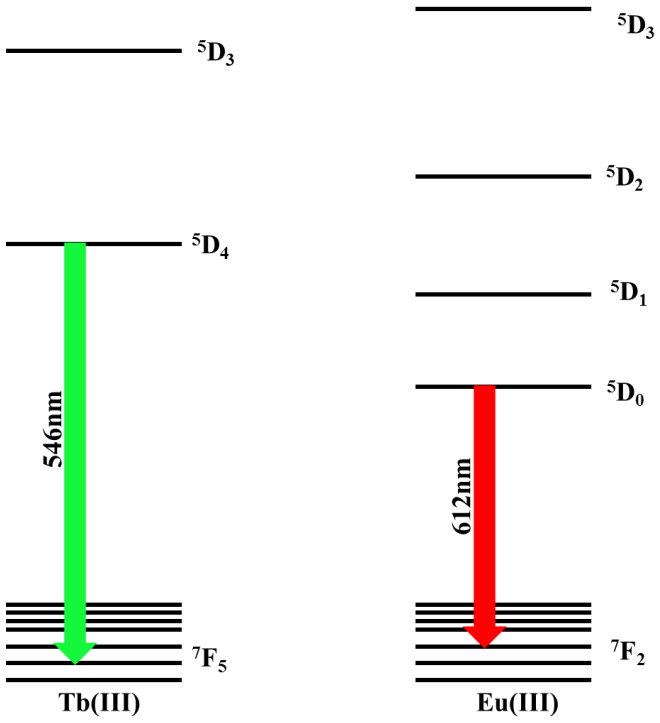

Figure 1.16 Energy level diagrams depicting the most intense transition of Tb(III) and Eu(III).

Many studies have been done to find the optimum triplet energy levels for ligands to sensitize Eu(III) and Tb(III). Latva *et al*. synthesized 41 different ligands and determined their triplet states by complexation with Gd(III).[81] This method was used in order to find the triplet state of the ligand as the accepting level of Gd(III) is too high in energy (~32000 cm^{-1}) to be accessed by triplet states of the ligands intended for Eu(III) or Tb(III) sensitization. The Gd(III) also causes singlet/triplet state mixing, which promotes the ligand phosphorescence. At 77 K, a phosphorescence measurement can be taken and the lowest energy triplet state is determined to be the band edge. Once these energy levels were known, the ligands were then used to complex Eu(III) and Tb(III) and the quantum yield of each complex was measured. A plot of

quantum yield vs triplet energy was made for Eu(III) and Tb(III). Figure 1.17a shows that in order to maximize the Eu(III) quantum yield, the triplet state of the ligand needs to be higher than the $^5D_1$ energy state. They concluded that this energy state is accepting the energy and transferring it to the emissive $^5D_0$. Figure 1.17b shows that to maximize Tb(III) emission, the triplet state of the ligand should be 2500-3000 cm^{-1} above the $^5D_4$ metal-centered excited state. This study demonstrated that different ligands need to be considered for targeted lanthanide sensitization.

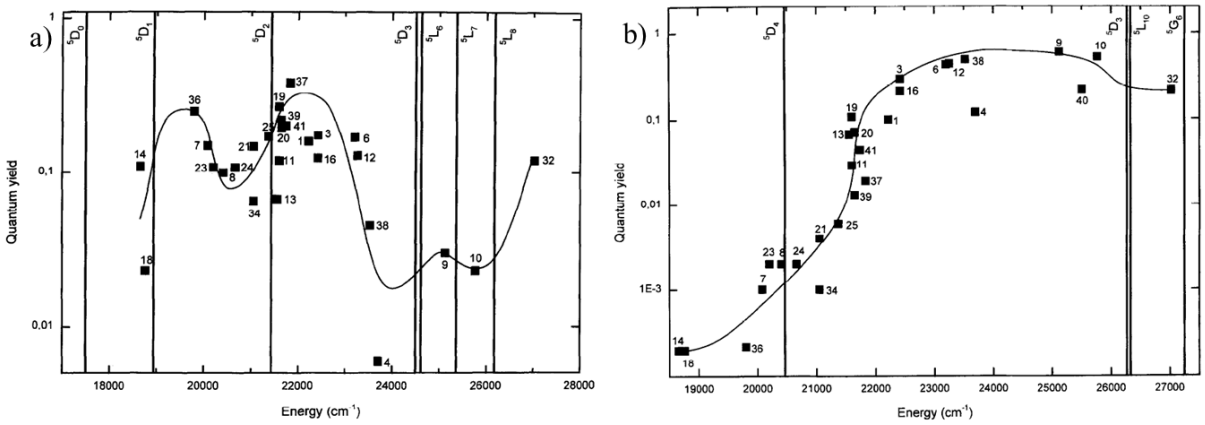

Figure 1.17 The effect of ligand triplet state on a)Eu(III) or b)Tb(III) quantum yield.[81]

One of the most common tunable ligand motifs for effecting Eu(III) or Tb(III) sensitization is the β-diketone and derivatives. In the following sections the use of these ligands on lanthanide emission sensitization and the use of the lanthanide complexes for sensing applications will be explored.

1.5.2 β-Diketones as Ligands for Sensitization of Lanthanide Emission

The first lanthanide β-diketonate complexes were prepared by Urbain in 1897.[82] Since then, these complexes have become the most popular and intensively investigated coordination compounds of lanthanides.[12] They have been used in many areas of applications including: the separation of lanthanides,[83] active compounds for lasers,[84] NMR shift reagents,[85] and electroluminescent materials for OLEDs.[86] The reason that they are so popular is because the ligands are highly tunable and commercially

available. As well, the synthesis of the complexes is relatively easy. In this thesis, only the tris-chelate complexes ($[Ln(L)_3(X)_n]$ where X = ancillary ligand) will be explored.

In a typical synthesis developed by Melby *et al*.[87] the β-diketone is deprotonated in the presence of a base in ethanol. The lanthanide hydrate salt in ethanol is then added dropwise to this solution, which typically results in the precipitation of the complex. The monoanionic bidentate ligands only fill six of the available coordination sites. Since lanthanides can have up to nine coordination sites, neutral ancillary ligands are required to fill the unoccupied sites. Solvent molecules, especially water, have been shown to reduce lanthanide emission.[12] The ancillary ligands are typically neutral Lewis bases such as the bidentate aromatic nitrogen donor 1,10-phenanthroline (phen)[88] or the oxygen donor trioctylphosphine oxide (TOPO).[89] Due to the mainly ionic character of the bonds, the β-diketonate ligands are relatively labile. In a study by Bhaumik *et al*.[90] it was shown that upon addition of a $Tb(NO_3)_3$ solution in ethanol to a similar solution of $Eu(acac)_3$ the red Eu(III) emission faded and the bright green emission of $Tb(acac)_3$ was observed, which suggested ligand exchange between the two different metal ions.

Many of the Eu(III) β-diketonate complexes display intense luminescence, such as $[Eu(tta)_3(phen)]$, which has been intensely studied for many applications due to its high quantum efficiency.[91] However, the 1,3 substituted aromatic β-diketonate ligands do not have a high enough triplet state to affect Tb(III) emission. Another important consideration in the synthesis of the β-diketonate tris-chelate lanthanide complexes is the choice of ancillary ligand. Neutral bidentate nitrogen donors, such as 1,10-phenathroline and 2,2'- bipyridine are commonly used for Eu(III). This is because their triplet state energy levels are ~2000 cm^{-1} higher than the $^5D_1$ energy level and so they improve Eu(III) sensitization. However, they are < 900 cm^{-1} above the Tb(III) $^5D_4$ energy level and so energy back transfer is possible.[92] To avoid this, other neutral ancillary ligands are used instead, such as trioctylphosphine oxide. Many of these considerations were accounted for in Chapter 3 of this thesis where four β-diketonate Ln(III) complexes have been synthesized.

1.5.3 Lanthanide complexes as fluoride sensors

While many studies have been done with lanthanide ions as sensors for analytes, such as anthrax spores,[93] the focus of this thesis will be the fluoride anion. As previously discussed, the amount of fluoride in a water sample has important implications on human health. The fluoride anion can be described as a hard Lewis base and since Ln(III) ions are hard Lewis acids, it is conceivable that lanthanides could be used to sense fluoride. Due to the high hydration enthalpy of lanthanide ions, only the Ln-F interaction can compete with coordination of water amongst the halides.[94] Unfortunately, in aqueous media the isoelectronic hydroxide anion is present, with a similar ionic radius (1.285 Å for F^- and 1.32 Å for OH^-).[95] Therefore, ligands must be designed with steric and charge considerations to further tune the selectivity. Many Ln(III) complexes with heptadentate ligands have been synthesized for this purpose.[96] The remaining open coordination sites are filled with H_2O ligands, which can be easily replaced by fluoride (Figure 1.18).

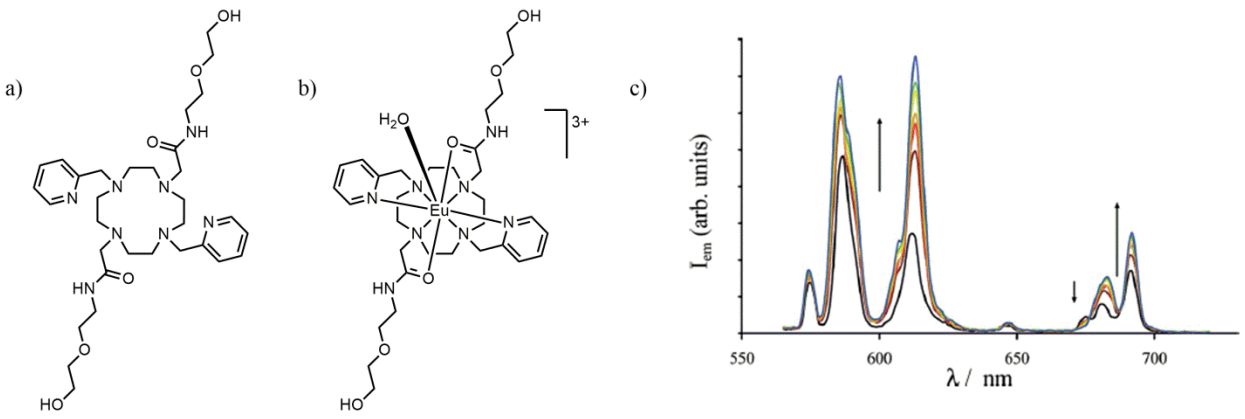

Figure 1.18 a) A heptadentate ligand b) Eu(III) complex using the heptadentate ligand c) ratiometric sensing of fluoride of the Eu(III) complex.[97]

In order to recognize that an anion has been bound, a sensitive and rapid method that can be calibrated is necessary. Lanthanide luminescence changes are highly sensitive and can be used to monitor the anion

binding. There are two ways that anions can bind to Ln(III) to cause changes in the emission intensity. The first type is reversible binding to the Ln(III) center by displacement of water. This changes the ligand field and the ratio of the emission band intensities will change.[97] The second type is reversible binding to the ligand. This can change the ligand's ground state energy or excited state energy, which can in turn influence the emission efficiency of the Ln(III) ion.[98]

Intriguing literature results in this field include the following two examples. Lui *et al*. designed a Eu(III) with a heptadentate ligand to make a $[Eu(L)]ClO_4$ salt in order to test the capabilities of the complex to sense fluoride in water (Figure 1.19).[99] Upon the addition of fluoride, the europium centered emission increased dramatically. The authors determined that increase in emission was coming from a fluoride bridged dimer of two complexes. They calculated their detection limit to be 0.46 ppb.

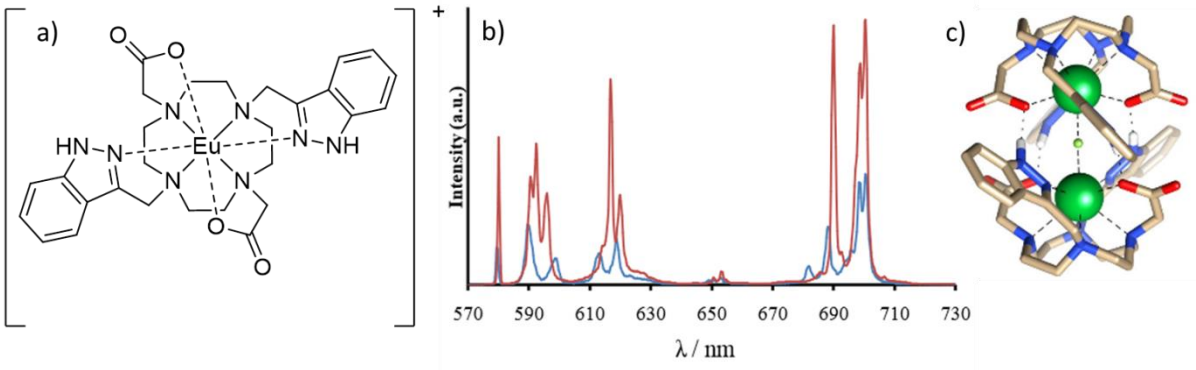

Figure 1.19 a) The structure of the $[Eu(L)]^+$ monomer. b) The intensity increase upon addition of fluoride. c) The structure of the dimer with bridging fluoride.[99]

Finally, Varlan *et al.* showed that a carboxylate functionalized triarylboron ligand, when bound to Tb(III) or Eu(III), could sense fluoride.[100] The addition of fluoride caused a change in the ligand triplet state, which caused quenching of the Ln(III) emission. These complexes are notable for being "turn-on" sensors in that as the Ln(III) emission is quenched, the ligand emission is enhanced with a distinct emission color change. These examples are just a few of the many Ln(III) ion complexes that are sensitive to fluoride

addition and can be used as versatile sensors. Either by binding to the metal center or the ligand, the Ln(III) emission is a sensitive tool for the detection of anions. By designing ligands for this purpose, the complexes can be tailored to be highly selective, useful tools for sensing devices.

1.6 Scope of the Thesis

The work described in this thesis demonstrates recent advances in utilizing triarylboron compounds as fluoride sensors with focus on the β-diketonate ligands as a useful system to chelate different moieties. The discussion above outlines the versatile applications of difluoroboron β-diketonates, triarylboron compounds, and lanthanide metal ions—especially in optical applications and in the context of fluoride sensing. My research has combined these components together to find new and interesting luminescent boron compounds and lanthanide compounds.

The work in Chapter 2 outlines the synthesis and characterization of four triarylboron functionalized β-diketonate ligands and their difluoroboron complexes. The effect of the triarylboron position on the absorption and emission of each complex was investigated. Chapter 3 outlines the synthesis of four lanthanide complexes using the ligands developed in Chapter 2. The ability of each ligand to sensitize Eu(III) or Tb(III) emission was evaluated by measuring their photophysical properties. Chapter 4 provides a general summary of the work in this thesis with key conclusions and proposed future work.

1.7 References

(1) Cariati, E.; Pizzotti, M.; Roberto, D.; Tessore, F.; Ugo, R. *Coord. Chem. Rev.* **2006**, *250*, 1210.

(2) Burnworth, M.; Rowan, S. J.; Weder, C. *Chem. Eur. J.* **2007**, *13*, 7828.

(3) Kalinowski, J. *Opt. Mater.* **2008**, *30*, 792.

(4) Hudson, Z.M.; Wang, S. *Dalton Trans.* **2011,** *40*, 7805.

(5) Feng, J.; Xiong, L.; Wang, S.; Li, S.; Li, Y.; Yang, G. *Adv. Func. Mater.* **2012,** *23*, 340.

(6) Hudson, Z.M.; Wang, S. *Acc. Chem. Res.* **2009,** *42*, 1584.

(7) Hudson, Z.M.; Sun, C.; Helander, M.G.; Change, Y-L.; Lu, Z-H.; Wang, S. *J. Am. Chem. Soc.* **2012,** *134*, 13930.

(8) Rao, Y-L.; Wang, S. *Inorg. Chem.* **2011,** *50*, 12263.

(9) Hu, J.; He, Z.; Wang, Z.; Li, X.; You, J.; Gao, G. *Tetrahedron* **2013,** *54*, 4167.

(10) Clegg, J.K.; Hayter, M.J.; Jolliffe, K.A.; Lindoy, L.F.; McMurtrie, J.C.; Meehan, G.V.; Neville, S.M.; Parsons, S.; Tasker, P.A.; Turner, P.; White, F.J. *Dalton Trans.* **2010**, *39*, 2804.

(11) Hudson, Z.M.; Sun, C.; Helander, M.G.; Amarne,H.; Lu, Z-H.; Wang, S. *Adv. Funct. Mater.* **2010,** *20*, 3426.

(12) Binnemans, K. *Handbook on the Physics and Chemistry of Rare Earths* **2005,** *35*, 107.

(13) Chow, Y.L.; Johansson, C.I.; Zhang, Y-H.; Gautron, R.; Yang, L.; Rassat, A.; Yang, S-Z. *J. Phys. Org. Chem.* **1996,** *9*, 7.

(14) Zhang, G.; St. Clair, T.L.; Fraser, C.L. *Macromolecules* **2009,** *42*, 3092.

(15) Zhang, G.; Evans, R.E.; Campbell, K.A.; Fraser, C.L. *Macromolecules* **2009**, *42*, 8627.

(16) Fedorenko, E.V.; Mirochnik, A.G.; Lvov, I.B.; Vovna, V.I. *Spectrochim. Acta, Part A.* **2014,** *120*, 119.

(17) Silberberg, M.S. *Chemistry: The Molecular Nature of Matter and Change;* McGraw-Hill:New York, **2003**; Vol. 3, pp 225, 256.

(18) Wiedemann, E. *Ann. Phys. Chem.* **1888,** *270*, 446.

(19) Braslavsky, S.E. *Pure Appl. Chem.* **2007,** *79*, 293.

(20) Valeur, B.; Berberan-Santos, M. *J. Chem. Ed.* **2011,** *88,* 731.

(21) Kasha, M. *Discuss. Faraday Soc.* **1950,** *9,* 14.

(22) McGown, L.B.; Nithipatikom, K. *Appl. Spectrosc. Rev.* **2000,** *35,* 353.

(23) Stokes, G.G. *Philos. Trans.* **1852,** *142,* 463.

(24) Porres, L.; Holland, A.; Palsson, L-O.; Monkman, A.P.; Kemp, C.; Beeby, A. *J. Fluoresc.* **2006,** *16,* 267.

(25) Brouwer, A.M. *Pure Appl. Chem.* **2011,** *83,* 2213.

(26) Sauer, M.; Hofkens,J.; Enderlain, J. *Handbook of Fluorescence Spectroscopy and Imaging;* Wiley-VCH: Weinheim, **2011,** pp 1-30.

(27) a) Rao, Y-L.; Armane, H.; Zhao, S-B.; McCormick, T. M.; Martic, S.; Sun, Y.; Wang, R-Y.; Wang, S. *J. Am. Chem. Soc.* **2008,** *130,* 12898. b) Rao, Y-L.; Amarne, H.; Chen, L.D.; Brown, M.L.; Mosey, N.J.; Wang, S. *J. Am. Chem. Soc.* **2013,** *135,* 3407.

(28) a) Kajiwara, Y.; Nagai, A.; Tanaka, K.; Chujo, Y. *J. Mater. Chem. C.* **2013,** *1,* 4437. b) Nagai, A.; Kokado, K.; Nagata, Y.; Arita, M.; Chujo. Y. *J. Org. Chem.* **2008,** *73,* 8605.

(29) a) Miyaura, N.; Suzuki, A. *Chem. Rev.* **1995,** *95,* 2457. b) Littke, A.F.; Dai, C.; Fu, G.C. *J. Am. Chem. Soc.* **2000,** *122,* 4020.

(30) a) Stephan, D.W. *Org. Biomol. Chem.* **2008,** *6,* 1535. b) Stephan, D.W. *Dalton Trans.* **2009,** 3129.

(31) a) Jia, W. L.; Moran, M.J.; Yuan, Y-Y.; Lu, Z. H.; Wang, S. *J. Mater. Chem.* **2005,** *15,* 3326. b) Li, D.; Zhang, H.; Wang, Y. *Chem. Soc. Rev.* **2013,** *42,* 8416.

(32) a) Hofmann, K.; Spange, S. *J. Org. Chem.* **2012,** *77,* 5049. b) Sartin, M.M.; Zhang, H.; Zhang, J.; Zhang, P.; Tian, W.; Wang, Y.; Bard, A. *J. Phys. Chem. C* **2007,** *111,* 16345. c) Brouwer, A.M.; Bakker, N.A.C.; Wiering, P.G.; Verhoeven, J.W. *Chem. Commun.* **1991,** 1094. d) Schwedler, S.; Eickhoff, D.; Brockhinke, R.; Cherian, D.; Weber, L.; Brockinke, A. *Phys. Chem. Chem. Phys.* **2011,** *13,* 9301.

(33) Doi, H.; Kinoshita, M.; Okumoto, K.; Shirota, Y. *Chem. Mater.* **2003,** *15,* 1080.

(34) Yang, X.; Bai, D.R.; Wang, S. *Angew. Chem. Int. Ed.* **2006,** *45,* 5475.

(35) Palmer, C.; Wolfe, S.H. *J. Am. Diet. Assoc.* **2005,** *105,* 1620.

(36) Kaminsky, L.S.; Mahoney, M.C.; Leach, J.; Melius, J.; Miller, M.J. *Crit. Rev. Oral. Biol. Med.* **1990,** *1,* 261.

(37) http://water.epa.gov/drink/contaminants/basicinformation/fluoride.cfm (accessed July 16, 2014)

(38) Xle, Y.; Popov, B.N. *Anal. Chem.* **2000,** *72,* 2075.

(39) Smith, D.W. *J. Chem. Ed.* **1977,** *54,* 541.

(40) Frant, M. S.; Ross, J. W. *Science* **1966,** *154,* 1553.

(41) Light, T.S.; Cappuccino, C.C. *J. Chem. Ed.* **1975,** *52,* 247.

(42) Yamaguchi, S.; Akiyama, S.; Tamao, A. *J. Am. Chem. Soc.* **2001,** *123,* 11372.

(43) Kubo, Y.; Yamamoto, M.; Ikeda, M.; Takeuchi, M.; Shinkai, S.; Yamaguchi, S.; Tamao, K. *Angew. Chem. Int. Ed.* **2003,** *42,* 2036.

(44) Wade, C.R.; Broomsgrove, A.E.J.; Aldridge, S.; Gabbai, F.P. *Chem. Rev.* **2010,** *110,* 3958.

(45) Sole, S.; Gabbai, F.P. *Chem. Commun.* **2004,** 1284.

(46) Hudnall, T.W.; Kim, Y-M.; Babbington, M.W.P.; Bourissou, D.; Gabbai, F.P. *J. Am. Chem. Soc.* **2008,** *130,* 10890.

(47) Kim, Y.; Gabbai, F.P. *J. Am. Chem. Soc.* **2009,** *131,* 3363.

(48) Hirai, M.; Gabbai, F.P. *Chem. Sci.* **2014,** *5,*1886.

(49) Mehrotra, R.C. *Pure Appl. Chem.* **1968,** *60,* 1349.

(50) Olmstead, W.N.; Bordwell, F.G.; *J. Org. Chem.* **1980,** *45,* 3299.

(51) Sager, W.F.; Filipescu, N.; Serafin, F.A. *J. Phys. Chem.* **1965,** *69,* 1092.

(52) Emsley, J. *Struct. Bonding.* **1984,** *57,* 147.

(53) Kates, S.A.; Dombroski, M.A.; Snider, B.B. *J. Org. Chem.* **1990,** *55,* 2427.

(54) Ranu, B.C.; Banerjee, S.; Jana, R. *Tetrahedron* **2007,** *63,* 776.

(55) Calvin, M.; Wilson, K.W. *J. Am. Chem. Soc.* **1945,** *67,* 2003.

(56) Schultz, B.G.; Larsen, E.M. *J. Am. Chem. Soc.* **1950,** *72,* 3610.

(57) Ligabue, R.A.; Monteiro, A.L.; Souza, R.F.; Souza, M.O. *J. Mol. Catal. A* **1998,** *130,* 101.

(58) Mou, X.; Wu, Y.; Liu, S.; Shi, M.; Liu, X.; Wang, C.; Sun, S.; Zhao, Q.; Zhou, X. Huang, W. *J. Mater. Chem.* **2011,** *21*,13951.

(59) Tsujimoto, H.; Yagi, S.; Honda, Y.; Tarao, H.; Maeda, T.; Nakazumi, H.; Sakurai, Y. *J. Lumin.* **2010,** *130,* 217.

(60) Blight. B.A.; Ko, S-B.; Lu, J-S.; Smith, L.F.; Wang, S. *Dalton Trans.* **2013,** *42*, 10089.

(61) Morgan, G.T.; Tunstall, R.B. *J. Chem. Soc., Trans.* **1924,** *125*, 1963.

(62) Xu, S.; Evans, R.E.; Liu, T.; Zhang, G.; Demas, J.N.; Trindle, C.O.; Fraser, C.L. *Inorg. Chem.* **2013,** *52*, 3597.

(63) Zhang, G.; Chen, J.; Payne, S.J.; Kooi, S.E.; Demas, J.N.; Fraser, C.L. *J. Am. Chem. Soc.* **2007,** *129,* 8942.

(64) Zhang, G.; Palmer, G.M.; Dewhirst, M.W.; Fraser, C.L. *Nat. Mat.* **2009,** *8,*747.

(65) Zhang, G.; Lu, J.; Sabat, M.; Fraser, C.L. *J. Am. Chem. Soc.* **2010,** *132,* 2160.

(66) Sun, X.; Zhang, X.; Li, X.; Liu, S.; Zhang, G. *J. Mater. Chem.* **2012,** *22*, 17332.

(67) Sakai, A.; Tanaka, M.; Ohta, E.; Yoshimoto, Y.; Mizuno, K.; Ikeda, H. *Tetrahedron Lett*. **2012,** 5*3,* 4138.

(68) Aspinall, H.C. *Chemistry of the f-Block Elements.* CRC Press: Amsterdam. **2001.** Vol 5. pp 1-29.

(69) Bunzli, J-C.; Svetlana, V.E. *Lanthanide Luminescence: Photophysical, Analytical and Biological Aspects,* Springer :Berlin. **2010**, pp 1-45.

(70) Moore, E.G.; Samuel, A.P.S.; Raymond, K.N. *Acc. Chem. Res.* **2009,** *42,* 542.

(71) Crookes, W.; *Philos. Trans. R. Soc. London., Ser. A* **1885,** *176,* 691.

(72) Urbain, G. *Ann. Chim. Phys., Ser. 8* **1909,** *18,* 222.

(73) Buzli, J-C.; Chauvin, A-S.; Kim, H.K.; Deiters, E.; Eliseeva, S.V. *Coord. Chem. Rev.* **2010,** *254,* 2623.

(74) Bunzli, J-C.; Piguet, C. *Chem. Soc. Rev.* **2005,** 1048.

(75) http://www.pitt.edu/~dave/Lanthanide_spec.html (accessed July 7, 2014)

(76) Weissman, S.I. *J. Chem. Phys.* **1942,** *10,* 214.

(77) Crosby, G.A.; Whan, R.E.; Alire, R.M. *J. Chem. Phys.* **1961,** *34,* 743.

(78) a) El-Sayed, M.A.; Bhaumik,M.A. *J. Phys. Chem.* **1965**, *69*, 275. b) El-Sayed, M.A.; Bhaumik, M.A. *J. Chem. Phys.* **1963**, *39*, 2391.

(79) a) Kido, J.; Okamoto, Y. *Chem. Rev.* **2002,** *102*, 2357. b) Kido, J.; Nagai, K.; Ohashi, Y. *Chem. Lett.* **1990,** 657.

(80) a) Chatterjee, D.K.; Rufaihah, A.J.; Zhang, Y. *Biomaterials* **2007,** *29,* 937. b) Thibon, A.; Pierre, V.C. *Anal. Bioanal. Chem.* **2009,** *394,* 107.

(81) Latva, M.; Takalo, H.; Mukkala, V-M.; Matachescu, C.; Rodriguez-Ubis, J.C.; Kankare, J. *J. Lumin.* **1997,** *75,* 149.

(82) Urbain, G.; Budischovsky, E. *Comp. Rend.* **1897,** *124,* 618.

(83) a) Mathur, J.N. *Solvent Extr. Ion Exch.* **1983,** *1,* 349. b)Sweet, T.R.; Parlett, H.W. *Anal. Chem.* **1968,** *40,*1885. c) Scribner, W.G.; Kotecki, A.M. *Anal. Chem.* **1965,** *37,* 1304.

(84) a)Wolff, N.E.; Pressley, R.J. *Appl. Phys. Lett*, **1963,** *2*, 152. b) Kuriki, K.; Koike, Y.; Okamoto, Y. *Chem. Rev.* **2002,** *102,* 2347. c) Huffmann, E.H. *Nature* **1963,** *200,* 158.

(85) a) Inagaki, F.; Miyazawa, T. *Prog. Nucl. Magn. Reson. Spectrosc.* **1981,** *14,* 67. b) Hinckley, C.C. *J. Am. Chem. Soc.* **1969,** *91,* 5160. c) Sanders, J.K.M.; Williams, D.H. *Chem. Comm.* **1970,** 422.

(86) a) Zheng, Y.X.; Lin, J.; Liang, Y.J.; Lin, Q.; Yu, Y.N.; Wang,S.B.; Guo, C.; Zhang, H.J. *Opt. Mater.* **2002,** *20,* 273. b) Hu, W.P.; Matsamura, M.; Wang, M.Z.; Jin, L.P. *Appl. Phys. Lett.* **2000,** *77,* 4271. c) Sun, P.P.; Duan, J.P.; Shih, H.T.; Cheng, C.H. *Appl. Phys. Lett.* **2002,** *81,* 792. d) Kido, J.; Nagai, K.; Okamoto, Y.; Skotheim, T. *Chem. Lett.* **1991,** 1267.

(87) Melby, L.R.; Rose, N.J.; Abramson, E.; Caris, J.C. *J. Am. Chem. Soc.* **1964,** *86,* 5517.

(88) Kang, J-G.; Kim, T-J.; Kang, H-J.; Kang, S.K. *J. Photochem. Photobiol. B* **2005,** *174,* 28.

(89) Zhu, G.; Si, Z.; Yang, J.; Ding, J. *Anal. Chim. Acta* **1990,** *231,* 157.

(90) Bhaumik, M.L. *J. Inorg. Nucl. Chem.* **1965**, *27*, 243.

(91) Nockemann, P.; Beurer, E.; Driesen, K.; Van Duen, R.; Van Hecke, K.; Van Meervelt, L; Binnemans, K. *Chem. Commun.* **2005,** 4354.

(92) Shi, J.; Hou, Y.; Chu, W.; Shi, X.; Gu. H.; Wang, B.; Sun, Z. *Inorg. Chem.* **2013,** *52,* 5013.

(93) Cable, M.L.; Kirby, J.P.; Sorasanee, K.; Gray, H.B.; Ponce, A. *J. Am. Chem. Soc.* **2007,** *129,* 1474.

(94) Natrajan, L.S.; Khoabane, N.M.; Dodds, B.L.; Muryn, C.A.; Pritchard, G.; Heath, S.L.; Kenwright, A.M.; Kuprov, I.; Faulkner, S. *Inorg. Chem.* **2010.** *49,* 7700.

(95) Shannon, R. D. *Acta Crystallogr. Sect. A* **1976,** *32,* 751.

(96) Butler, S.J.; Parker, D. *Chem. Soc. Rev.* **2013,** *42,* 1652.

(97) Tripier R.; Platas-Iglesias, C.; Boos, A.; Morfin, J-F.; Charbonniere, L. *Eur. J. Inorg. Chem.* **2010,** 2735.

(98) a) Pal, R.; Parker, D.; Costello, L.C. *Org. Biomol. Chem.* **2009,** *7,* 1525. b) Bretonniere, Y.; Cann, M.J.; Parker, D.; Slater, R. *Org. Biomol. Chem.* **2004,** *2,* 1624. c) Parker, D.; Yu, J. *Chem. Commun.* **2005,** 3141.

(99) Liu, T.; Nonat, A.; Beyler, M.; Regueiro-Figueroa, M.; Nono, K. N.; Jeannin, O.; Camerel, F.; Debaene, F.; Cianférani-Sanglier, S.; Tripier, R.; Platas-Iglesias, C.; Charbonnière, L. J. *Angew. Chem. Int. Ed.* **2014,** *53,* 7259.

(100) Varlan, M.; Blight, B.A.; Wang, S. *Chem. Commun.* **2012,** *48,* 12059.

Chapter 2

Boron Functionalized β-Diketonate Difluoroboron Complexes

2.1 Introduction

As outlined in Chapter 1, difluoroboron β-diketonate compounds have been widely studied due to their emissive properties. While the chelated boron center does not participate in the HOMO or LUMO energy levels, the chelate complexes have higher molar absorptivities and quantum yields than the parent β-diketones.[1] Due to these improved photophysical qualities, difluoroboron β-diketonate compounds have been used in many applications including: photochemical reagents,[2] two-photon materials,[3] oxygen sensors,[4] mechanochromic materials,[5] conjugated polymers,[6] and white-light emitters.[7] Meanwhile, triarylboron compounds are well known for enhancing the fluorescence of organic compounds.[8] In addition, the empty low energy p_π orbital on boron (combined with the steric bulk of the aryl groups) allows these molecules to be highly selective centers for the binding of small anions such as CN^- and F^-.[9]

The motivation for the work in this chapter was two-fold. First, the triarylboron functionalized ligands described in this chapter were initially developed for lanthanide sensitization, as outlined in Chapter 3. In order to study the photophysical properties of the ligands in a similar bonding environment, but without the interference of a metal ion, chelation of difluoroboron was explored. This was an attractive option due to the passive role the difluorboron plays in difluoroboron β-diketonate photophysical properties. Second, the Fraser group has successfully used dibenzoylmethane-BF_2 (dbm-BF_2) embedded in a polymer matrix to create a phosphorescent oxygen sensor that can be used in early cancer detection.[10] They have also explored the solid state mechanochromic properties of dbm-BF_2.[5] Meanwhile, Ikeda and coworkers have investigated the dbm-BF_2 concentration dependent excimer emission for white light applications.[7] Inspired by these results, we anticipated that by adding a triarylboron moiety to the diketonate backbone, both at the 1 and 3 positions or on the α-carbon, we would be able to use the extended conjugation and charge transfer abilities of boron to further tune the photophysical properties of this class of compounds.

Furthermore, by adding a triarylboron to the backbone, the LUMO will contain significant contributions from the boron and the resulting molecules should be good ideal candidates for fluorometric fluoride sensing.

The research included in this chapter details the synthesis of four triarylboron β-diketone ligands and their use in the formation of boron difluoride chelate compounds (Scheme 2.1). Two of the complexes have a triarylboron located at the 1 and/or 3 positions of the backbone with a relatively planar structure that is similar to dibenzoylmethane. These compounds have been studied for their white light emission properties. The other two complexes have a triarylboron located orthogonally from the backbone of the diketone on the α-carbon. Towards the completion of this work, the two α-carbon substituted systems were reported by Thilagar and coworkers.[11] The crystal structures of three of the BF_2 compounds have been investigated in this work and all molecules have been characterized with NMR spectroscopy and elemental analyses. The BF_2 chelate compounds were also investigated computationally to establish the optimized structures and to determine singlet and triplet energy levels by TD-DFT methods. The photophysical properties of the chelates were studied including quantum yields and fluorescence lifetimes. Following this investigation, they were then tested as viable fluoride sensors and the titration of each compound was followed with UV-Visible and fluorescence spectroscopy. The binding constant of each compound with fluoride was estimated using non-linear regression.

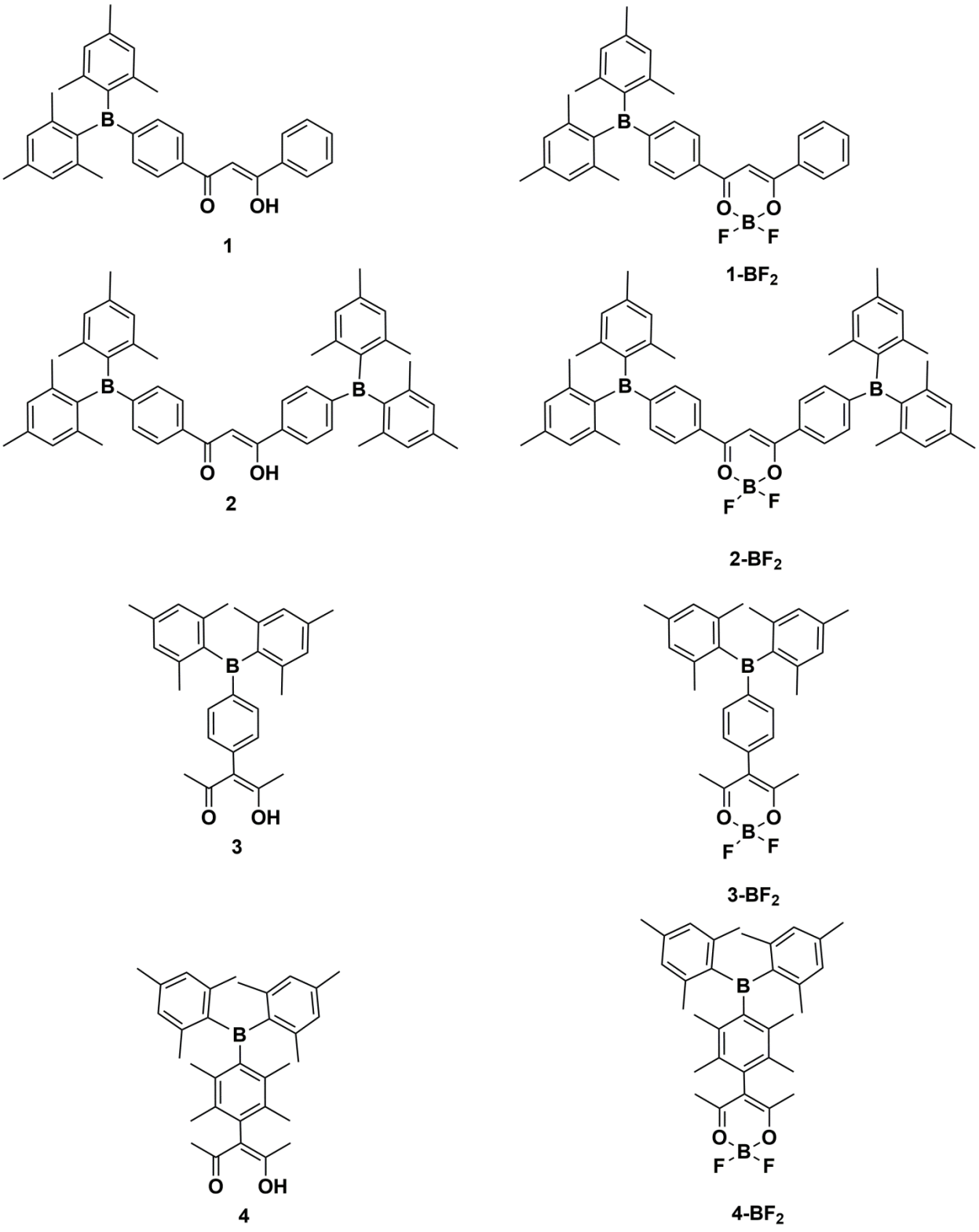

Scheme 2.1 The structures of the molecules investigated in this chapter.

2.2 Experimental Section

2.2.1 General Procedures

All starting reagents, unless otherwise specified, were received from Sigma-Aldrich and used without further purification. 2,2,2-Trimethoxy-4,5-dimethyl-1,3,2-dioxaphosphole was purchased from Alfa Aesar. Solvents were purchased from Fischer Scientific and purified by a solvent purification system (Innovation Technologies). Deuterated solvents were purchased from Cambridge Isotopes and used without further drying or purification. Column chromatography was carried out on silica. NMR spectra were acquired on a Bruker Advance 400 MHz spectrometer. Elemental analyses (CHN) were performed by the analytical laboratories at University of Montreal. The UV-visible spectra were obtained on a Varian Cary 50 UV−Visible spectrophotometer and all solutions for photophysical experiments were degassed under a nitrogen atmosphere. Excitation and emission spectra were recorded on a Photon Technologies International QuantaMaster model 2 spectrometer. Photoluminescent lifetimes were measured on a Photon Technology International Phosphorescent lifetime spectrometer, Timemaster C-631F equipped with an LED lamp (λ_{em}= 360 nm) and digital emission photon multiplier tube for emission. Solution quantum yields were calculated using optically dilute solutions (A ≈ 0.1), using 9,10-diphenylanthracene in ethanol (ϕ= 0.95)[12] as the standard at 298 K. Solid state quantum yields were obtained by using a PTFE-coated integrating sphere mounted onto a Jobin Yvon Horiba Fluoromax-3 by means of a known spectroscopic method. The computational calculations were performed using the Gaussian09, revision D.01,[13] software package and the High Performance Computing Virtual Laboratory (HPCVL) at Queen's University. The ground-state geometries were fully optimized at the B3LYP level using the 6-311+G(d,p) basis set for all atoms. The initial geometric parameters in the calculations were employed from crystal structure data for geometry optimization. TD-DFT calculations were performed to obtain the singlet and triplet excitation energies. X-ray crystallographic data was acquired and analyzed by Dr. Suning Wang. A single crystal was collected and mounted on glass fibers for analysis using a Bruker Apex II single-crystal defractometer operating at 50 kV and 30 mA at 180 K with a graphite

monochromated Mo Kα radiation source. The data was collected and processed using the Bruker SHEXTL software and were corrected for absorption effects. All structures were solved by direct method with non-hydrogen atoms refined anisotropically. The positions of the hydrogen atoms were calculated and their contributions in structural factor calculations were included.

2.2.2 Synthesis of 1-BF_2

Ligand 1 followed the synthetic procedure as previously reported from our group.[14]

1-A: Under N_2, 4-bromoacetophenone diethylketal (3.05 g, 11.2 mmol, 1 eq.) was dissolved in anhydrous THF (125 mL) and cooled to -78^{o}C. 1.6 M n-BuLi (7.72 mL, 12.0 mmol, 1.1 eq.) was added dropwise over 40 minutes and then allowed to stir for 60 minutes at -78^{o}C. In one portion, solid dimesitylboron fluoride (3.00 g, 11.2 mmol 1 eq.) was added to the reaction mixture at -78^{o}C, and the reaction was warmed to room temperature while stirring overnight. The reaction was quenched and stirred with 2 M HCl, extracted with diethyl ether, and washed with distilled water. The organic layer was dried with $MgSO_4$, filtered, and volatiles were removed under reduced pressure to afford a pale yellow solid (Scheme 2.2). The residue was purified by column chromatography (1:5 hexanes:CH_2Cl_2) to afford a colorless oil that solidified upon standing (3.36 g, 9.51 mmol, 85 % yield). ^{1}H NMR (400 MHz, 298 K, $CDCl_3$, ppm): δ 7.91 (d, J = 8.3 Hz, 2H), 7.59 (d, J = 8.3 Hz, 2H), 6.84 (s, 4H), 2.63 (s, 3H), 2.32 (s, 6H), 1.98 (s, 12H); ^{13}C NMR (100 MHz, 298 K, $CDCl_3$, ppm): δ 198.5, 141.4, 140.8, 139.2, 138.8, 135.7, 128.3, 127.6, 26.8, 23.4, 21.2; ^{11}B NMR (128 MHz, 298 K, $CDCl_3$, ppm): δ 78.7; Anal. Calc. for $C_{26}H_{29}BO$: C, 84.78; H, 7.94; Found: C, 84.46; H, 8.17.

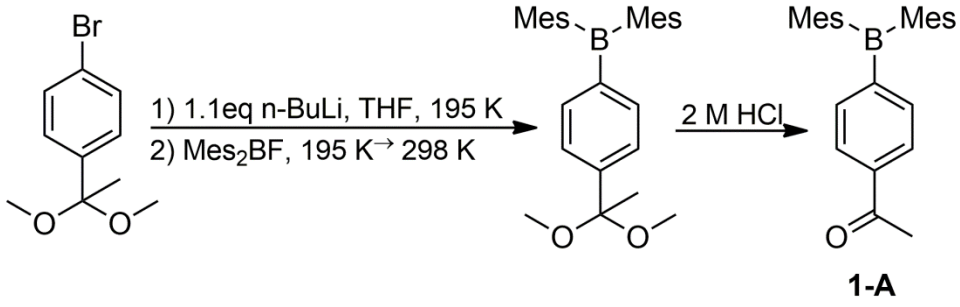

Scheme 2.2 Synthesis of the intermediate 1-A.

1: Under N_2, Compound **1-A** (0.60 g, 1.7 mmol, 1 eq.) was dissolved in anhydrous THF (10 mL) and cooled to 0°C. Separately, lithium hexamethyldisilazide (LHMDS, 0.57 g, 3.4 mmol, 2.1 eq.) was dissolved in anhydrous THF (15 mL) and then added dropwise to the cooled THF solution of **1-A**. The reaction was allowed to stir for 20 minutes allowing the enolate to quantitatively form. Benzoyl chloride (0.18 mL, 1.6 mmol, 0.95 eq.) was added dropwise to the reaction mixture and the reaction was allowed to stir for 1 hour at 0°C, and then 1 hour at room temperature (Scheme 2.3). The reaction mixture was diluted with diethyl ether, and sequentially washed with a saturated NH_4Cl solution, water, and brine. The organic layer was then dried with $MgSO_4$, filtered, and volatiles were removed under reduced pressure. The crude was recrystallized in CH_2Cl_2/CH_3OH to afford yellow crystals (0.67 g, 1.4 mmol, 87 % yield). ^{1}H NMR (400 MHz, 298 K, $CDCl_3$, ppm): δ 16.87 (s, 1H), 8.02 (d, J = 7.1 Hz, 2H), 7.95 (d, J = 8.1 Hz, 2H), 7.64 (d, J = 8.1 Hz, 2H), 7.57 (t, J = 7.1 Hz, 1H), 7.50 (dd, J = 7.1 Hz, 7.1 Hz), 6.97 (s, 1H), 6.86 (s,4H), 2.34 (s, 6H), 2.03 (s, 12H); ^{13}C NMR (100 MHz, 298 K, $CDCl_3$, ppm): δ 186.7, 184.8, 141.6, 140.9, 139.2 137.9, 136.1, 135.7, 132.6, 128.7, 128.4, 123.3, 126.5, 93.7, 23.5, 21.3; ^{11}B NMR (128 MHz, 298 K, $CDCl_3$, ppm): δ 83.5; Anal. Calc. for $C_{33}H_{33}BO_2$: C, 83.90; H, 7.04; Found: C, 83.70; H, 7.17.

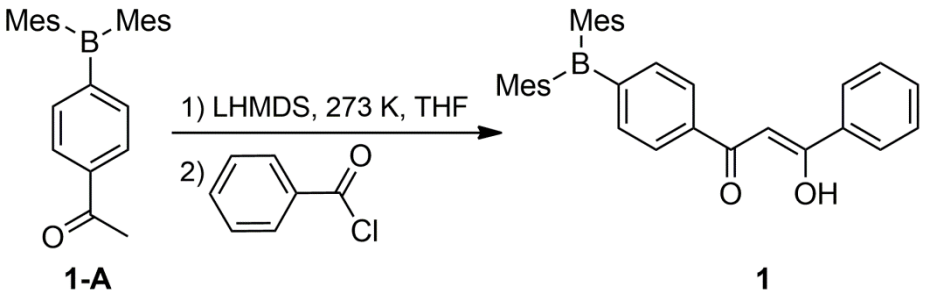

Scheme 2.3 Synthesis of ligand **1**.

1-BF_2: 0.10 g of **1** (0.21 mmol, 1 eq.) was dissolved in 10 mL distilled CH_2Cl_2 in a nitrogen-filled round bottom flask. The solution was heated to reflux and 2.1eq BF_3·OEt_2 (0.055 mL, 0.44 mmol) was added (Scheme 2.4). The mixture immediately changed colour from pale yellow to orange. The reflux was

continued overnight. In the morning, the solution was washed with distilled water in order to wash away any coordinating fluorides, dried with brine and $MgSO_4$, and the CH_2Cl_2 was removed under reduced pressure. The compound was purified by column chromatography (CH_2Cl_2). 32% yield. ^{1}H NMR (400 MHz, 298 K $CDCl_3$, ppm): δ 8.17 (d, J = 7.9 Hz, 2H), 8.10 (d, J = 7.9 Hz, 2H), 7.72 (t, J = 7.4, 1H) 7.67 (d, J = 8.1 Hz 2H) 7.58 (dd, J = 8.1 Hz, J = 7.4 Hz, 2H) 7.24(s, 1H), 6.86(s, 4H), 2.34 (s, 6H), 2.00 (s, 12H); ^{13}C NMR (100 MHz, 298 K, $CDCl_3$, ppm) δ 183.50, 183.15, 140.92, 139.63, 135.85, 135.37, 134.05, 132.00, 129.23, 129.00, 128.46, 128.17, 115.63, 93.93, 23.45, 21.25; ^{11}B NMR (128 MHz, 298 K, $CDCl_3$, ppm): δ 81.92 (broad), 1.35; ^{19}F NMR (376 MHz, 298 K, $CDCl_3$, ppm): -140.49, -140.56 Anal. Calc. for $C_{33}H_{32}B_2F_2O_2$: C, 76.19 H, 6.20; found: C, 73.45, H, 6.34. This can be attributed to 0.3 CH_2Cl_2, which is corroborated with data from the crystal structure. Anal. Calc.: $C_{33.3}H_{32.6}B_2Cl_{0.6}F_2O_2$: C, 73.29, H, 6.02.

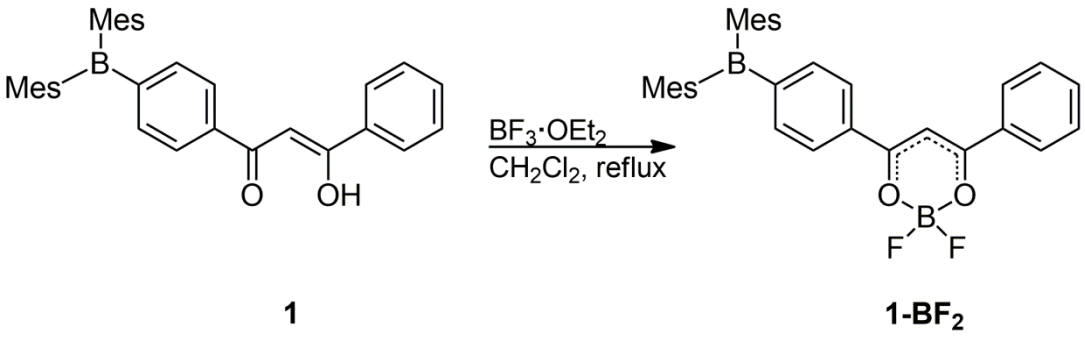

1 **1-BF$_2$**

Scheme 2.4 Synthesis of **1-BF$_2$**.

2.2.3 Synthesis of 2-BF$_2$

2-A: 1.00 g of (4-bromophenyl)dimesitylborane[15] (2.47 mmol, 1 eq.), under a nitrogen atmosphere, was dissolved in 30 mL anhydrous THF. It was then cooled to -78^{o}C and 1.6 M n-BuLi (1.70 mL, 2.71 mmol, 1.1 eq.) was added dropwise. The mixture was allowed to stir for one hour. After the one hour stir period, a CO_2 filled balloon was vented into the mixture and the mixture was allowed to warm slowly to room temperature overnight (Scheme 2.5). In the morning, the reaction was quenched with 2 M HCl and the

product was separated into diethyl ether. The diethyl ether was washed with distilled water, dried with brine and $MgSO_4$, filtered, and the volatiles were removed under reduced pressure. The solid was washed with hexanes and filtered to recover 0.65 g white solid (70 % yield). ^{1}H NMR (300 MHz, 298 K, $CDCl_3$, ppm): δ 8.10 (d, J = 7.4 Hz, 2H), 7.62 (d, J = 7.4 Hz, 2H), 6.86 (s, 4H), 2.33 (s, 6H), 2.01 (s, 12H).

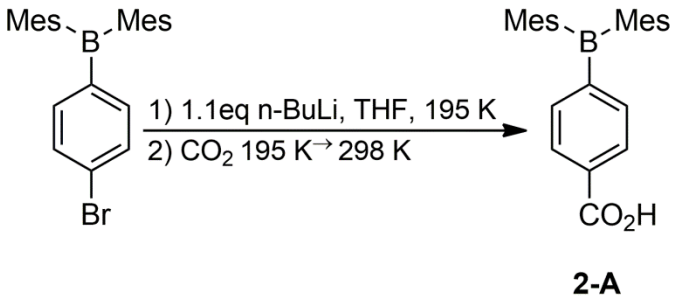

Scheme 2.5 Synthesis of the intermediate **2-A**.

2-B: 310 mg of **2-A** (0.805 mmol, 1 eq.) was dissolved in 75 mL absolute ethanol (1.28 mol, excess) and heated to reflux. Three drops of concentrated H_2SO_4 (cat.) was added and the mixture was refluxed overnight (Scheme 2.6). In the morning, the mixture was separated into diethyl ether and washed with twice with water, dried with brine and $MgSO_4$, filtered, and the ether was removed under reduced pressure. The resulting oil was then purified by column chromatography (CH_2Cl_2) to yield 310 mg recovered (93 %). ^{1}H NMR (300 MHz, 298 K, $CDCl_3$, ppm): δ 8.05 (d, J = 7.9 Hz, 2H), 7.62 (d, J = 7.9Hz, 2H), 6.86(s, 4H), 4.41 (q, J = 7.0 Hz, 2H) 2.33 (s, 6H), 2.03 (s, 12H) 1.41 (t, J = 7.0 Hz, 3H).

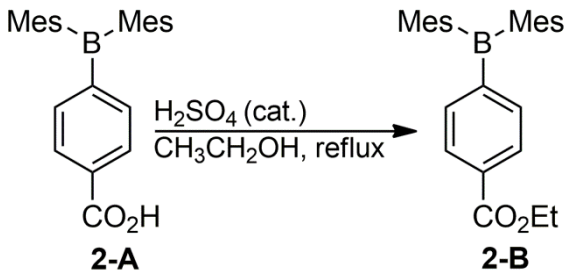

Scheme 2.6 Synthesis of the intermediate **2-B**.

2: 310 mg of **2-B** (0.750 mmol, 1 eq.), 265 mg of **1-A** (0.750 mmol, 1 eq.), and 264 mg LHMDS (1.58 mmol, 2.1 eq.) were added together into a dry schlenk flask. The three solids were dissolved in 10 ml of distilled THF and stirred under N_2 for one hour. The mixture was then refluxed for three hours and then allowed to stir at room temperature for 40 hours (Scheme 2.7). It was quenched with ammonium chloride, separated into diethyl ether and washed with water, and then dried with brine and $MgSO_4$. The slurry was filtered and diethyl ether was removed in vacuo. The crude mixture was purified by column chromatography (CH_2Cl_2). 251 mg isolated (47 % yield). ^{1}H NMR (300 MHz, 298 K, $CDCl_3$, ppm): δ 16.90 (s, 1H), 7.99 (d, J = 8.1 Hz, 4H), 7.67 (d, J = 8.1Hz, 4H), 6.97 (s, 1H) 6.89 (s, 8H), 2.36 (s, 12H), 2.05 (s, 24H).

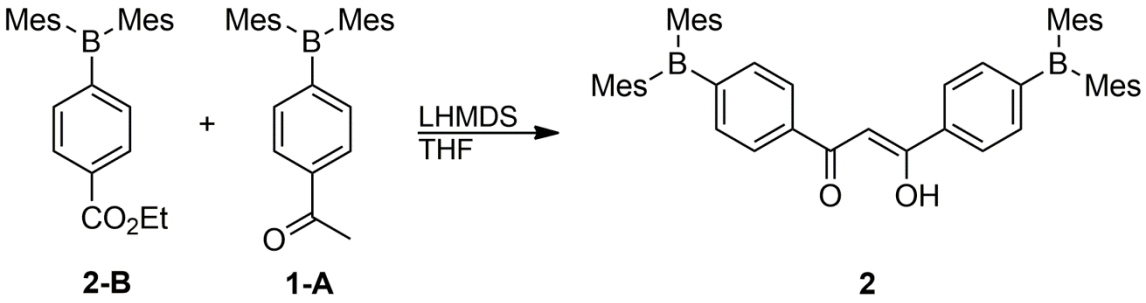

Scheme 2.7 Synthesis of ligand **2**.

2-BF_2: 0.10 mg of 2 (0.14 mmol, 1 eq.) was dissolved in 10 mL distilled CH_2Cl_2 in a nitrogen filled round bottom flask. The solution was heated to reflux and 2.1 eq. $BF_3{\cdot}OEt_2$ (0.041 mL, 0.29 mmol) was added. The mixture immediately changed colour from yellow to brown (Scheme 2.8). The reflux continued overnight. In the morning, the solution was washed with distilled water in order to wash away any coordinating fluorides, dried with brine and $MgSO_4$, and the CH_2Cl_2 was removed under reduced pressure. The compound was purified by column chromatography (CH_2Cl_2). 48 % yield. ^{1}H NMR (400 MHz, 298 K, CD_2Cl_2, ppm): δ 8.12 (d, J = 8.3 Hz, 4H), 7.66 (d, J = 8.3 Hz 4H) 7.33(s, 1H), 6.86 (s, 4H), 2.32 (s, 6H), 1.99 (s, 12H); ^{13}C NMR (100 MHz, 298 K, CD_2Cl_2,, ppm) δ 183.93, 141.45, 140.25, 136.43,

134.61, 128.97, 128.82, 95.24, 23.78, 21.56; ^{11}B NMR (128 MHz, 298 K, CD_2Cl_2, ppm): δ 79.56 (broad), 1.30; ^{19}F NMR (376 MHz, 298 K, CD_2Cl_2, ppm): -140.58, -140.66 Anal. Calc. for $C_{51}H_{53}B_3F_2O_2$: C, 79.72 H, 6.95; found: C, 78.87, H, 7.14. This can be attributed to 0.5 H_2O. Anal. Calc. for $C_{51}H_{54}B_3F_2O_{2.5}$: C, 78.79, H, 7.00.

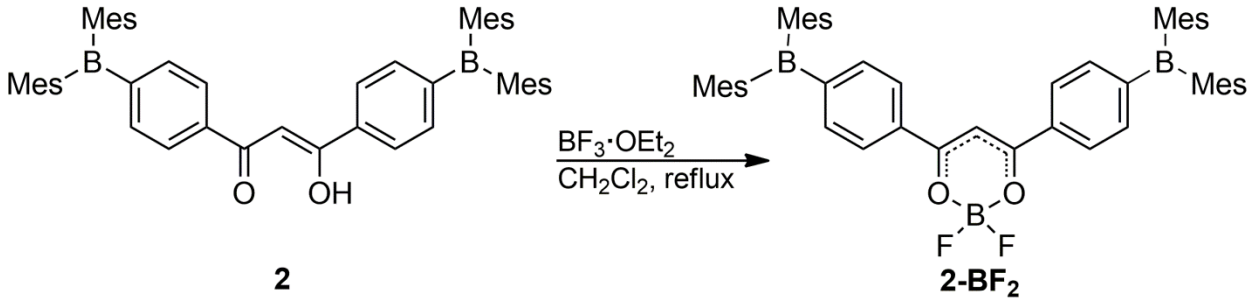

Scheme 2.8 Synthesis of **2-BF_2**.

2.2.4 Synthesis of 3-BF_2

Ligand 3 was synthesized as previously reported.[11]

3-A: (4-Bromophenyl)dimesitylborane (2.19 g, 5.40 mmol, 1 eq.) was dissolved in 80 mL of THF and the mixture was cooled to -78^{o}C. To the mixture was added n-BuLi (1.6 M, 3.4 mL, 5.9 mmol, 1.1 eq.) under N_2 atmosphere at -78^{o}C. After stirring for 1 hour, dried DMF (0.84 mL, 11 mmol, 2 eq.) was added to the mixture. After warming to room temperature, the mixture was stirred for 6 hours. After that, 7.5 mL of 2 M HCl was added dropwise, and the mixture was stirred for 5 hours (Scheme 2.9). Water was then added to the reaction mixture and the mixture was extracted with diethyl ether. Hydrophobic extracts were dried over $MgSO_4$. The product was purified by column chromatography using hexanes:ethyl acetate (9:1) as eluent. Yield: 0.77 g (40 %). ^{1}H NMR (300 MHz, 298 K, $CDCl_3$, ppm): δ 10.10 (s, 1 H), 7.87 (d, 7.8 Hz, 2 H), 7.68 (d, 7.5 Hz, 2 H), 6.87 (s, 4 H), 2.35 (s, 6 H), 2.01 (s, 12 H). ^{13}C NMR (75 MHz, 298 K, $CDCl_3$, ppm): δ 192.70, 152.80, 141.42, 140.85, 139.43, 138.01, 135.96, 129.04, 128.41, 23.44, 21.26.

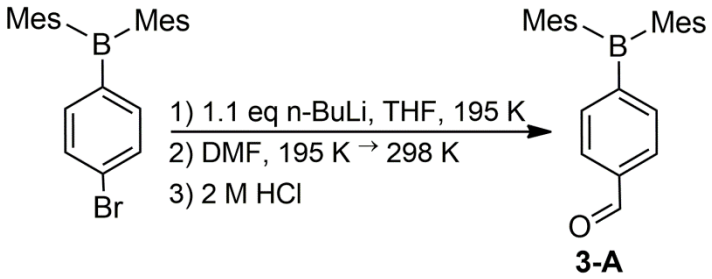

Scheme 2.9 Synthesis of the intermediate **3-A**.

3: A mixture of **3-A** (0.77 g, 2.2 mmol, 1 eq.) and 2,2,2-trimethoxy-4,5-dimethyl-1,3,2-dioxaphosphole (2.27 g, 13.2 mmol, 6 eq.) was stirred for 13 hours at room temperature. Then, 4.0 mL of dried methanol was added and the resultant mixture was stirred for 5 hours (Scheme 2.10). The white precipitate was filtered and washed with methanol. Yield: 0.58 g (62 %). ^{1}H NMR (300 MHz, 298 K, $CDCl_3$, ppm): δ 16.68 (s, 1 H), 7.55 (d, 7.8 Hz, 2 H), 7.18 (d, 8.1 Hz, 2 H), 6.86 (s, 4 H), 2.34 (s, 6 H), 2.04 (s, 12 H), 1.93 (s, 6 H). ^{13}C NMR (75 MHz, 298 K, $CDCl_3$, ppm): δ 190.65, 145.30, 141.66, 140.77, 140.54, 138.83, 136.58, 130.74, 128.26, 115.22, 24.12, 23.38, 21.24.

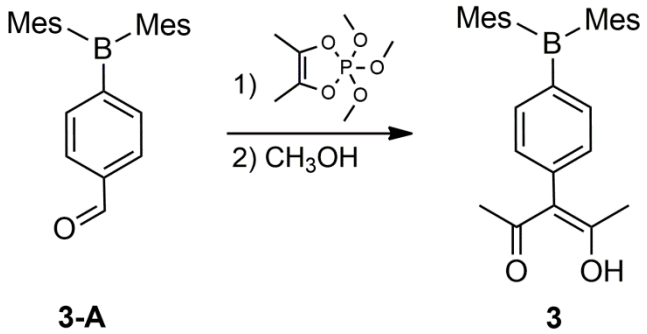

Scheme 2.10 Synthesis of the ligand **3**.

3-BF_2: 100 mg of **3** (0.236 mmol, 1 eq.) was dissolved in 10 mL distilled CH_2Cl_2 in a nitrogen filled round bottom flask. The solution was heated to reflux and 2.1 eq. BF_3˙OEt_2 (0.0611 mL, 0.495 mmol) was added. The reflux continued overnight (Scheme 2.11). In the morning, the solution was washed with

distilled water in order to wash away any coordinating fluorides, dried with brine and $MgSO_4$, and the CH_2Cl_2 was removed under reduced pressure. The compound was purified by crystallization (CH_2Cl_2/ diethyl ether) in a 33 % yield. ^{1}H NMR (400 MHz, 298 K, CD_2Cl_2, ppm): δ 7.56 (d, J = 8.04 Hz, 2H), 7.20 (d, J = 8.04 Hz, 2H), 6.85 (s, 4H), 2.31 (s, 6H), 2.13 (s, 6H), 2.00 (s, 12H); ^{13}C NMR (100 MHz, 298 K, CD_2Cl_2,, ppm) δ 190.98, 140.73, 139.12, 136.79, 136.21, 130.24, 128.24, 23.55, 23.08, 20.89; ^{11}B NMR (128 MHz, 298 K, CD_2Cl_2, ppm): δ 75.65 (broad), 0.40; ^{19}F NMR (376 MHz, 298 K, CD_2Cl_2, ppm): -139.16, -139.23.

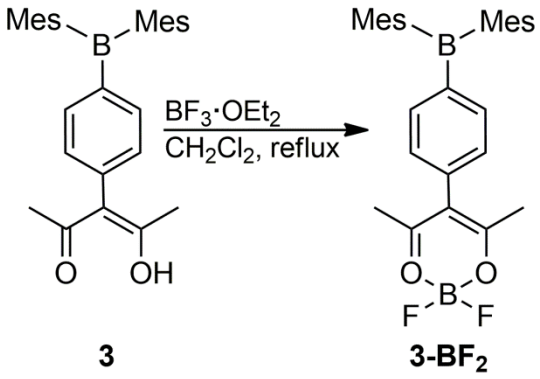

Scheme 2.11 Synthesis of **3-BF_2**.

2.2.5 Synthesis of 4-BF_2

Ligand 4 was synthesized as previously reported.[11]

4-A: (4-bromo-2,3,5,6-tetramethylphenyl)dimesitylborane (0.23 g, 0.50 mmol, 1 eq.) was dissolved in 8 mL of THF and the mixture was cooled to -78^{o}C. To the mixture was added n-BuLi (1.6 M, 0.32 mL, 0.50 mmol, 1 eq.) under a N_2 atmosphere at -78^{o}C. After stirring for 1 hour, dried DMF (0.080 mL, 1.0 mmol, 2 eq.) was added to the mixture. After warming to room temperature, the mixture was stirred for 6 hours. 0.70 mL of 2 M HCl was added dropwise and the mixture was stirred for 5 hours (Scheme 2.12). After an addition of water, the mixture was extracted with diethyl ether and the combined hydrophobic extracts were dried over $MgSO_4$. A yellow solid was purified by column chromatography using hexanes:

ethyl acetate (9:1) as eluent. Yield: 127 mg (62 %). ^{1}H NMR (300 MHz, 298 K, $CDCl_3$, ppm): δ 10.69 (s, 1 H), 6.77 (s, 4 H), 2.33 (s, 6 H), 2.29 (s, 6 H), 2.05 (s, 6 H), 1.98 (s, 12 H). ^{13}C NMR (75 MHz, 298 K, $CDCl_3$, ppm): δ 197.11, 141.11, 140.68, 139.73, 136.11, 135.29, 134.05, 128.96, 23.31, 22.76, 21.23, 19.99, 15.31.

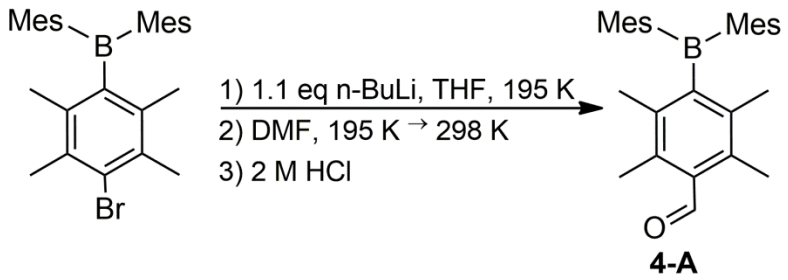

Scheme 2.12 Synthesis of the intermediate **4-A**.

4: A mixture of **4-A** (0.45 g, 1.1 mmol, 1 eq.) and 2,2,2-trimethoxy-4,5-dimethyl-1,3,2-dioxaphosphole (1.3 g, 6.4 mmol, 6 eq.) was stirred for 24 hour at 60^{o}C. Then, 6.0 mL of dried methanol is added and stirred for 4 hours (Scheme 2.13). The white precipitate was filtered and washed with methanol. Yield: 157 mg (30 %). ^{1}H NMR (300 MHz, 298 K. $CDCl_3$, ppm): δ 16.52 (s, 1 H), 6.77 (s, 4 H), 2.29 (s, 6 H), 2.02 (m, 24 H), 1.77 (s, 6 H). ^{13}C NMR (75 MHz, 298 K, $CDCl_3$, ppm): δ 190.43, 144.43, 140.92, 140.60, 139.36, 136.01, 135.84, 133.06, 128.92, 128.81, 113.66, 23.26, 23.22, 22.70. 21.23, 20.42, 16.76.

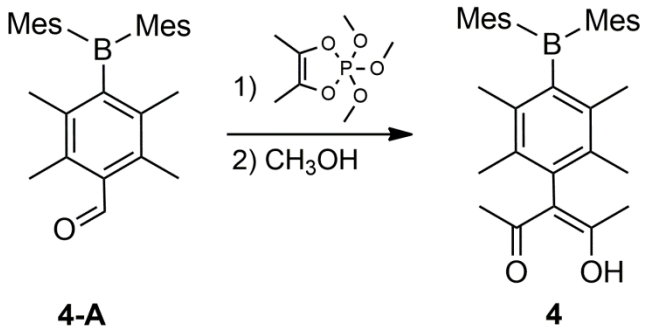

Scheme 2.13 Synthesis of ligand **4**.

4-BF_2: 0.10 g of **4** (0.21 mmol, 1 eq.) was dissolved in 10 mL distilled CH_2Cl_2 in a nitrogen-filled round bottom flask. The solution was heated to reflux and 2.1eq. $BF_3{\cdot}OEt_2$ (0.054 mL, 0.44 mmol) was added. The reflux continued overnight (Scheme 2.14). In the morning, the solution was washed with distilled water in order to wash away any coordinating fluorides, dried with brine and $MgSO_4$, and the CH_2Cl_2 was removed under reduced pressure. The compound was crystallized from (CH_2Cl_2/ether) in a 41 % yield. ^{1}H NMR (400 MHz, 298 K, CD_2Cl_2, ppm): δ 6.77 (s, 4H), 2.26 (s, 6H), 2.03-1.96 (m, 30H); ^{13}C NMR (100 MHz, 298 K, CD_2Cl_2, ppm) δ 191.11, 140.98, 140.63, 139.69, 136.49, 132.78, 131.97, 128.90, 128.83, 115.36, 22.94, 22.64, 20.90, 20.16, 16.48; ^{11}B NMR (128 MHz, 298 K, CD_2Cl_2, ppm): δ 78.37 (broad), 0.59; ^{19}F NMR (376 MHz, 298 K, CD_2Cl_2, ppm): -140.32, -140.38.

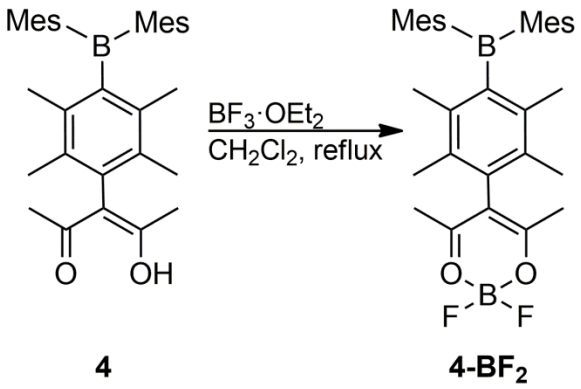

Scheme 2.14 Synthesis of **4-BF_2**.

2.2.6 X-Ray Crystallographic Data

Single crystals of **1-BF_2**, **2-BF_2**, were acquired by slow evaporation under air from a methylene chloride solution. **3-BF_2** crystals were acquired by solvent diffusion of diethyl ether into a saturated solution of methylene chloride. The crystal data are located in Table 2.1.

Table 2.1 Crystallographic details for **1-BF_2**, **2-BF_2**, and **3-BF_2**.

Compound	**1-BF_2**	**2-BF_2**	**3-BF_2**
Formula	C33.50 H33 B2 Cl F2 O2	C51 H53 B3 F2 O2	C14.50 H16 B F O
FW	562.67	768.36	236.08
Space Group	P-1	P2(1)	P2(1)2(1)2(1)
a, Å	9.8714(9)	9.9391(16)	8.7973(7)
b, Å	14.9480(13)	16.595(3)	15.1847(14)
c, Å	21.2648(19)	14.119(2)	23.674(2)
α, °	105.9140(10)	90	90
β, °	92.1230(10)	109.870(3)	90
γ, °	100.8790(10)	90	90
V, $Å^3$	2950.2(5)	2190.2(6)	3162.5(5)
Z	4	2	8
D_{calc}, g cm^{-1}	1.267	1.165	0.992
T, K	180(2)	185(2)	150(2)
μ, mm^{-1}	0.172	0.074	0.068
2θmax, °	54.14	51	55.06
Reflns measured	23443	11124	53721
Reflns used (Rint)	12596 (0.0412)	5839(0.0801)	7244 (0.0384)
Parameters	1180	816	1000
Final R Values [I > 2σ(I)]:			
R_1[a]	0.0648	0.0653	0.0459
wR_2[b]	0.1542	0.1259	0.1271
R Values (all data)			
R_1[a]	0.1403	0.1628	0.0525
wR_2[b]	0.1903	0.1702	0.1312
Goodness-of-fit on F^2	1.011	0.998	1.096

[a] $R_1 = \sum[(|F_0| - |F_c|) / \sum|F_0|$

[b] $wR_2 = [\sum w[(F_0^2-F_c^2)^2]/ \sum[w(F_0^2)^2]]^{1/2}$

$w = 1 / [\sigma^2(F_0^2) + (0.075P)^2]$, where $P = [Max (F_0^2,0) + 2F_c^2]/3$

Table 2.2 Selected bond lengths (Å) and angles (°) for **1-BF_2**, **2-BF_2**, and **3-BF_2**.

		Compound 1-BF_2	
B(1)-F(1)	1.362(4)	B(1)-F(2)	1.366(4)
B(1)-O(1)	1.479(4)	B(1)-O(2)	1.479(4)
B(2)-C(7)	1.573(4)	B(2)-C(16)	1.576(5)
B(2)-C(25)	1.583(5)	O(1)-C(1)	1.303(3)
O(2)-C(3)	1.299(3)	C(1)-C(2)	1.375(4)
C(1)-C(10)	1.463(4)	C(2)-C(3)	1.383(4)
C(3)-C(4)	1.466(4)		
F(1)-B(1)-F(2)	111.1(3)	F(1)-B(1)-O(1)	108.9(3)
F(2)-B(1)-O(1)	108.5(3)	O(1)-B(1)-O(2)	110.7(2)
C(7)-B(2)-C(16)	118.0(3)	C(7)-B(2)-C(25)	119.6(3)
C(16)-B(2)-C(25)	122.4(3)	C(1)-O(1)-B(1)	123.7(2)
C(3)-O(2)-B(1)	123.8(2)	O(1)-C(1)-C(2)	120.1(2)
O(1)-C(1)-C(10)	115.1(2)	C(2)-C(1)-C(10)	124.8(2)
C(1)-C(2)-C(3)	121.2(3)	O(2)-C(3)-C(4)	115.4(2)
O(2)-C(3)-C(2)	120.0(3)	C(8)-C(7)-B(2)	121.5(3)
C(2)-C(3)-C(4)	124.5(3)	C(5)-C(4)-C(3)	122.4(2)
C(6)-C(7)-B(2)	122.0(3)	C(15)-C(10)-C(1)	119.3(3)
C(9)-C(4)-C(3)	118.7(3)	C(17)-C(16)-B(2)	119.3(3)
C(11)-C(10)-C(1)	121.9(3)	C(26)-C(25)-B(2)	121.0(3)
C(21)-C(16)-B(2)	122.6(3)	C(30)-C(25)-B(2)	122.0(3)
		Compound 2-BF_2	
B(1)-F(2)	1.324(11)	B(1)-F(1)	1.353(11)
B(1)-O(2)	1.461(9)	B(1)-O(1)	1.494(10)
B(2)-C(19)	1.572(8)	B(2)-C(7)	1.583(9)
B(2)-C(10)	1.615(8)	B(3)-C(31)	1.559(9)
B(3)-C(34)	1.587(8)	B(3)-C(43)	1.602(8)
O(1)-C(1)	1.283(6)	O(2)-C(3)	1.298(7)
C(1)-C(2)	1.374(8)	C(1)-C(28)	1.478(8)
C(2)-C(3)	1.392(8)	C(3)-C(4)	1.476(8)
F(2)-B(1)-F(1)	111.9(9)	F(2)-B(1)-O(2)	109.9(8)
F(1)-B(1)-O(2)	109.5(8)	F(2)-B(1)-O(1)	108.3(8)
F(1)-B(1)-O(1)	106.7(8)	O(2)-B(1)-O(1)	110.3(7)
C(19)-B(2)-C(7)	119.2(6)	C(19)-B(2)-C(10)	124.4(5)
C(7)-B(2)-C(10)	116.3(6)	C(31)-B(3)-C(34)	121.0(6)
C(31)-B(3)-C(43)	117.6(5)	C(34)-B(3)-C(43)	121.4(5)

C(1)-O(1)-B(1)	123.9(6)	C(3)-O(2)-B(1)	124.1(6)
O(1)-C(1)-C(2)	121.3(6)	O(1)-C(1)-C(28)	115.0(6)
C(2)-C(1)-C(28)	123.8(6)	C(1)-C(2)-C(3)	119.4(6)
O(2)-C(3)-C(2)	120.9(6)	O(2)-C(3)-C(4)	115.6(6)
C(2)-C(3)-C(4)	123.5(6)	C(9)-C(4)-C(3)	121.9(6)
C(5)-C(4)-C(3)	118.7(6)	C(6)-C(7)-B(2)	122.3(6)
C(8)-C(7)-B(2)	120.9(6)	C(11)-C(10)-B(2)	119.0(4)
C(15)-C(10)-B(2)	120.7(4)	C(20)-C(19)-B(2)	119.8(4)
C(24)-C(19)-B(2)	120.2(4)	C(32)-C(31)-B(3)	122.5(6)
C(30)-C(31)-B(3)	121.3(6)	C(35)-C(34)-B(3)	120.1(5)
C(39)-C(34)-B(3)	119.9(5)	C(44)-C(43)-B(3)	120.3(4)
C(48)-C(43)-B(3)	119.3(4)	C(33)-C(28)-C(1)	122.0(6)
C(29)-C(28)-C(1)	119.2(5)		

Compound 3-BF_2

O(1)-C(4)	1.2985(16)	O(1)-B(1)	1.489(2)
O(2)-C(2)	1.2990(16)	O(2)-B(1)	1.492(2)
F(1)-B(1)	1.376(2)	B(1)-F(2)	1.356(2)
C(1)-C(2)	1.497(2)	C(2)-C(3)	1.392(2)
C(3)-C(4)	1.401(2)	C(3)-C(6)	1.4941(18)
C(4)-C(5)	1.484(2)	C(9)-B(2)	1.575(2)
C(12)-B(2)	1.585(2)	C(21)-B(2)	1.588(2)
C(4)-O(1)-B(1)	122.01(12)	C(2)-O(2)-B(1)	122.36(12)
O(2)-C(2)-C(3)	122.11(13)	O(2)-C(2)-C(1)	114.11(13)
C(3)-C(2)-C(1)	123.75(13)	C(2)-C(3)-C(4)	117.40(12)
C(2)-C(3)-C(6)	122.12(13)	C(4)-C(3)-C(6)	120.22(13)
O(1)-C(4)-C(3)	122.19(13)	O(1)-C(4)-C(5)	114.40(13)
C(3)-C(4)-C(5)	123.33(13)	C(7)-C(6)-C(3)	120.32(13)
C(11)-C(6)-C(3)	120.79(13)	C(17)-C(12)-B(2)	121.24(14)
C(8)-C(9)-B(2)	121.08(13)	C(13)-C(12)-B(2)	121.04(13)
C(10)-C(9)-B(2)	121.68(14)	C(22)-C(21)-B(2)	121.34(14)
C(26)-C(21)-B(2)	121.11(13)	F(2)-B(1)-F(1)	112.33(14)
F(2)-B(1)-O(1)	108.92(16)	F(1)-B(1)-O(1)	108.62(14)
F(2)-B(1)-O(2)	108.79(14)	F(1)-B(1)-O(2)	108.69(15)
O(1)-B(1)-O(2)	109.47(12)	C(9)-B(2)-C(12)	119.18(13)
C(9)-B(2)-C(21)	119.27(13)	C(12)-B(2)-C(21)	121.54(12)

2.3 Results and Discussion

2.3.1 Synthesis

The synthesis of the ligands and the chelate compounds was carried out using the procedures as described below. During the synthesis of complexes **3-BF_2** and **4-BF_2**, the ligands and complexes were published by Thilagar *et al.*[11] Therefore, they have only been characterized by NMR spectroscopy.

2.3.1.1 Synthesis of Ligand 1

The multi-step synthesis of ligand **1** is illustrated in Scheme 2.15. The synthesis was previously reported in Blight *et al.*[14] 4-Dimesitylboron-acetophenone (**1-A)** was synthesized by a lithiation of 4-bromoacetophenone diethylketal at 195 K, followed by the addition of dimesitylboron fluoride. The diethylketal was chosen in order to protect the ketone from the nucleophilic attack of n-BuLi. The ketal was converted to the ketone by acid hydrolysis. The ketone (**1-A)** was collected as an off-white solid purified by column chromatography (85% yield) and characterized by NMR spectroscopy. **1-A** was then reacted with LHMDS and benzoyl chloride at 273 K in a Claisen condensation and allowed to stir for one hour. After this, **1** was purified by column chromatography and collected as a bright yellow solid (87% yield). It was characterized by NMR and EA.

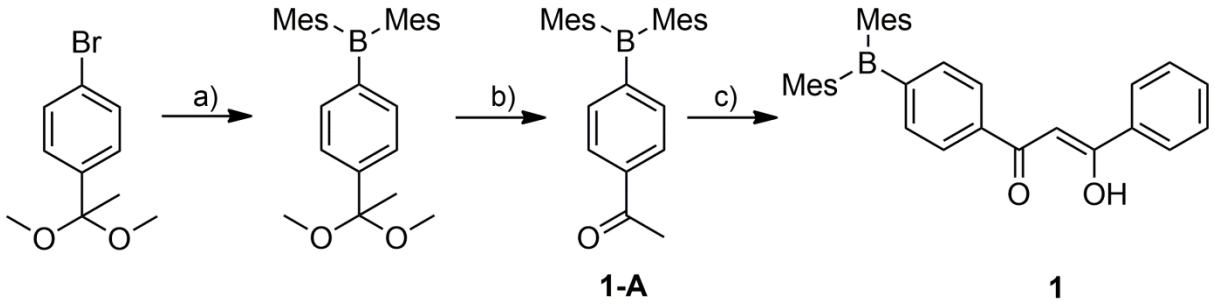

Reagents and Conditions: a) 1.1 eq. n-BuLi, 1 eq. Mes_2BF (Mes = 2,4,6-trimethylphenyl), THF, 195 K→298 K, overnight; b) 2 M HCl, 20 minutes; c) LHMDS, benzoyl chloride, THF, 273 K, 3 hours.

Scheme 2.15 Synthesis of ligand **1**.

2.3.1.2 Synthesis of Ligand 2

Similar to the synthesis of ligand **1**, 4-dimesitylboron-acetophenone (**1-A**) was synthesized. Also synthesized was (4-bromophenyl) dimesitylborane by lithiation of 1,4 dibromobenzene[15] at 195 K, which was purified by washing the collected solid with acetonitrile. (4-bromophenyl) dimesitylborane was further reacted with n-butyllithium at 195 K for one hour before bubbling CO_2 gas through the reaction overnight. After acidification and aqueous work-up, the product (**2-A**) is purified by washing with hexane (70 % yield). **2-A** was converted to an ester (**2-B**) by acidic conversion with ethanol (93% yield). Then, **1-A** and **2-B** were reacted with LHMDS at 273 K for one hour and then at reflux in THF for 40 hours. The orange di-boron functionalized β-diketone (**2**) was collected by column chromatography in CH_2Cl_2 (47% yield). This procedure can be visualized in Scheme 2.16.

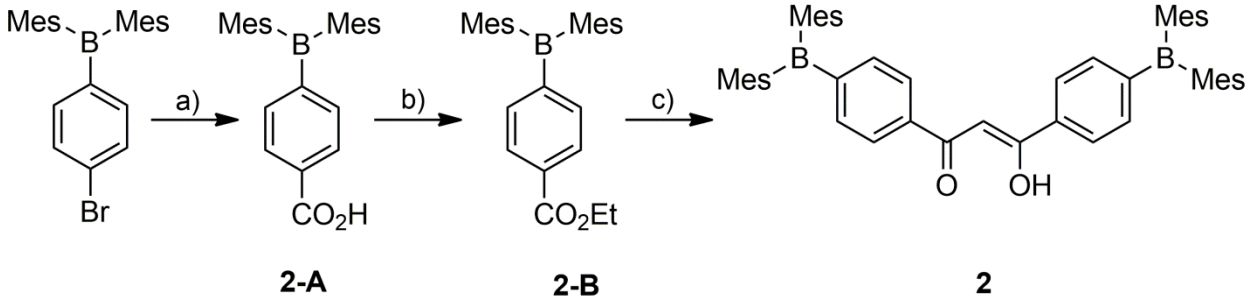

Reagents and Conditions: a) 1.1 eq. n-BuLi, $CO_{2(g)}$, THF, 195 K→ 298 K, overnight; b) ethanol, H_2SO_4; c) LHMDS, **1-A**, THF, 0°C, 1 hour, reflux, 3 hours, 298 K, 40 hours.

Scheme 2.16 Synthesis of compound **2**.

2.3.1.3 Synthesis of Ligand 3

As decribed by Thiligar *et al.*,[11] 4-bromophenyl-dimesitylborane was converted to 4-dimesitylborane-benzaldehyde (**3-A**) by lithiation with n-BuLi at 195 K followed by addition of DMF. After warming to room temperature and stirring for 6 hours, the reaction mixture was acidified with HCl and stirred for a further 5 hours. **3-A** was purified by column chromatography (9:1 hexanes: ethyl acetate) in a 40% yield.

The aldehyde, **3- A**, was then stirred in 2,2,2-trimethoxy-4,5-dimethyl-1,3,2-dioxaphosphole for 12 hours at room temperature and then methanol. The resulting β-diketone, **3**, is a white solid which was then collected by filtration and washed with cold methanol (62% yield). The scheme can be found in Scheme 2.17.

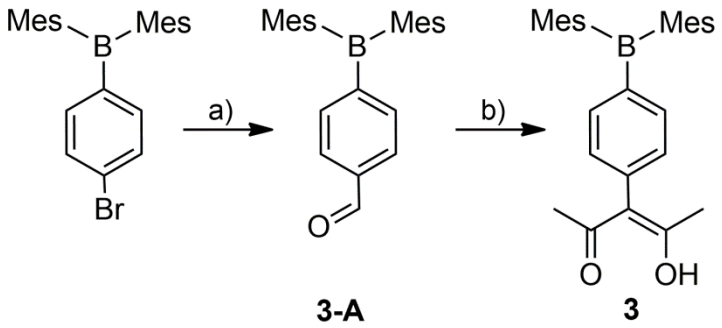

Reagents and Conditions: a) 1.1 eq. n-BuLi, THF, 195 K→298 K, DMF, 6 hours, H^+, 5 hours b) 6 eq. 2,2,2-trimethoxy-4,5-dimethyl-1,3,2-dioxaphosphole, 12 hours, methanol.

Scheme 2.17 Synthesis of compound **3**.

2.3.1.4 Synthesis of Ligand 4

Ligand **4** was synthesized according to literature procedure.[11] 4-Bromoduryl-dimesitylborane was converted to an aldehyde (**4-A**) by lithiation with n-BuLi at 195 K followed by addition of DMF. After warming room temperature for and stirring for 6 hours, the reaction mixture was acidified with HCl and stirred for a further 5 hours. **4-A** was purified by column chromatography (9:1 hexanes: ethyl acetate) in 62 % yield. **4-A** was then stirred in 2,2,2-trimethoxy-4,5-dimethyl-1,3,2-dioxaphosphole for 12 hours at 60^{o}C and then methanol was added. The reaction mixture had to be heated due to the steric bulk of the product (**4**). This is also explains why the yield (30%) is low. The resulting white solid was then collected by filtration and washed with cold methanol. The scheme can be found in Scheme 2.18.

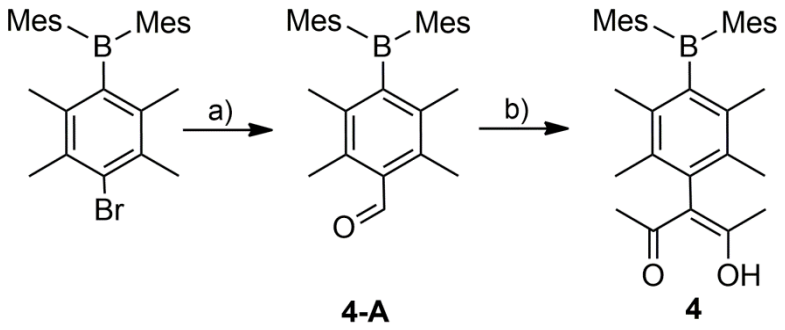

Reagents and Conditions: a) 1.1 eq. n-BuLi, THF, 195 K→298 K, DMF, 6 hours, H^+, 5 hours b) 6 eq. 2,2,2-trimethoxy-4,5-dimethyl-1,3,2-dioxaphosphole, 12 hours, methanol.

Scheme 2.18 Synthesis of compound **4**.

2.3.1.5 Synthesis of the BF_2 Chelates

All of the chelate complexes were synthesized similarly. Under N_2, the β-diketones were dissolved in distilled CH_2Cl_2 and excess BF_3·OEt_2 was added dropwise via syringe. The mixture was refluxed overnight. In the morning, the reaction mixture was washed with water to remove any coordinating fluorides. The 1,3 substituted β-diketonates, **1-BF_2** (32% yield) and **2-BF_2** (48% yield), were purified by column chromatography (CH_2Cl_2) while **3-BF_2** (41% yield) and **4-BF_2** (33% yield) were purified by crystallization (CH_2Cl_2/ diethyl ether). The low yields are characteristic of a difluorboron complex with an electron withdrawing group.[16] The electron withdrawing group makes the β-diketone less nucleophilic, which reduces the yield. The general synthesis of the complexes can be found in scheme 2.19. The complexes were characterized with NMR; as well, **1-BF_2** and **2-BF_2** were characterized with EA. This data can be found in the experimental section.

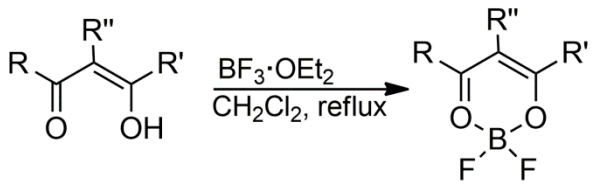

1 - R=(Ph)$BMes_2$, R'=Ph, R''=H
2 - R=R'=(Ph)$BMes_2$, R''=H
3 - R=R'=Me, R''=(Ph)$BMes_2$
4 - R=R'=Me, R''=(Ph)$BMes_2$

Scheme 2.19 General synthesis of the chelate complexes.

2.3.2 X-Ray Crystallographic Analysis

The ORTEP and packing diagram for **1-BF_2**, **2-BF_2,** and **3-BF_2** are pictured in Figure 2.1, 2.2, and 2.3, respectively. The crystal structure of **1-BF_2** shows that it belongs in the triclinic P-1 space group. There are two molecules in the asymmetric unit. As shown in the packing diagram, there is one set of molecules with a parallel arrangement of stacked dimers that have F···H bonds of 2.610 Å. The other molecules are tilted ~60^o with F···H bonds of 2.467 Å. These molecules form F···H bonds to CH_2Cl_2 (not shown). There are also extensive CH···π bonds within the lattice. Compared to the crystal structure of dibenzoylmethane difluoroboron (dbm-BF_2), published by Ikeda and coworkers,[17] the molecular structures are highly similar. The B-O and B-F bond lengths are almost identical between the structures (1.479 Å and 1.362 Å in **1-BF_2** compared to 1.481 Å and 1.363 Å in dbm-BF_2). The O-B-O angle in each molecule (110.7° in **1-BF_2** and 110.9° in dbm-BF_2) shows slight deviation from an idealized tetrahedron. The torsion angle of the boron-functionalized phenyl in **1-BF_2** is 16.1° while the torsion angle of the unfunctionalized phenyl ring is 8.1°. The torsion angle of the phenyl rings of dbm-BF_2 is 18.3°. However, in the extended structure of dbm-BF_2 there is extensive overlap of the phenyl rings. This does not occur in **1-BF_2** because of the steric hindrance of the mesityl groups.

The dbm-BF_2 structure can also be compared to that of **2-BF_2,** which crystallizes in the monoclinic $P2_1$ space group with one molecule in the asymmetric unit. The extended diagram shows no stacked dimers, but extensive π-π stacking involving the mesityl rings and the core of the molecule. There are also F···H

bonds 2.488 Å long and CH···π bonds from the core to the mesityl rings. It displays similar bond lengths (B-O: 1.461 Å, B-F: 1.353 Å) and bond angles (O-B-O: 111.9°) to the previous two structures. It also has dihedral angles of 0.1° and 7.5°. When the triarylboron moieties of **1-BF$_2$** and **2-BF$_2$** are examined, it can be shown that the C-B-C bond angles are slightly distorted from an idealized trigonal planar center (ranges from 118.0° to 122.4° in **1-BF$_2$** and 116.3° to 124.4° in **2-BF$_2$**. This is due to the steric hindrance of the mesityls.

The crystal structure of **3-BF$_2$** was found to belong to the $P2_12_12_1$ space group. It has only molecule in the asymmetric unit. The phenyl ring has a torsion angle of 100.9° with respect to the β-diketonato backbone. Emsley and Freeman studied the crystal structure of 2,2-difluoro-4,6-dimethyl-5-(4'-nitrophenyl)-1,2,3-dioxaborinane and discovered a torsion angle of 99°.[16] The bond length of the C-C bond between the two rings is 1.494 Å in **3-BF$_2$** but 1.499 Å in the literature structure. This bond distance is closer to a C-C single bond than double bond, preventing any π overlap between the rings. The packing diagram of **3-BF$_2$** shows F···H bonds 2.655 Å long and O···H bonds 2.506 Å long, as seen in Figure 2.3. The relatively coplanar phenyl rings on **1-BF$_2$** and **2-BF$_2$** contrast with the orthogonal phenyl linker on **3-BF$_2$** which has implications on the singlet and triplet energy levels.

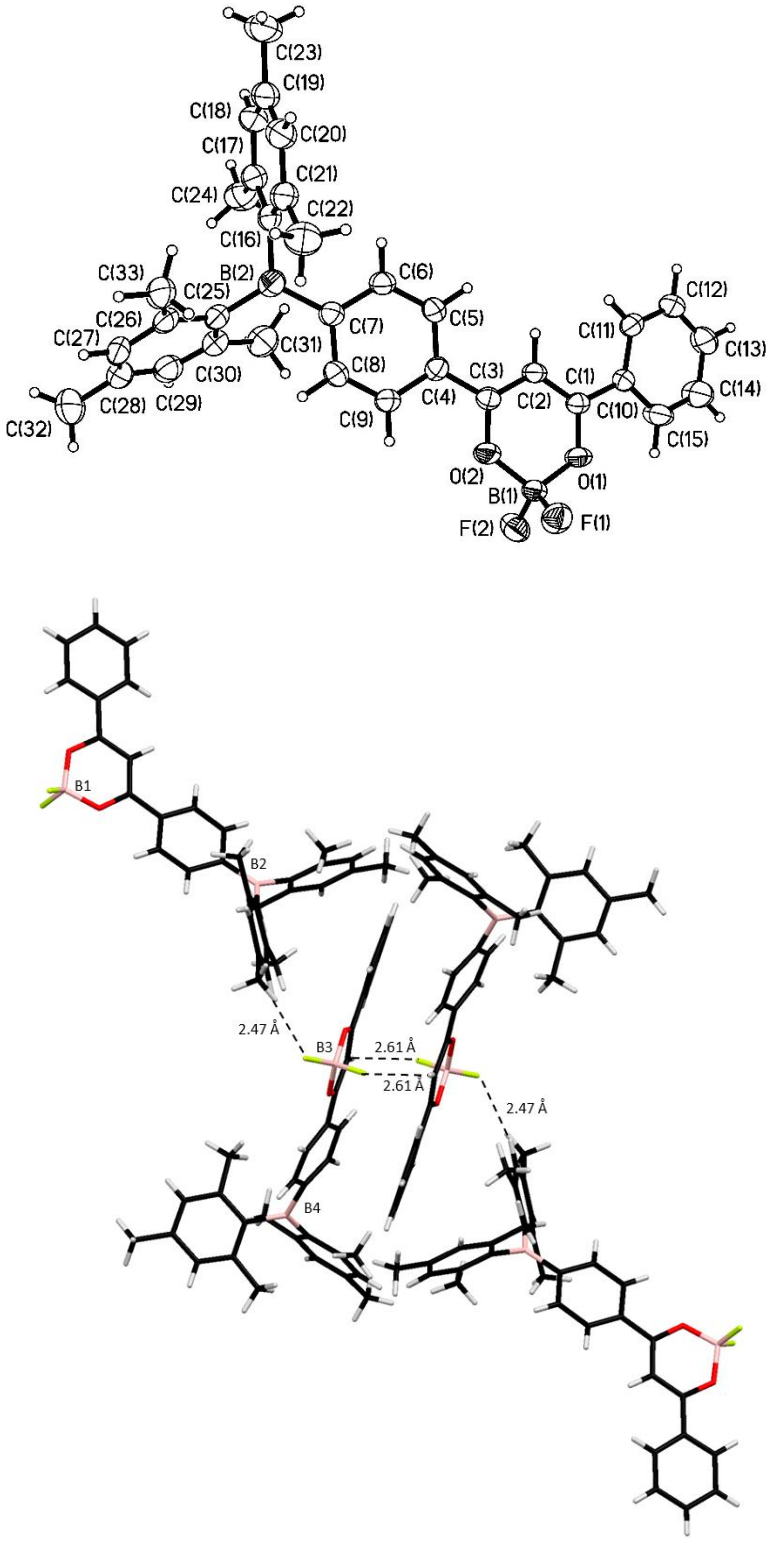

Figure 2.1 The ORTEP and packing diagram of **1-BF_2**.

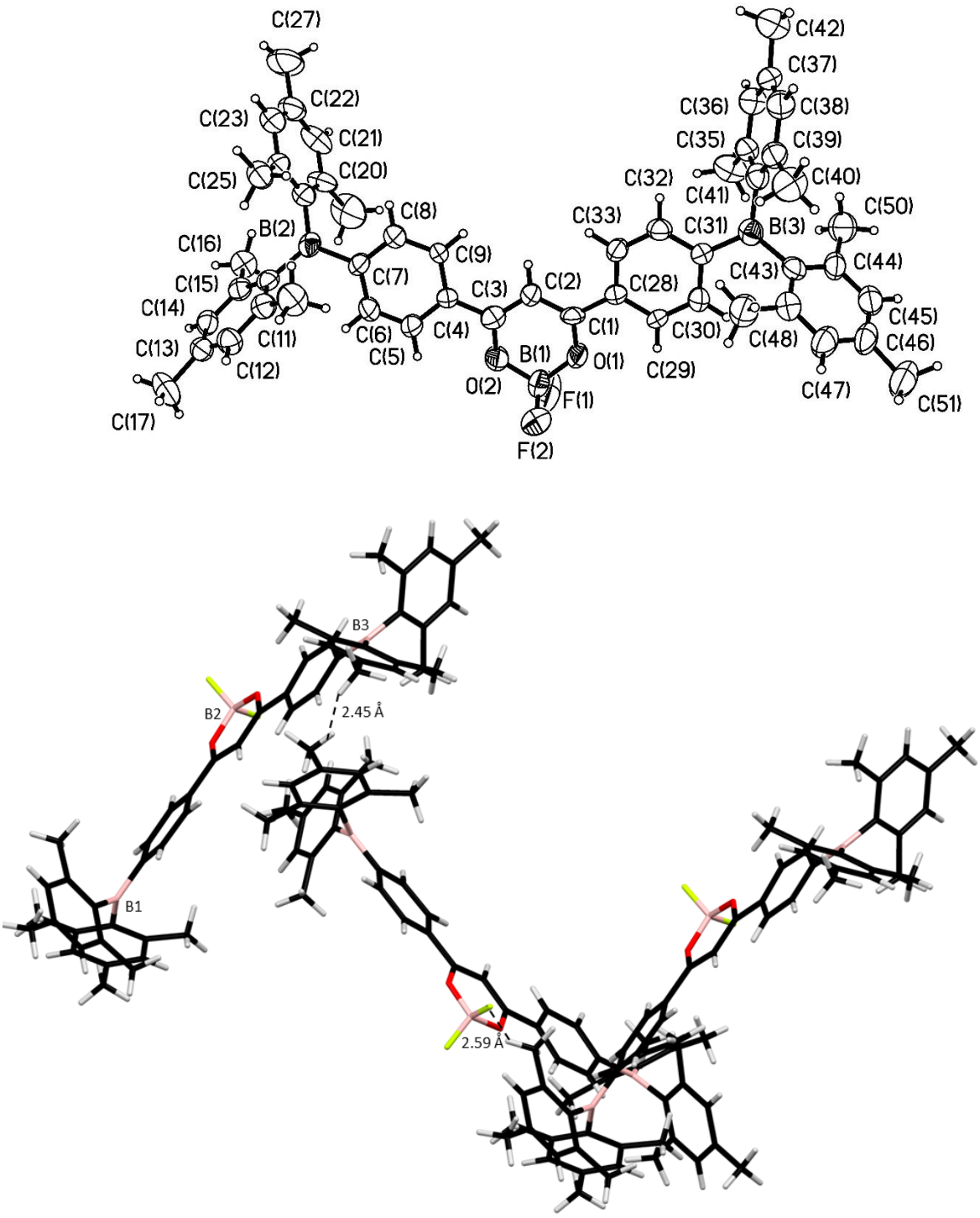

Figure 2.2 The ORTEP and packing diagram of **2-BF_2**.

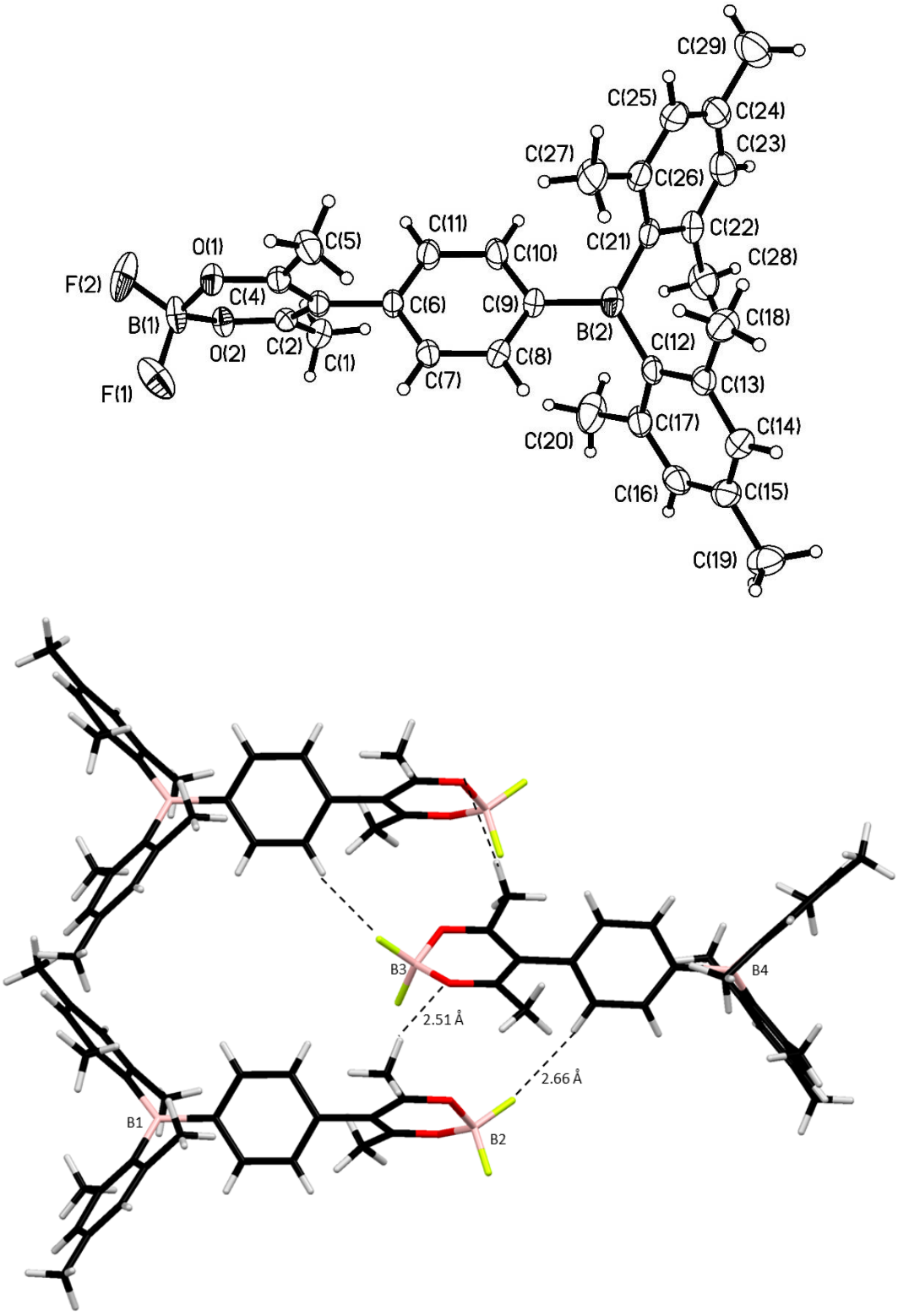

Figure 2.3 The ORTEP and packing diagram of **3-BF_2**.

2.3.3 DFT Computational Studies

The structural and photophysical properties of the chelate complexes were studied computationally. First, their geometries were optimized using 6-311+G(d,p) basis set and the B3LYP level of theory. The initial geometries were based on crystal structures **1-BF$_2$** and **2-BF$_2$** while modeled geometries were used for **3-BF$_2$** and **4-BF$_2$.** In each case, the HOMO was calculated to be located on the mesityl moieties and the LUMO was calculated to be on the β-diketo backbone. The three-coordinate boron has a large contribution to the LUMO in **1-BF$_2$** and **2-BF$_2$**. There is little to no electron density located on the BF_2 moiety. The HOMO and LUMO diagrams can be visualized in Figure 2.4a and 2.4b, respectively.

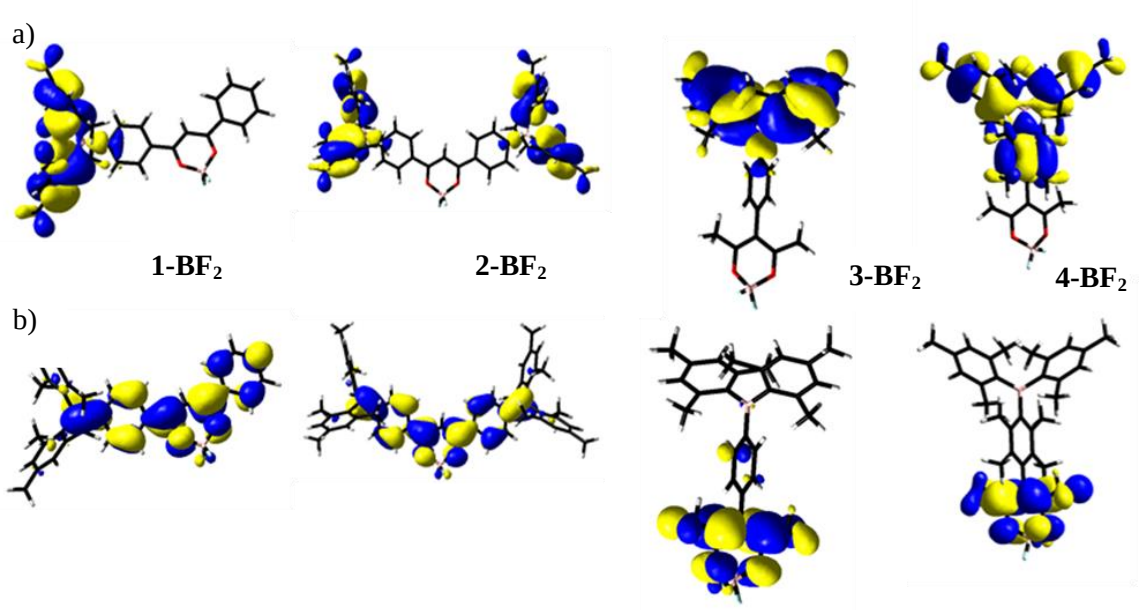

Figure 2.4 The a) HOMO and b) LUMO diagrams of **1-BF$_2$**, **2-BF$_2$**, **3-BF$_2$**, and **4-BF$_2$**.

In agreement with the crystal structures, the optimized structures show that the aryl linker is coplanar with the β-diketonate unit in **1-BF$_2$** and **2-BF$_2$** and orthogonal to the β-diketonate unit in the structures of **3-BF$_2$**, and **4-BF$_2$** (Figure 2.5). Based on this structural data, it is clear that **3-BF$_2$**, and **4-BF$_2$** are not conjugated with the β-diketonate unit while the structures of **1-BF$_2$** and **2-**

BF_2 show extended conjugation. This will have a significant impact on the electronic properties of the ligands.

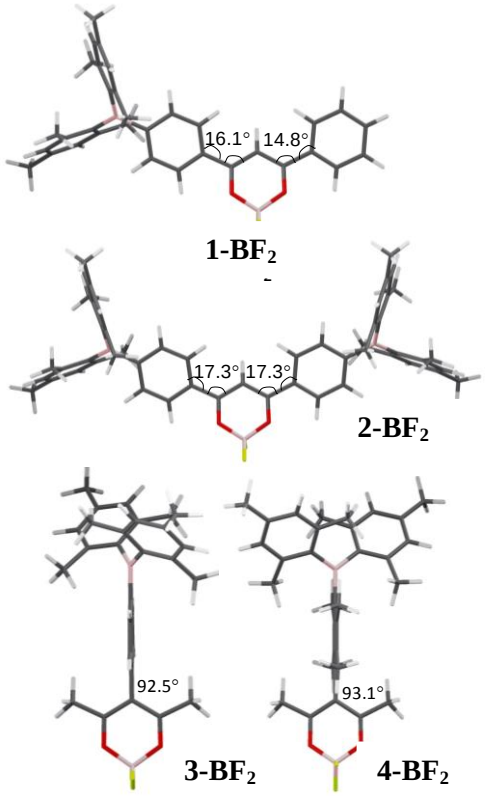

Figure 2.5 The optimized structures of the BF_2 chelates and their dihedral angles.

TD-DFT was performed on the optimized structures with the same basis set and level of theory. Both triplet and singlet states were calculated. The calculated $S_0 \rightarrow S_1$ and $S_0 \rightarrow T_1$ transitions are detailed in Table 2.3 and the orbitals that have a major contribution to the transitions can be visualized in Figure 2.6. The $S_0 \rightarrow S_1$ transition in **1-BF_2** and **2-BF_2** shows the charge transfer from the mesityl groups to the π-conjugated backbone and the three-coordinate boron. In each case, the HOMO→LUMO transition is the major contributor to the transition. In **3-BF_2**, the transition to the first excited state involves a charge transfer from the mesityl π to the B-phenyl π* and the 1,3 β-diketonato backbone π*. The major contributor to this transition is the HOMO→LUMO+1. In **4-BF_2**, the transition is the mesityl-duryl π system charge transfer to the 1,3 β-diketonato

backbone π*. This transition is mostly from the HOMO-1→LUMO. In both cases, the increased energy transition energy of the $S_0 \rightarrow S_1$ is due to the twisted arrangement between the backbone and the phenyl rings leading to decreased π conjugation. The calculated triplet state energies follow the same energy pattern as the singlet states with **2-BF_2** being the lowest energy and **3-BF_2** being the highest. This shows that by controlling the amount of π-conjugation between the mesityls and the aryl-diketo leads to tuning of the triplet state. This has important implications for Chapter 3 of this thesis. The calculations were also performed in the presence of methylene chloride as a solvent.

Table 2.3 Summary of TD-DFT results for **1-BF_2**, **2-BF_2**, **3-BF_2**, and **4-BF_2**.

Compound	**Transition**	**Major MO contributions**	**Oscillator Strength**	**λ (nm)**
1-BF_2	S_1	HOMO→LUMO (84%)	0.0291	439.00
	T_1	HOMO-4 → LUMO (59%)	0.0000	499.36
1-BF_2 with CH_2Cl_2	S_1	HOMO→LUMO (86%)	0.0269	458.09
	T_1	HOMO-4 → LUMO (58%)	0.0000	513.64
2-BF_2	S_1	HOMO→LUMO (83%)	0.0184	442.83
	T_1	HOMO-8→LUMO (83%)	0.0000	511.38
2-BF_2 with CH_2Cl_2	S_1	HOMO → LUMO (85%)	0.0384	465.30
	T_1	HOMO-8→ LUMO (52%)	0.0000	525.93
3-BF_2	S_1	HOMO→LUMO+1 (76%)	0.0864	357.88
	T_1	HOMO-5→LUMO (53%)	0.0000	416.58
		HOMO-4→LUMO (47%)	0.0000	
3-BF_2 with CH_2Cl_2	S_1	HOMO→LUMO (58%)	0.0472	361.24
	T_1	HOMO-6→LUMO (100%)	0.0000	419.08
4-BF_2	S_1	HOMO-1→LUMO (69%)	0.0044	360.49
	T_1	HOMO-6→LUMO (100%)	0.0000	427.91
4-BF_2 with CH_2Cl_2	S_1	HOMO→LUMO (54%)	0.0059	396.20
		HOMO-1→LUMO (46%)		
	T_1	HOMO-6→ LUMO(100%)	0.0000	433.88

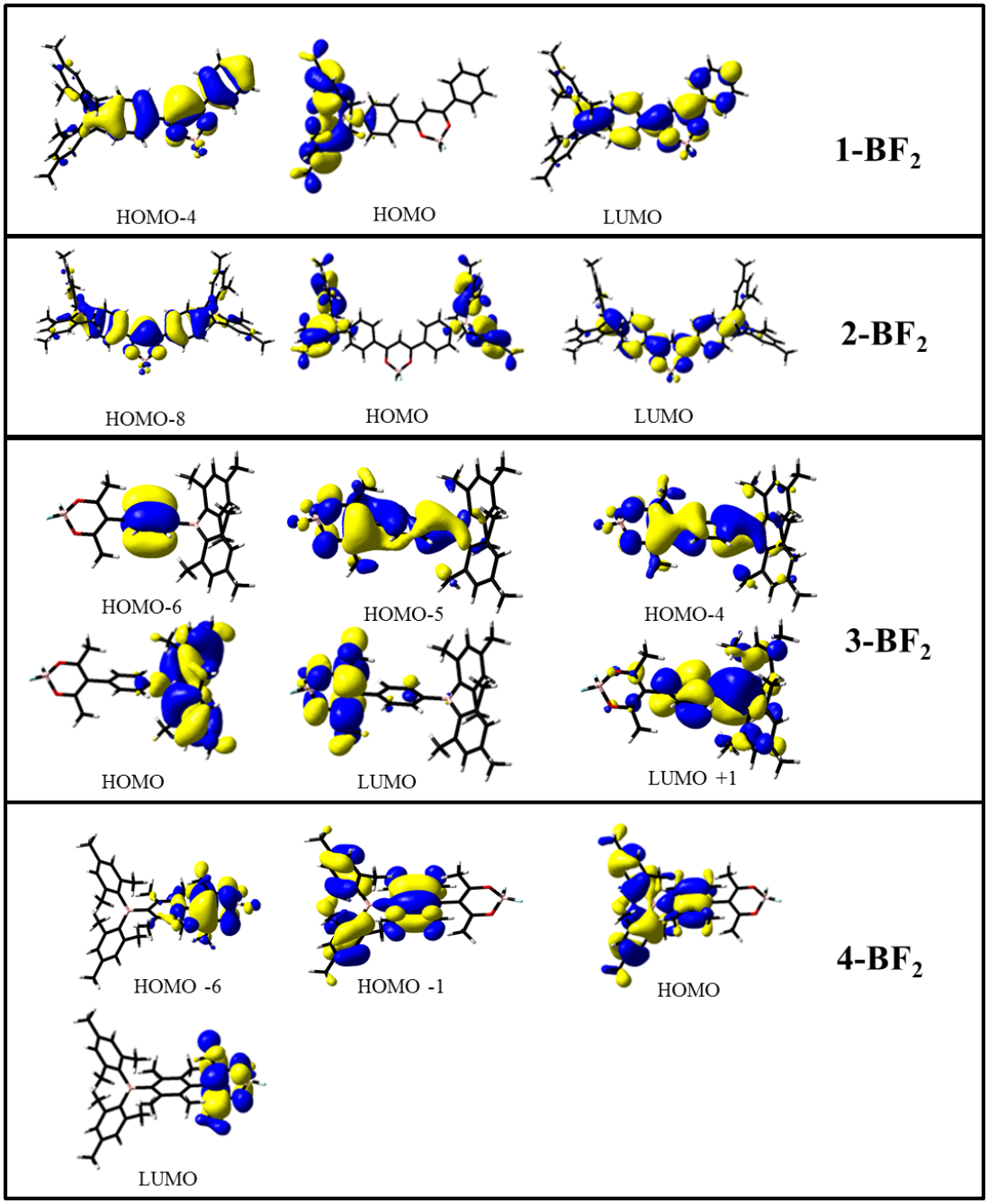

Figure 2.6 The major contributing orbitals to the calculated transitions of **1-BF_2**, **2-BF_2**, **3-BF_2**, and **4-BF_2**.

2.3.4 UV-Vis Absorption Spectra

To better understand the electronic properties of the complexes, the UV-visible spectra were recorded. The absorption of all four complexes are overlaid in Figure 2.7. **1-BF$_2$** and **2-BF$_2$** have similar absorbance profiles and large extinction coefficients. The molar absorptivity of **2-BF$_2$** is significantly higher than the others because of the extended conjugation in the system. The extended conjugation is also why the two complexes are more red-shifted in their absorption energy than the disrupted conjugation *meso*-substituted complexes, **3-BF$_2$** and **4-BF$_2$**. These complexes are weakly absorbing because of the small amount of conjugation. Table 2.4 shows a summary of all the photophysical data in CH_2Cl_2.

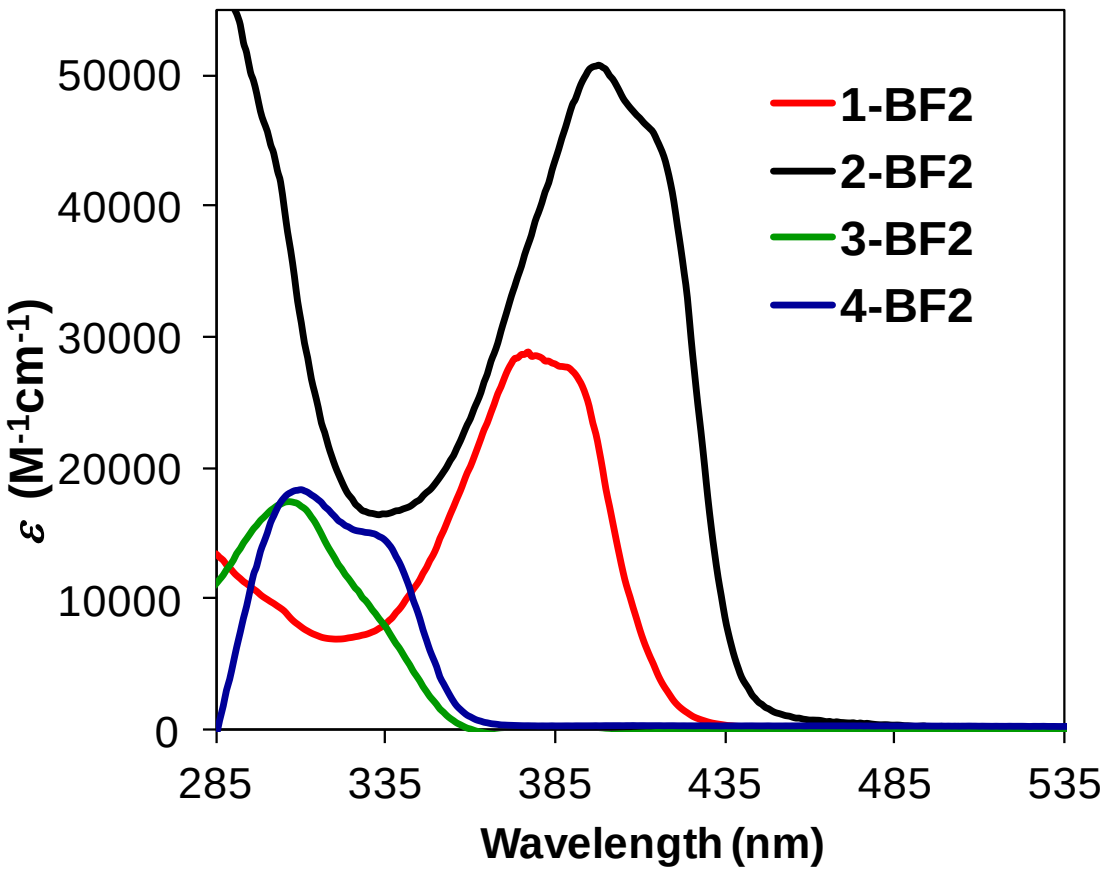

Figure 2.7 The absorption spectrum of **1-BF$_2$**, **2-BF$_2$**, **3-BF$_2$**, and **4-BF$_2$** in CH_2Cl_2 at 298 K.

2.3.5 Fluorescence Spectra

The fluorescence spectra were also recorded to investigate the electronic properties of each difluoroboron compound. The normalized emission spectra can be found overlaid in Figure 2.8. The emission wavelength red-shifts as the conjugation in the system increases and the HOMO-LUMO gap shrinks. The *meso* substituted complexes show emission in the UV region and, therefore, it is not visible to the human eye. All of the spectra were recorded at the same concentration: 1.0 x 10^{-5} M in CH_2Cl_2.

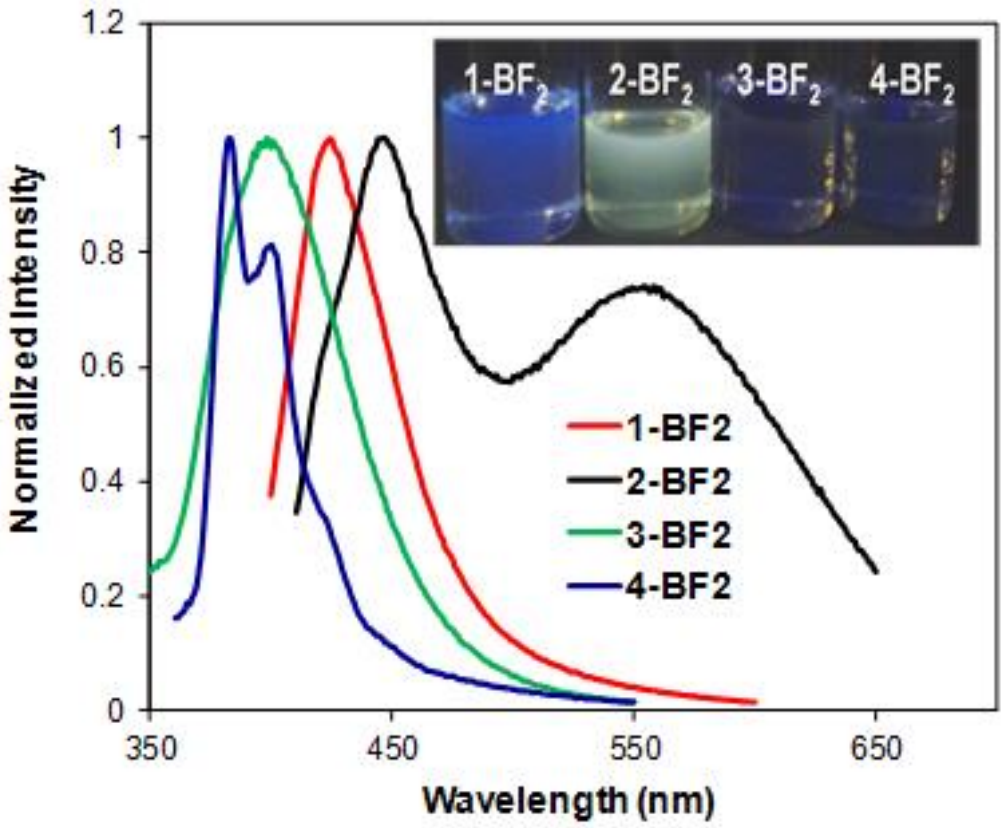

Figure 2.8 The normalized emission spectrum of **1-BF_2**, **2-BF_2**, **3-BF_2**, and **4-BF_2** in CH_2Cl_2 at 298 K.

Similar to other phenyl-substituted 1,3-β-diketonate-BF_2 compounds, **1-BF_2** and **2-BF_2** show a concentration dependent excimer emission at higher wavelengths. This can be visualized in Figure 2.9. Due to the wavelength of the complex emission and excimer emission, white light emission can be obtained from the complexes at higher concentrations.

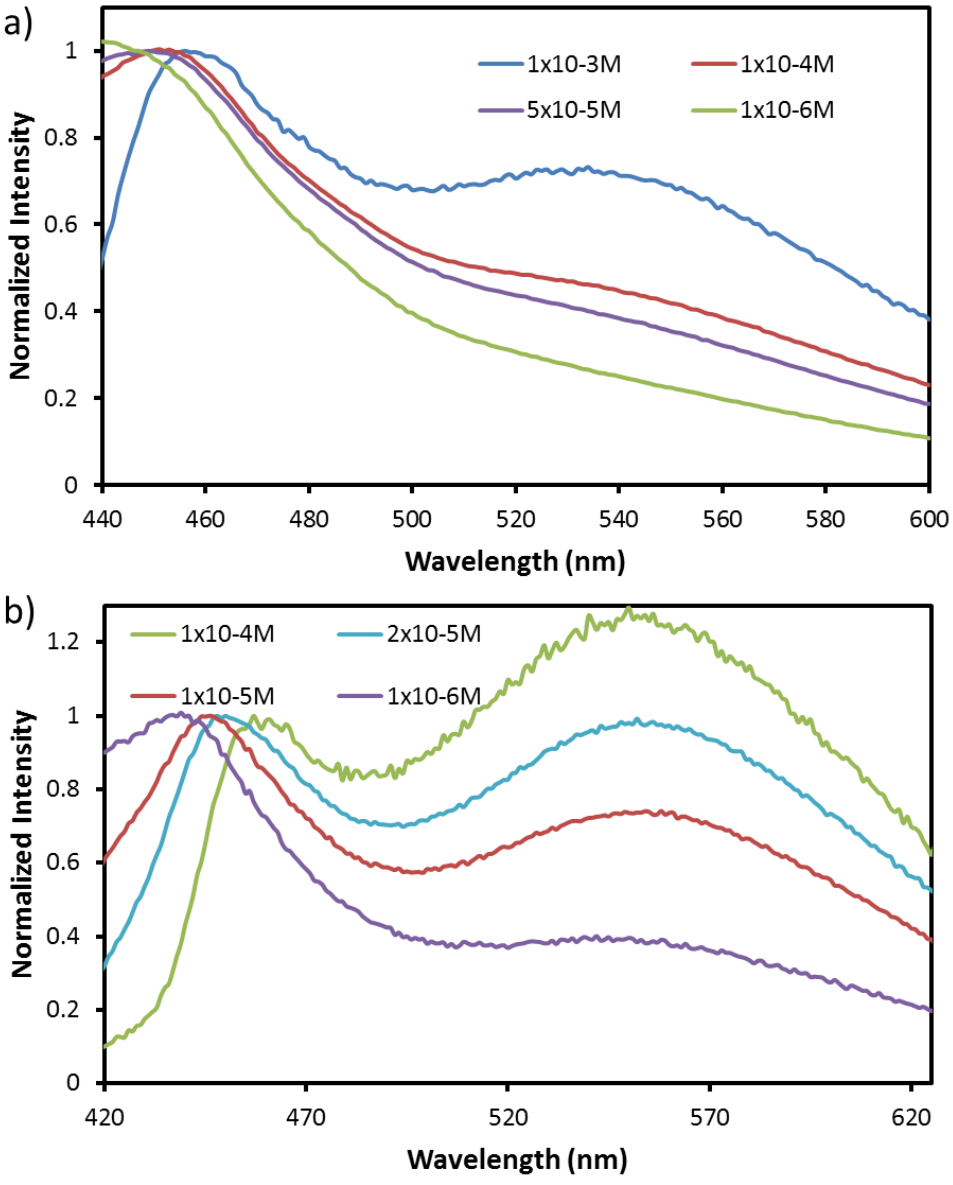

Figure 2.9 The emission spectral change with concentration of a) **1-BF_2** (λ_{ex} = 380 nm) and b) **2-BF_2** (λ_{ex}= 394 nm) 298 K in CH_2Cl_2.

The quantum yield of each complex was measured in CH_2Cl_2 against 9,10-diphenylanthracene. All of the solution quantum yields are relatively low. In the solid state, **1-BF$_2$** and **2-BF$_2$** have much higher quantum yields, whereas the solid state quantum yield of **3-BF$_2$** and **4-BF$_2$** is very small. The lifetime of the emission of **1-BF$_2$** and **2-BF$_2$** was measured in 2-Me-THF at 77 K. The relatively short lifetimes of the emission peaks indicate that the emission is fluorescence. The emission data of all the complexes is summarized in Table 2.4. Attempts to measure the triplet states at 77 K were unsuccessful.

Table 2.4 Photophysical properties of **1-BF$_2$**, **2-BF$_2$**, **3-BF$_2$**, and **4-BF$_2$**.

Compound	**Absorption (Emission) Maxima (nm)**	**ε ($M^{-1}cm^{-1}$)**	**Solution ϕ[a] (ϕ_{ss})[b]**	**Emission Decay Lifetime (ns)**
1-BF$_2$	377 (424)	$2.9x10^4$	0.06 (0.17)	1.551± 0.034
2-BF$_2$	398 (445)	$5.1x10^4$	0.04 (0.12)	1.869 ± 0.035
3-BF$_2$	306 (398)	$1.7x10^4$	0.05 (<0.01)	--
4-BF$_2$	310 (383)	$1.8x10^4$	0.14 (<0.01)	--

[a]Solution quantum yield vs 9,10-diphenylanthracene in ethanol (0.95).[15]
[b]The solid state quantum yield was found via integration sphere in a 20% w/w PMMA film.

2.3.6 Fluoride Sensing

In order to test the fluoride sensing ability of each chelate compound, 3.0 mL of a 1.0 x 10^{-5} M solution in distilled CH_2Cl_2 was prepared in a quartz cuvette. The solution was degassed with N_2. Similarly, a solution of tetrabutylammonium fluoride (TBAF) in distilled CH_2Cl_2 was made such that 1 µL of this solution was 0.1 equivalents of the chelate solution. The chelate was then titrated with the solution of TBAF and the absorption and fluorometric response was measured until no change was observed in the fluorescence spectrum.

In **1-BF$_2$**, as fluoride is added, the absorbance and the fluorescence decrease until 10 equivalents have been added (see Figure 2.10 and 2.11). This can be attributed to the bound fluoride

interrupting the HOMO→LUMO charge transfer as the boron center is no longer available to accept charge transfer in the LUMO. In **2-BF_2**, there are two wavelengths that exhibit change in the absorbance. As fluoride is added, the peak at 397 nm decreases in absorbance while the secondary peak at 430 nm increases (Figure 2.12). The emission shows a decrease in intensity until 5 equivalents of fluoride have been added (Figure 2.13). Again, this can be attributed to the boron center no longer being a part of the LUMO.

The titrations of **3-BF_2** (Figure 2.14 and 2.15) and **4-BF_2** (Figure 2.16 and 2.17) are very similar. The initial absorbance wavelength increases. As well, a second lower energy absorbance peak increases at ~430 nm. This can be attributed to a charge transfer from the [$BMes_2$(Ar)F] → 1,3-β diketonato backbone charge transfer. The computational data indicated that there was no boron contribution to the LUMO in these complexes, so the fluoride binding would not alter the LUMO. Instead it would destabilize the HOMO, leading to a decrease in the $S_0 \rightarrow S_1$ transition energy. Both complexes also demonstrated a small increase in the emission intensity upon addition of fluoride with **3-BF_2** being more affected by the titration than **4-BF_2**.

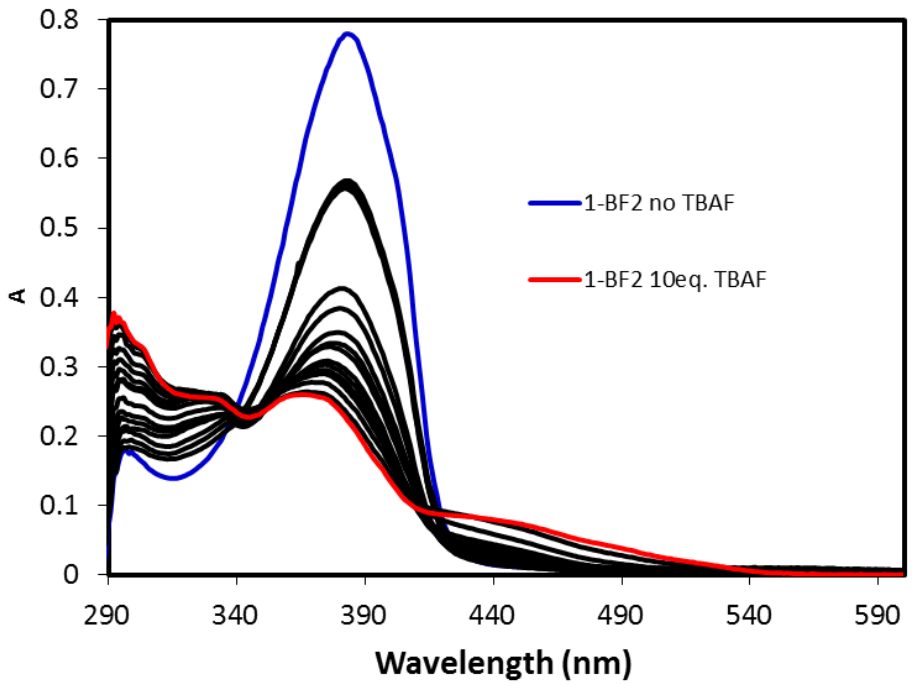

Figure 2.10 The absorption spectral change of **1-BF_2** with the addition of TBAF at 298 K in CH_2Cl_2.

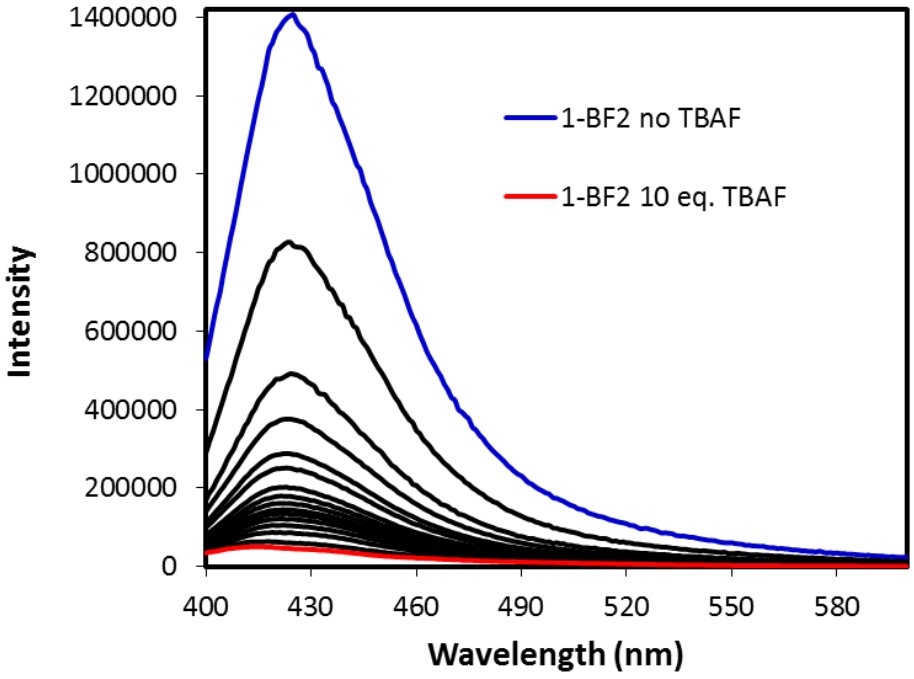

Figure 2.11 The fluorescence spectral change of **1-BF_2** with the addition of TBAF in CH_2Cl_2 at 298 K (λ_{ex} = 380 nm).

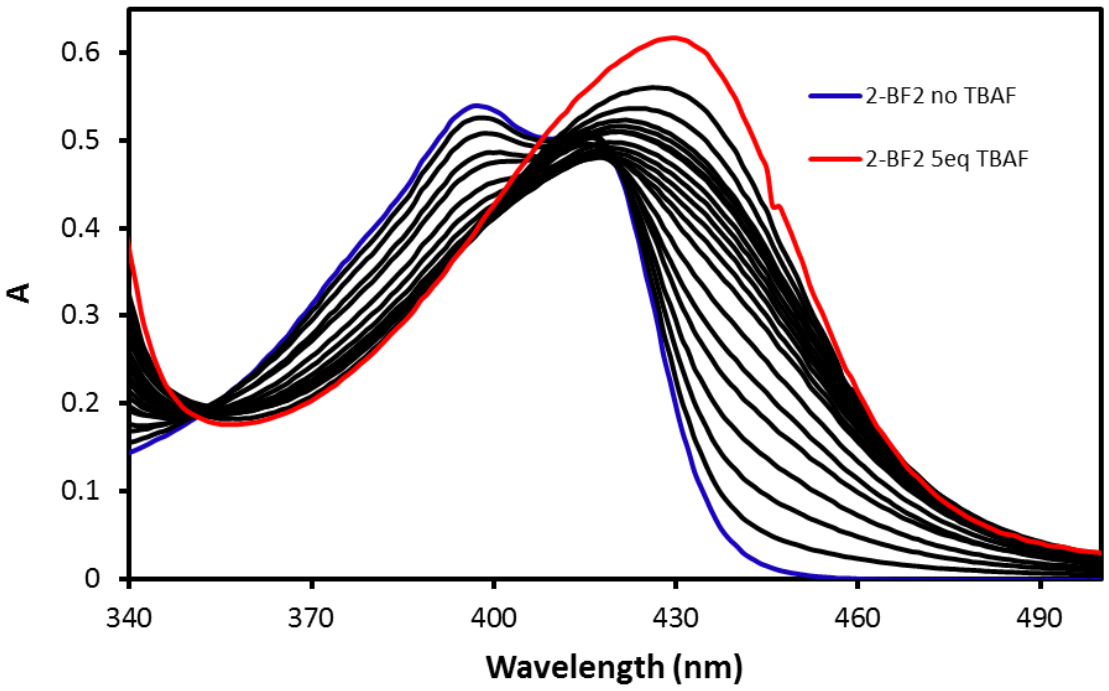

Figure 2.12 The absorption spectral change of **2-BF$_2$** with the addition of TBAF at 298 K in CH_2Cl_2.

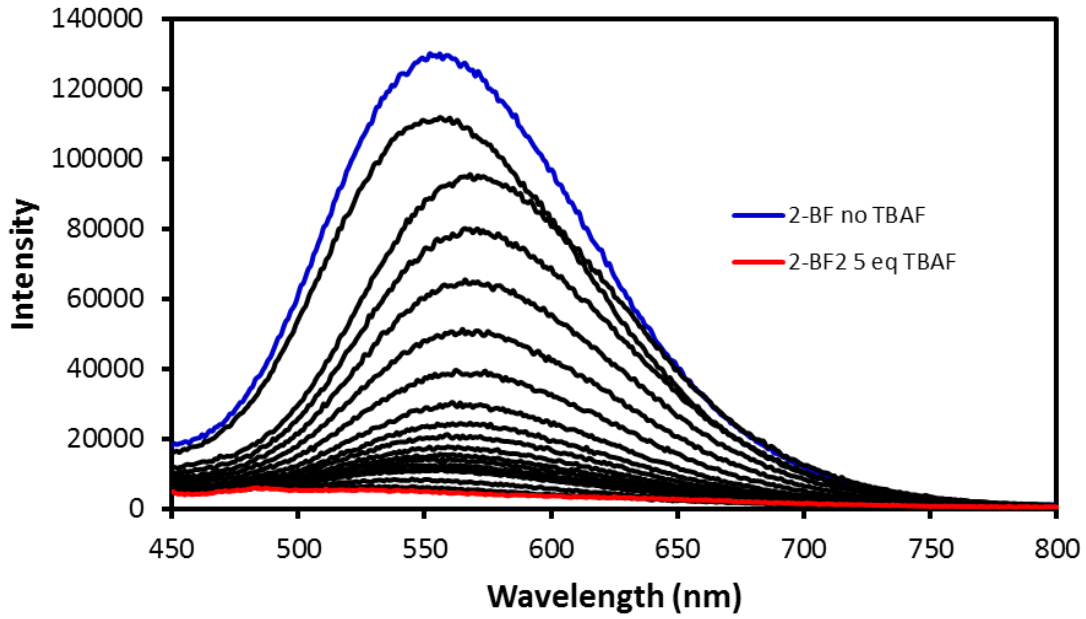

Figure 2.13 The fluorescence spectral change of **2-BF$_2$** with the addition of TBAF at 298 K in CH_2Cl_2 (λ_{ex} = 397 nm).

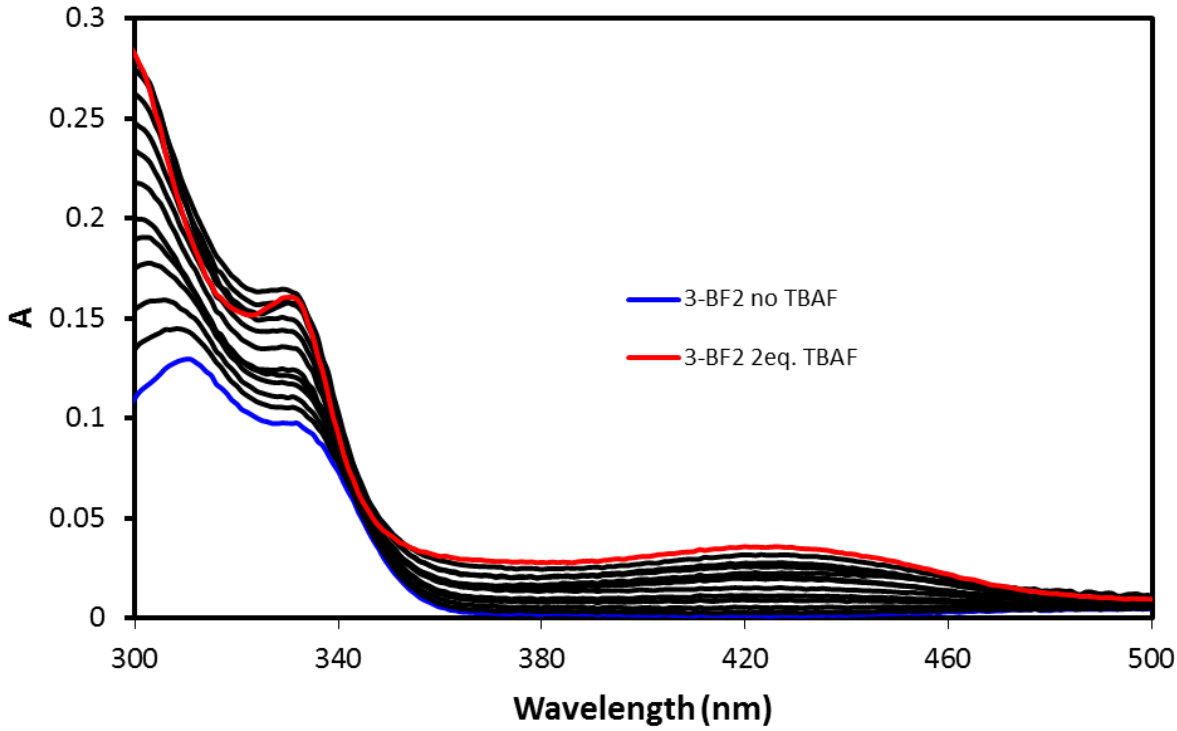

Figure 2.14 The absorption spectral change of **3-BF$_2$** with the addition of TBAF at 298 K in CH_2Cl_2.

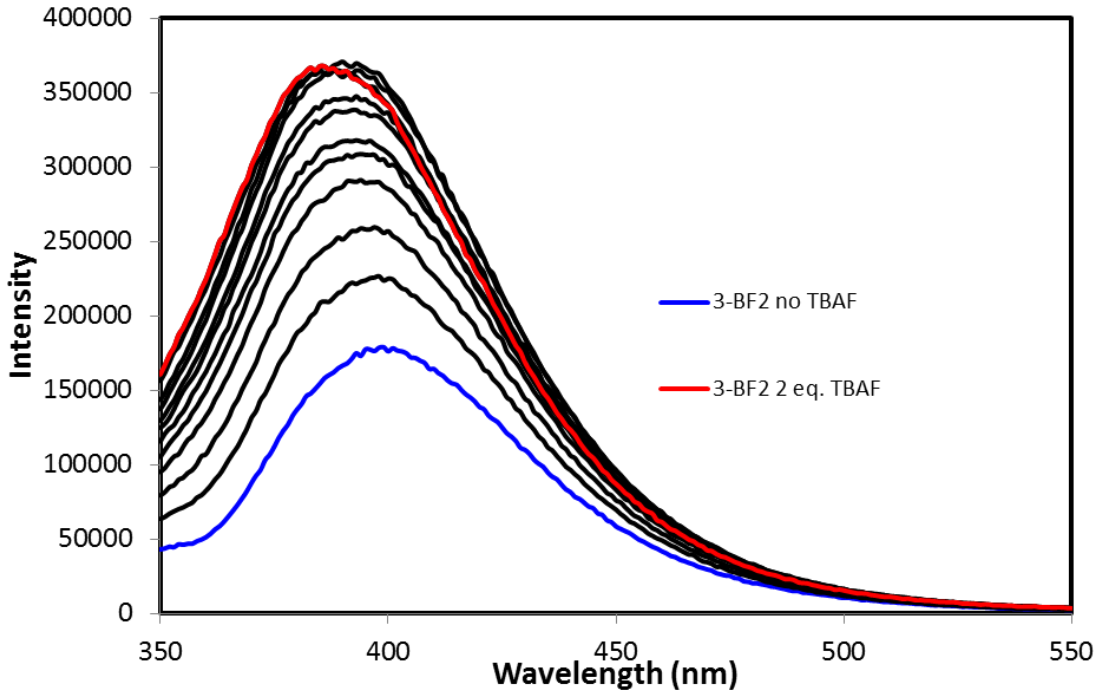

Figure 2.15 The fluorescence spectral change of **3-BF$_2$** with the addition of TBAF at 298 K in CH_2Cl_2 (λ_{ex} = 330 nm).

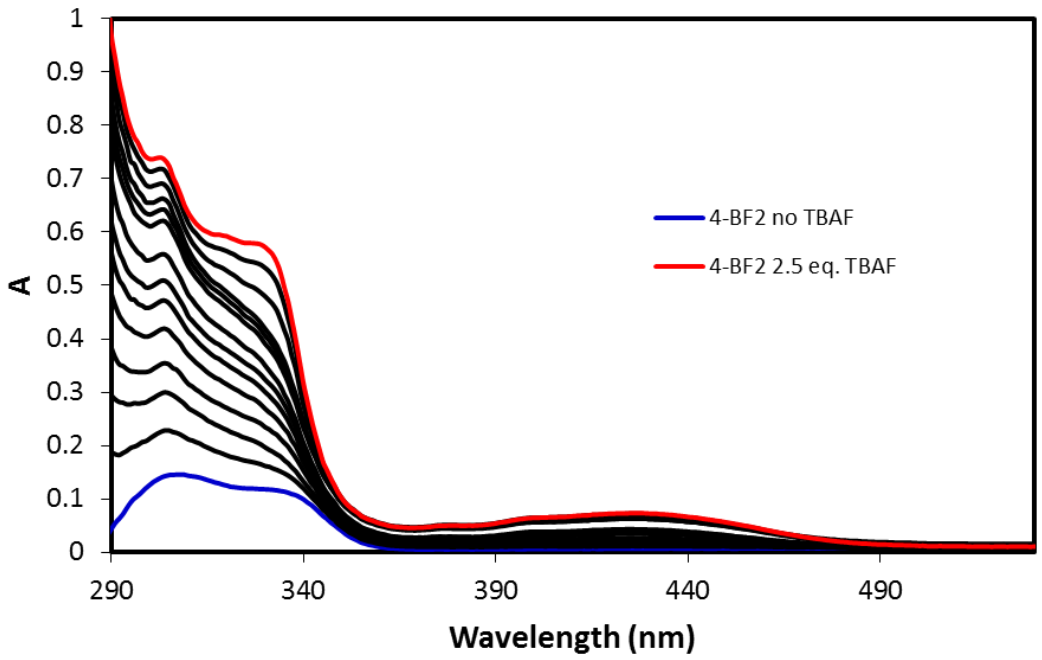

Figure 2.16 The absorption spectral change of **4-BF_2** with the addition of TBAF at 298 K in CH_2Cl_2.

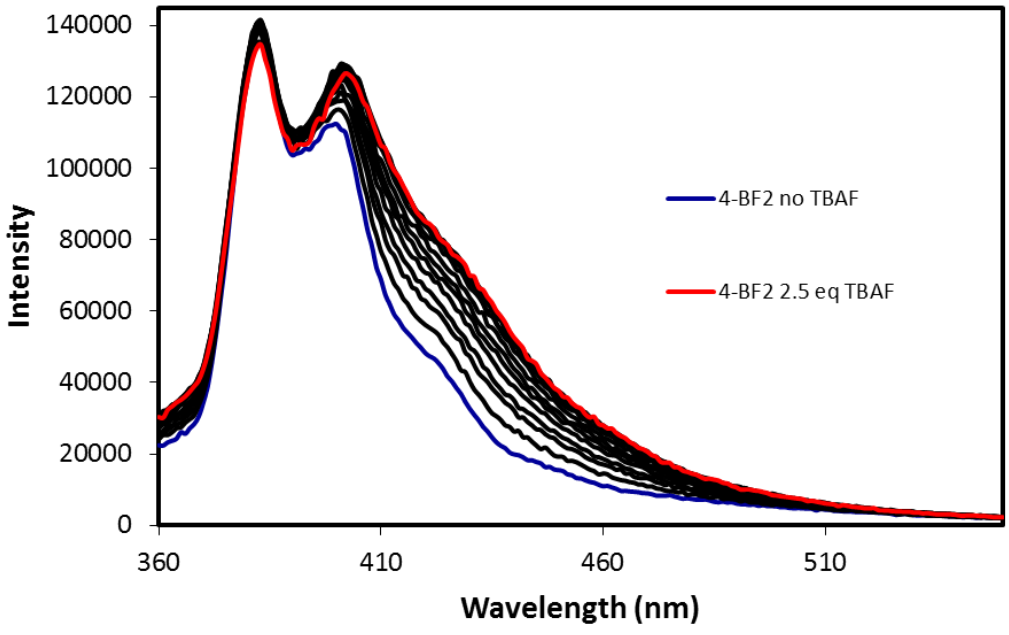

Figure 2.17 The fluorescence spectral change of **4-BF_2** with the addition of TBAF at 298 K in CH_2Cl_2 (λ_{ex} = 345 nm).

The fluoride binding constant of each chelate compound can be calculated using a simple mathematical model assuming a 1:1 binding model with fluoride. The binding constants with this isotherm can be calculated using the non-linear regression model previously used by Wylie and Macartney.[18] The model can be derived by:[19]

$$aL + bF^- \rightleftharpoons LF$$

Using this, the equilibrium can be stated as:

$$K = \frac{[LF]}{[L]^a[F]^b} \qquad \text{Equation 2.1}$$

In a 1:1 binding isotherm, the molar equivalents, a and b, are both 1 and can be ignored. In the mixture, the total concentration of each component can be calculated by:

$$[L]_t = [L] + [LF] \qquad \text{Equation 2.2}$$

$$[F]_t = [F] + [LF] \qquad \text{Equation 2.3}$$

Where $[L]_t$ and $[F]_t$ represent the total concentrations of the ligand and the fluoride ions. Substituting these terms into the equilibrium equation:

$$K = \frac{[LF]}{([L]_t - [LF])([F]_t - [LF])} \qquad \text{Equation 2.4}$$

Solving this for [LF]:

$$[LF] = \frac{\left([L]_t + [F]_t + \left(\frac{1}{K}\right)\right) \pm \sqrt{([L]_t + [F]_t + (\frac{1}{K}))^2 - 4[L]_t[F]_t}}{2} \qquad \text{Equation 2.5}$$

If

$$b = [L]_t + [F]_t + K^{-1} \qquad \text{Equation 2.6}$$

Then Equation 5 can be simplified to:

$$[LF] = \frac{b \pm \sqrt{b^2 - 4[L]_t[F]_t}}{2} \qquad \text{Equation 2.7}$$

In order to measure the changes in the concentration of each species, the titration was followed spectroscopically and the change in absorbance was measured. The change in absorbance can be predicted with:

$$\Delta A_{predicted} = \Delta A_{limiting}(\frac{[LF]}{[F]_t}) \qquad \text{Equation 2.8}$$

where $\Delta A_{limiting}$ is the limiting change in the absorbance intensity. In the binding isotherm, the binding constant (K) and the limiting change ($\Delta A_{limiting}$) are taken as floating values. When the plot of predicted change versus the fluoride concentration is compared to the observed absorbance change versus the fluoride concentration, the limiting change and the binding constant can be modeled. All of the binding constants of the 1:1 binding systems have been determined using this method. Figure 2.18 shows the plot of **1-BF$_2$** as the maximum absorbance decreases. **3-BF$_2$** and **4-BF$_2$** were followed by the low energy absorption band that increased with increasing fluoride and is pictured in Figure 2.19 and Figure 2.20, respectively. The dilution of the chelate compound by the addition of fluoride was accounted for in these calculations.

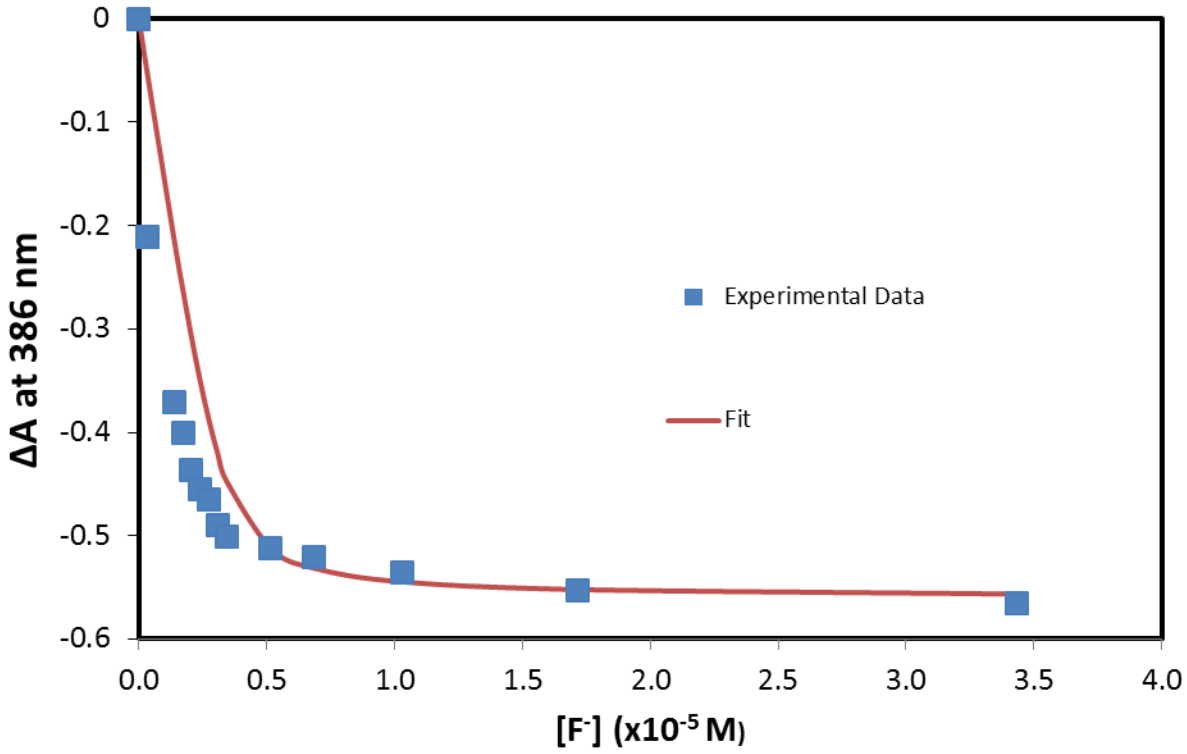

Figure 2.18 The change in absorbance plot at 386 nm and the fit (K = ~1.8 x 10^6 M^{-1}) for **1-BF$_2$** titration by TBAF at 298 K.

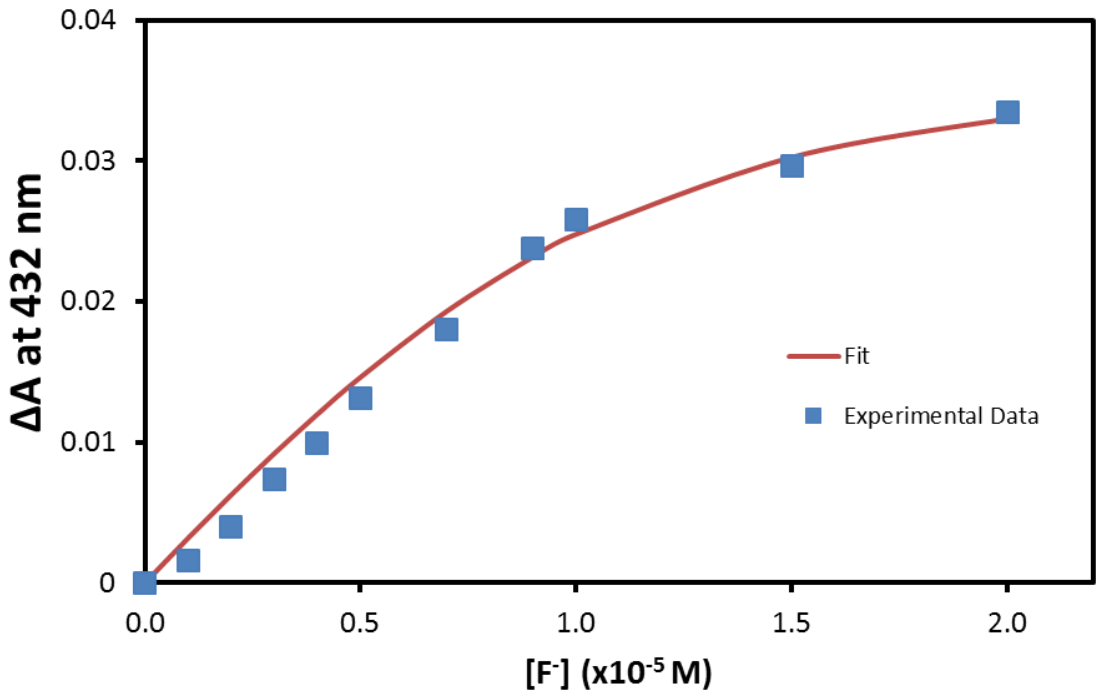

Figure 2.19 The change in absorbance plot at 432 nm and the fit (K = ~1.1 x 10^5 M^{-1}) for **3-BF_2** titration by TBAF at 298 K.

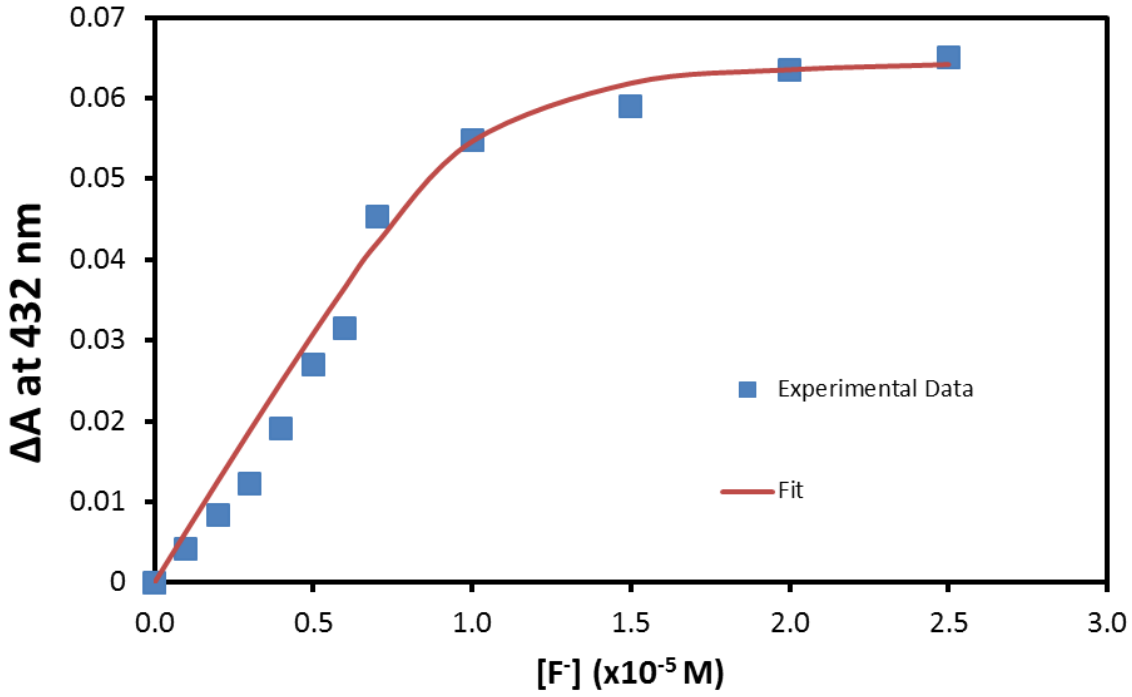

Figure 2.20 The change in absorbance plot at 432 nm and the fit (K = ~2.8 x 10^5 M^{-1}) for the titration of **4-BF_2** with TBAF at 298 K.

The absorption titration of **2-BF$_2$** shows significant changes at two wavelengths. As the first equivalent of fluoride is added, the absorption band at 397 nm decreases. Then, as more fluoride is added, the other absorption band at 430 nm increases. Because there are two triarylboron centers on **2-BF$_2$**, it is anticipated that this complex will participate in 1:2 binding with fluoride. To estimate the binding constant of each boron center the binding events were first isolated by selecting wavelengths where there was limited change occurring during the opposite binding event. For example, 460 nm was chosen because the spectrum exhibited large changes at this wavelength as the first equivalent of fluoride is added and only small fluctuations as the second equivalent is bound. Also, in order to fit only the 1:1 (or 2:1) binding, the data points that had a high certainty of containing both species were not included. It was determined that the binding constant for binding to the first fluoride ion is approximately 30 times stronger than that for the second fluoride ion. This deviates from statistical binding behavior[20] and implies that the binding of the first fluoride causes the second boron center to become less Lewis acidic for binding fluoride. Figure 2.21 shows the change in absorbance plot to estimate K_1 at 460 nm and Figure 2.22 shows the change in absorbance plot to estimate K_2 at 419 nm. A summary of the binding constants can be found in Table 2.5.

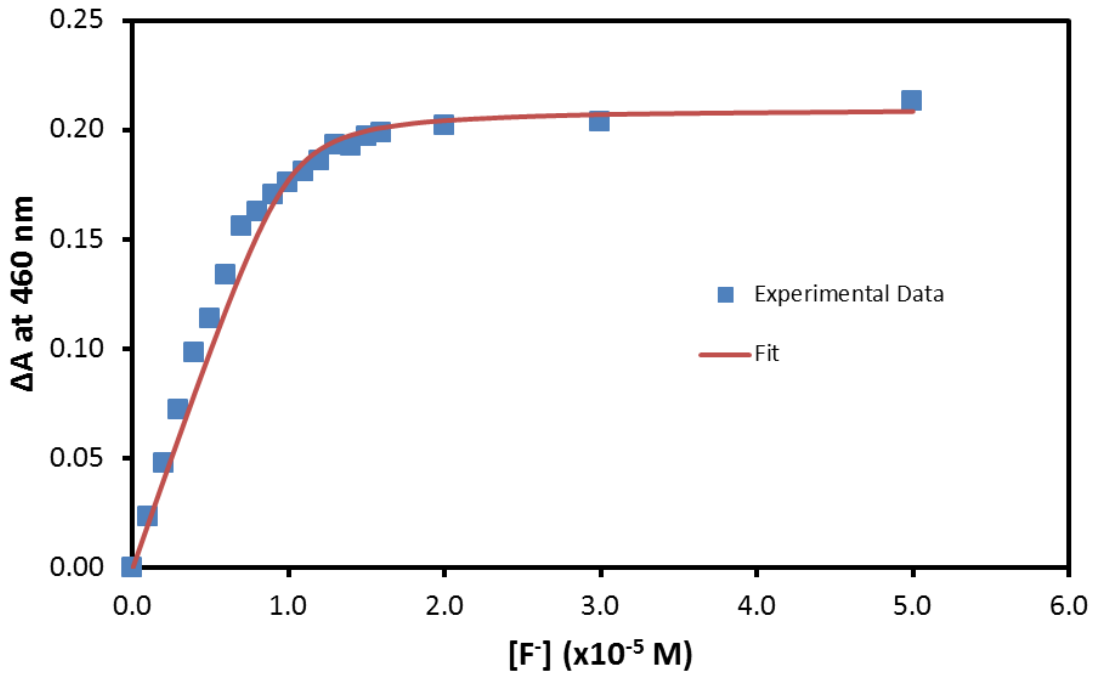

Figure 2.21 The change in absorbance plot at 460 nm and the fit (K_1 = ~3.5 x 10^6 M^{-1}) for the titration of **2-BF$_2$** with TBAF at 298 K.

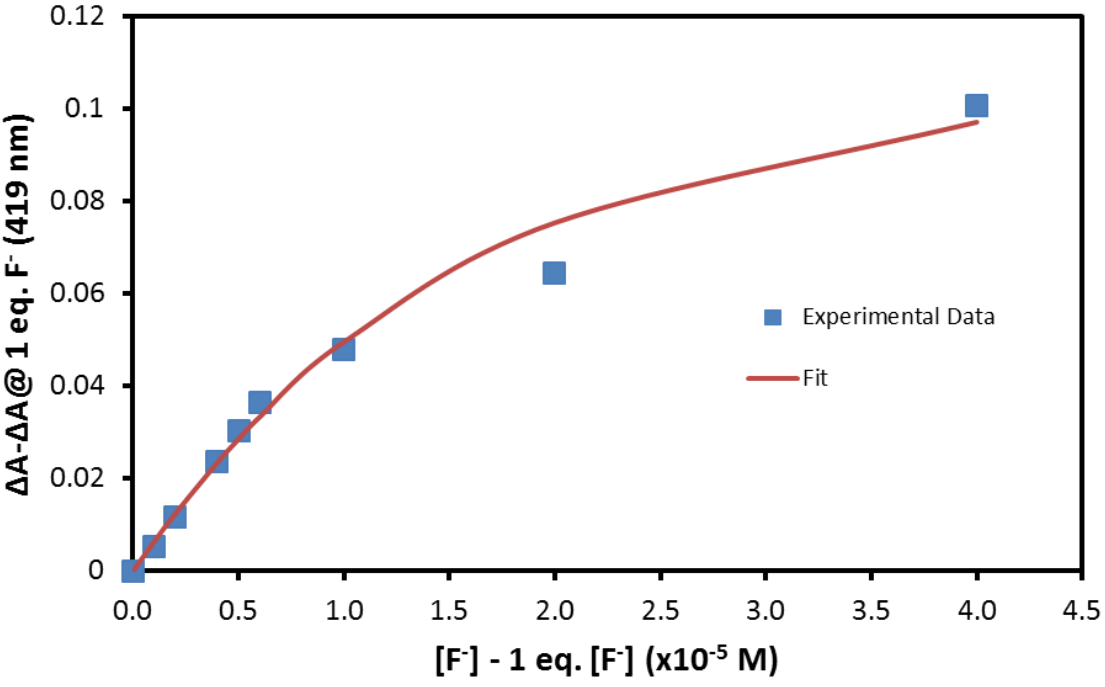

Figure 2.22 The change in absorbance plot at 419 nm and the fit (K_2 = ~1.1x 10^5 M^{-1}) for the titration of **2-BF$_2$** with TBAF at 298 K.

Table 2.5 Estimated binding constants of **1-BF_2**, **2-BF_2**, **3-BF_2**, and **4-BF_2**.

Compound	**Binding Constant (M^{-1})**
1-BF_2	1.8×10^6
2-BF_2	$K_1 = 3.5 \times 10^6$
	$K_2 = 1.1 \times 10^5$
3-BF_2	1.1×10^5
4-BF_2	2.8×10^6

The binding constants of the 1:1 binding chelates are approximately similar for all compounds, implying that the location of the triarylboron on the β-diketone does not influence the Lewis acidity of the complex. However, the binding of the second equivalent to **2-BF_2** is weaker. All these binding constants are similar to $B(Mes)_3$ (K = 3.3 (±0.3) x 10^5 M^{-1}),[21] Mes_2PhB (K = 5 x 10^6 M^{-1}),[22] and the initial studies done by Yamaguchi *et al.*(K = 2.8 (±0.3) x 10^5 M^{-1}).[23] It is, therefore, assumed that the B-F binding would be reversible upon addition of water. This has not been attempted experimentally. The titrations were not repeated three times and certain assumptions were made with regard to the binding behavior, especially for the 2:1 system. Therefore, these binding constants should be considered as estimated values.

2.4 Conclusions

Four triarylboron functionalized β-diketone ligands were synthesized and chelated with boron difluoride. Two of the ligands were substituted in the 1 and 3 positions (**1-BF_2** and **2-BF_2**) while the remaining two chelates were substituted in the *meso* position (**3-BF_2** and **4-BF_2**). **1-BF_2**, **2-BF_2**, and **3-BF_2** were studied crystallographically. The boron-phenyl unit in **1-BF_2** and **2-BF_2** was found to be coplanar with the 1,3-β-diketonate backbone while the boron-phenyl or boron-duryl unit in **3-BF_2** and **4-BF_2** was found to be twisted orthogonally to the backbone. This is in agreement to similar literature structures. Computational studies revealed that the HOMO-LUMO transition is the mesityl moieties performing a charge transfer to the β-diketonate backbone. TD-DFT results revealed the singlet and triplet energy levels and their major contributing orbitals.

The singlet and triplet states of **1-BF_2** and **2-BF_2** have a relatively lower energy due to the extended conjugation afforded by their planar structure, compared to **3-BF_2** and **4-BF_2**, which have higher singlet and triplet energies due to the disrupted conjugation between the aryl linker and the diketonato backbone. All four chelate complexes were studied for their photophysical properties and it was found that the chelate complexes followed the same trend as established by the computational data. The complexes have low fluorescent quantum efficiencies in solution; **1-BF_2** and **2-BF_2** have an improved quantum yield in the solid state but **3-BF_2** and **4-BF_2** have little emission in the solid state. Finally, all four complexes were investigated for their fluoride sensing ability. It was discovered that **1-BF_2** is a "turn-off" sensor because both its absorption band and fluorescence band decreases upon the addition of fluoride. **2-BF_2** experiences emission quenching while one absorption wavelength is quenched and another enhanced. **3-BF_2** and **4-BF_2** both show an increase in the absorption intensity when fluoride is added and a new, lower energy absorption peak evolves, which can be attributed to the [$BMes_2$(Ar)F] → diketonato backbone charge transfer. They also display an increase in emission intensity upon addition of fluoride. The fluoride binding constants of each chelate complex were also estimated. They were determined to be on the same order of magnitude as the previously reported triarylboron compounds reported.

2.5 References

(1) Chow, Y.L.; Johansson, C.I.; Zhang, Y-H.; Gautron, R.; Yang, L.;Rassat, A.; Yang, S-Z. *J. Phys. Org. Chem.* **1996,** *9*, 7.

(2) Chow, Y. L.; Ouyang, X. *Can. J. Chem.* **1991,** *69*, 423.

(3) (a) Padilha, L. A.; Webster, S.; Przhonska, O. V.; Hu, H.; Peceli, D.;Ensley, T. R.; Bondar, M. V.; Gerasov, A. O.; Kovtun, Y. P.; Shandura, M. P.; Kachkovski, A. D.; Hagan, D. J.; Stryland, E. W. V. *J. Phys. Chem. A.* **2010**, *114*, 6493. (b) Cogné-Laage, E.; Allemand, J.-F.; Ruel, O.; Baudin, J.-B.; Croquette, V.; Blanchard-Desce, M.; Jullien, L. *Chem. Eur. J.* **2004,** *10*, 1445.

(4) Zhang, G.; Chen, J.; Payne, S. J.; Kooi, S. E.; Demas, J. N.; Fraser, C. L. *J. Am. Chem. Soc.* **2007**, *129*, 8942.

(5) Liu, T.; Chien, A. D.; Lu, J.; Zhang, G.; Fraser, C. L. *J. Mater. Chem.* **2011**, *21*, 8401. (b) Zhang, G.; Lu, J. Sabat, M.; Fraser, C.L. *J. Am. Chem. Soc.* **2010,** *132*, 2160.

(6) Xu, S.; Evans, R.E.; Liu, T.; Zhang, G.; Demas, J.N.; Trindle, C.O.; Fraser, C.L. *Inorg. Chem.* **2013,** *52*, 3597.

(7) Sakai, A.; Tanaka, M.; Ohta, E.; Yoshimoto, Y.; Mizuno, K.; Ikeda, H. *Tetrahedron Lett.* **2012,** *53*, 4138.

(8) Hoffend, C.; Diefenbach, M.; Januszewski, E.; Bolte, M.; Lerner, H-W.; Holthausen, M.C.; Wagner, M. *Dalton Trans.* **2013,** *43*, 13826.

(9) Wade, C.R.; Broomsgrove, A. E. J.; Aldridge, S.; Gabbai, F.P. *Chem. Rev.* **2010**, *110*, 3958.

(10) Zhang, G.; Palmer, G.M.; Dewhirst, M.W.; Fraser, C.L. *Nat. Mater.* **2009,** *8*, 747.

(11) Kumar, R. G.; Thilagar, P. *Dalton Trans.* **2014**, *43*, 3871.

(12) Brouwer, A.M. *Pure Appl. Chem.* **2011,** *83*, 2213.

(13) Frisch, M. J.; Trucks, G. W.; Schlegel, H. B.; Scuseria, G. E.; Robb, M. A.; Cheeseman, J. R.; Scalmani, G.; Barone, V.; Mennucci, B.; Petersson, G. A.; Nakatsuji, H.; Caricato, M.; Li, X.; Hratchian, H. P.; Izmaylov, A. F.; Bloino, J.; Zheng, G.; Sonnenberg, J. L.; Hada, M.; Ehara, M.;

Toyota, K.; Fukuda, R.; Hasegawa, J.; Ishida, M.; Nakajima, T.; Honda, Y.; Kitao, O.; Nakai, H.; Vreven, T.; Montgomery, J. A.; Peralta, Jr. J. E.; Ogliaro, F.; Bearpark, M.; Heyd, J. J.; Brothers, E.; Kudin, K. N.; Staroverov, V. N.; Keith, T.; Kobayashi, R.; Normand, J.; Raghavachari, K.; Rendell, A.; Burant, J.C.; Iyengar, S. S.; Tomasi, J.; Cossi, M.; N. Rega, N.; Millam, J. M.; Klene, M.; Knox, J. E.; Cross, J. B.; Bakken, V.; Adamo, C.; Jaramillo, J.; Gomperts, R.; Stratmann, R. E.; Yazyev, O.; Austin, A.J.; Cammi, R.; Pomelli, C.; Ochterski, J. W.; Martin, R. L.; Morokuma, K.; Zakrzewski, V. G.; Voth, G. A.; Salvador, P.; Dannenberg, J. J.; Dapprich, S.; Daniels, A. D.; Farkas, O.; Foresman, J. B.; Ortiz, J. V.; Cioslowski, J.; Fox, D. J. Gaussian, Inc., Wallingford CT, 2010. Revision B.01.

(14) Blight, B.A.; Ko, S-B.; Lu, J-S.; Smith, L.F.; Wang, S. *Dalton Trans*. **2013**, *42*, 10089.

(15) Jia, W-L.; Bai, D-R.; McCormick, T.; Liu, Q-D.; Motala, M.; Wang, R-Y.; Seward, C.; Tao, Y.; Wang, S. *Chem. Eur. J.* **2004**, *10*, 994.

(16) Emsley, J.; Freeman, N. *J. Mol. Struct.***1989,** *196,* 249.

(17) Tanaka, M.; Ohta, E.; Sakai, A.; Yoshimoto, Y.; Mizuno, K.; Ikeda, H. *Tetrahedron Lett.* **2013,** *54,* 4380.

(18) (a) Wylie, R. S.; Macartney, D. H. *Inorg. Chem.* **1993**, *32*, 1830. (b) Connors, K. A. *Binding Constants. New York: John Wiley & Sons*, **1987**, 52.

(19) Hirose, K.; *J. Inclusion Phenom. Macrocyclic Chem.* **2001,** *39.* 193.

(20) Ercolani, G. *J. Am. Chem. Soc.* **2003,** *125*, 16097.

(21) Sole, S.; Gabbaı, F. P. *Chem. Commun.* **2004,** 1284.

(22) Huh, J. O.; Kim, H.; Lee, K. M.; Lee, Y. S.; Do, Y.; Lee, M. H. *Chem. Commun.* **2010,** 138.

(23) Yamaguchi, S.; Akiyama, S.; Tamao, A. *J. Am. Chem. Soc.* **2001,** *123,* 11372.

Chapter 3

Sensitization of Lanthanide Luminescence with Boron-Functionalized β-Diketonate Ligands

3.1 Introduction

The lanthanide metal ions have been extensively studied due to their intriguing photophysical properties. These properties include long excited state lifetimes, large Stoke's shifts, and extremely narrow emission bands.[1] Additionally, trivalent lanthanide complexes have optically pure emission colors that are unique to this group of metal ions. Unfortunately, the quantum yield of lanthanide luminescence is very low, due to the Laporte forbidden f→f transitions. In order to stimulate the emission, one must sensitize the f→f transitions by using the Absorption-Energy Transfer-Emission (AETE) mechanism. In the AETE mechanism, a ligand acts as an antenna to harvest energy followed by an intersystem crossing and an energy transfer to the metal ion. This can promote lanthanide emission by three orders of magnitude or more.[2] Unlike the phosphorescence of transition metal complexes, lanthanide emission is less sensitive to oxygen quenching[3] and as a result, luminescent lanthanide complexes have found many applications in ambient conditions such as lasers,[4] sensors,[5] counterfeiting tags,[6] electroluminescent devices,[7] and cellular imaging.[8]

It is very important in the AETE mechanism that the T_1 energy level of the chelating ligands is matched to that of the emissive state of the lanthanide ion. If the energy level is too low, no sensitization will be achieved. If the energy level is too high, other possible non-radiative transitions can occur. In order to tune these energy levels, many ligand systems were developed for lanthanide sensitization, as discussed in Chapter 1. Previous work in the Wang group has incorporated a triarylboron with a carboxylate binding site for Eu(III) and Tb(III).[9] Initial absorption of energy causes a $\pi \rightarrow \pi^*$ transition to the empty p_π orbital on boron which then

promotes energy transfer to the lanthanide. Scheme 3.1 shows the two ligand systems that were investigated previously. It was found that ligand **M1** was effective at sensitizing both Eu(III) and Tb(III), but **M2** was ineffective at sensitizing Tb(III) because its triplet state was too low. Unfortunately, the carboxylate ligands led to oligomer and aggregate formation instead of discrete molecules, which limit their applications.

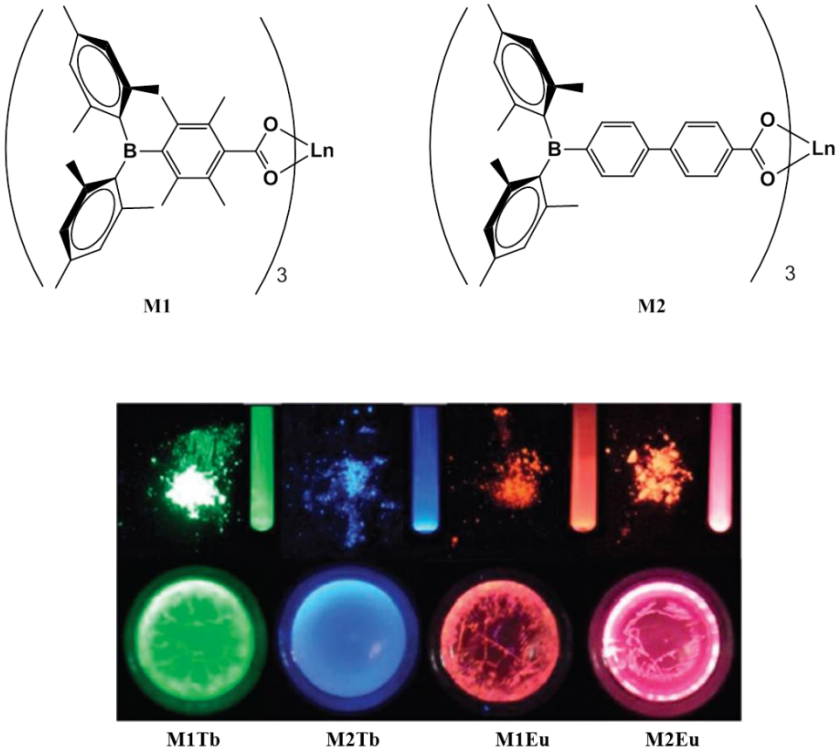

Scheme 3.1 Previous ligand systems developed by the Wang group for lanthanide ion sensitization.

In this chapter, in order to promote discrete molecule formation and further tuning of the triplet state energy, the four triarylboron functionalized β-diketone ligands described in Chapter 2 of this thesis were investigated for their triplet states by making complexes with gadolinium. Once the triplet energy levels were established, the complexes that were predicted to exhibit lanthanide emission sensitization were synthesized and their photophysical properties were investigated. The applications of the new lanthanide complexes in fluoride sensing were also investigated.

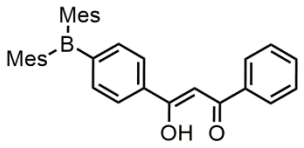

1

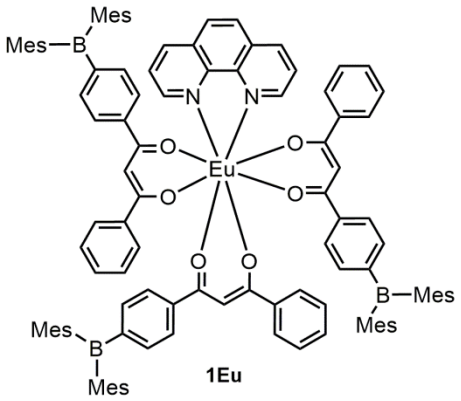

1Eu

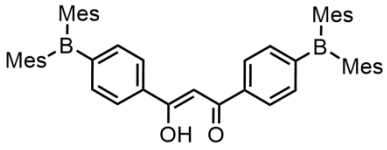

2

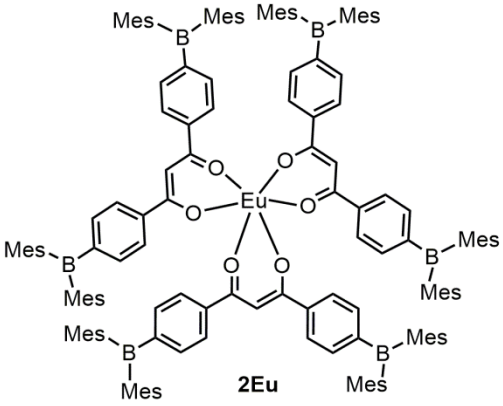

2Eu

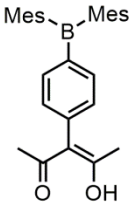

3

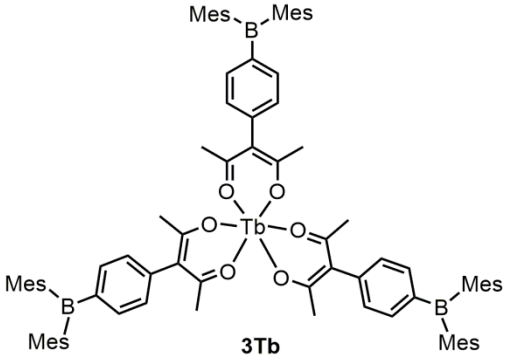

3Tb

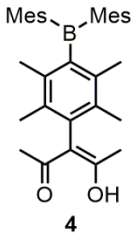

4

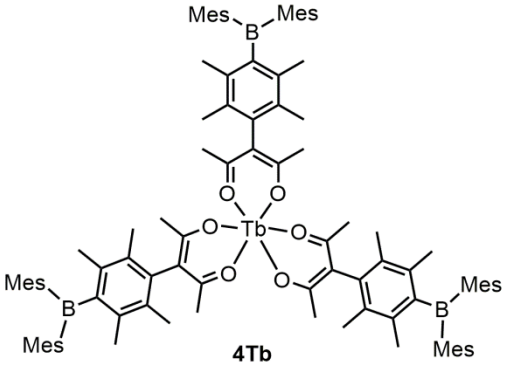

4Tb

Scheme 3.2 Ligands and lanthanide complexes investigated in this Chapter.

3.2 Experimental Section

3.2.1 General Procedures

Experimental techniques and instruments are similar to those described in Section 2.2. The syntheses of the ligands **1**, **2**, **3**, and **4** are described in Section 2.2. Cresyl Violet was used as quantum yield standard ($\Phi = 0.54$).[10] No crystals of the lanthanide complexes were obtained.

3.2.2 Synthesis of 1Eu

1Eu: In a 20 mL sample vial, **1** (48 mg, 0.10 mmol, 3 eq.) and 1,10-phenanthroline (6.0 mg, 0.033 mmol, 1 eq.) were suspended in 2 mL of ethanol and heated gently. 0.10 mL of 1 M NaOH (from a 1 M stock solution in H_2O, 3 eq.) was added, at which point the suspension dissolved and turned bright yellow. $EuCl_3 \bullet 6H_2O$ (12 mg, 0.033 mmol, 1 eq.) was dissolved in 1 mL of ethanol and this solution was added dropwise to the solution containing **1** and allowed to stir at room temperature for 10 minutes. A pale yellow precipitate formed very quickly. The reaction mixture was then stirred overnight, followed by a vacuum filtration to isolate the yellow solid, which was rinsed with distilled water and then ethanol. The yellow solid was further purified by dissolving in CH_2Cl_2, and precipitated from cold ethanol and filtered to produce a yellow powder in 62% yield (41 mg, 0.020 mmol). ^{1}H NMR (400 MHz, 298 K, $CDCl_3$): δ10.91 (d, J = 7.9 Hz, 2H), 10.49 (s, 2H), 9.85 (s, 2H), 8.90 (d, J = 7.9 Hz, 2H), 6.91-6.71 (m, 27H), 6.41 (s, 6H), 5.45 (s, 6H), 2.30 (s, 18H), 1.82 (s, 36H). ^{13}C NMR (100 MHz, 298 K, $CDCl_3$): δ 207.28, 150.05, 141.60, 140.69, 138.54, 132.25, 131.06, 128.04, 125.07, 124.78, 123.49, 116.63, 111.16, 109.77, 23.28, 21.18. Anal. Calc. for $C_{111}H_{104}B_3O_6N_2Eu$: C, 76.34; H, 6.00; N, 1.60; Found: C, 75.11; H, 5.84; N, 1.41. This can be attributed to 1.5 H_2O. Anal. Calc. for $C_{111}H_{107}B_3O_{7.5}N_2Eu$ ($[Eu(\mathbf{1})_3(phen)(H_2O)_{1.5}]$): C, 75.18; H, 6.08; N, 1.58.

3.2.3 Synthesis of 2Eu

2Eu: 50 mg of **2** (0.069 mmol, 3 eq.) was placed in a 20 mL vial and 6.3 mg 1,10-phenanthroline (0.023 mmol, 1 eq) and 6 mL absolute ethanol were added. Potassium t-butoxide (0.060 mL, 1 M

in THF, 3 eq.) was added dropwise to this suspension. To another 20 mL vial, 8.5 mg $EuCl_3 \cdot 6H_2O$ (0.023 mmol, 1 eq.) was dissolved in 4 mL of absolute ethanol. The Eu(III) solution was then added dropwise to the solution containing **2** and immediately a precipitate formed. The mixture was stirred overnight in a warm water bath. The mixture was filtered and washed with H_2O and ethanol. 32 mg of yellow powder was collected (58% yield). ^{1}H NMR (400 MHz, 298 K, $CDCl_3$): δ 6.76 (multiplet, 27H), 2.29 (s, 36H), 1.92 (s, 72H). Anal. Calc. for $C_{153}H_{179}B_6EuO_{16}$ ([Eu(**2**)$_3$(H_2O)$_{10}$]): C, 73.77; H, 7.24; found: C, 74.31; H, 6.74.

3.2.4 Synthesis of 3Tb

3Tb: 100 mg of **3** (0.24 mmol, 3 eq.) was placed in a 20 mL vial and 3 eq. of trioctylphosphine oxide (TOPO) (91 mg, 0.24 mmol) was added. These solids were suspended in 5 mL of ethanol. 0.24 mL of 1 M NaOH (3 eq. from a stock solution in H_2O) was added dropwise and the mixture was allowed to stir at room temperature until all solids were dissolved. To another 20 mL vial, 1 eq. of $TbCl_3 \bullet 6H_2O$ (29 mg, 0.082 mmol) was added and dissolved in 5 mL of ethanol. The Tb(III) solution was then added dropwise to the ligand solution and the mixture was stirred for three hours. Almost immediately, a white precipitate formed. The precipitate was filtered, dissolved in CH_2Cl_2 and washed with water. The product was then precipitated from CH_2Cl_2 with ethanol. 41 mg, 32% yield. Anal. Calc. for $C_{87}H_{112}B_3O_{14}Tb$. ([Tb(**3**)$_3$(H_2O)$_8$]): C, 66.42; H, 7.18 Found: C,66.50; H, 7.25.

3.2.5 Synthesis of 4Tb

4Tb: 100 mg of **4** (0.21 mmol, 3 eq.) was placed in a 20 mL vial and 3 eq. of TOPO (80 mg, 0.21 mmol) was added. These solids were suspended in 5 mL of ethanol. 1M NaOH (0.21 mL, 3 eq. from a stock solution in H_2O) was added dropwise and allowed to stir at room temperature until all solids were dissolved. To another 20 mL vial, 1eq. of $TbCl_3 \bullet 6H_2O$ (26 mg, 0.070 mmol) was added and dissolved in 5 mL of ethanol. The Tb(III) solution was then added dropwise to the solution containing **4** and the mixture was stirred for three hours. Almost immediately, a white

precipitate formed. The precipitate was filtered, dissolved in CH_2Cl_2 and washed with water. The product was then precipitated from CH_2Cl_2 with ethanol. 43 mg, 34% yield. Anal. Calc. for: $C_{99}H_{140}B_3O_{16}Tb$ ([Tb(**4**)$_3$(H_2O)$_{10}$]) : C, 66.89; H, 7.94 Found: C, 67.04; H, 7.51.

3.3 Results and Discussion

3.3.1 Synthesis

3.3.1.1 Synthesis of 1Eu and 2Eu

Both complexes **1Eu** and **2Eu** were synthesized similarly, as shown in Scheme 3.3, following the synthesis as described by Melby *et. al.*[11] By mixing ligand **1** or **2** from Chapter 2, 1,10-phenanthroline (phen), and $EuCl_3$•$6H_2O$, complexes in ethanol were immediately formed at 298 K and a yellow precipitate was observed. The complex was collected by filtration from ethanol. The NMR spectrum and elemental analyses showed that **1Eu** also had 1.5 equivalents of water. They also revealed that **2Eu** did not contain 1,10-phenanthroline, possibly because ligand **2** is too large, and as a consequence, the extra coordination sites are occupied by H_2O molecules.

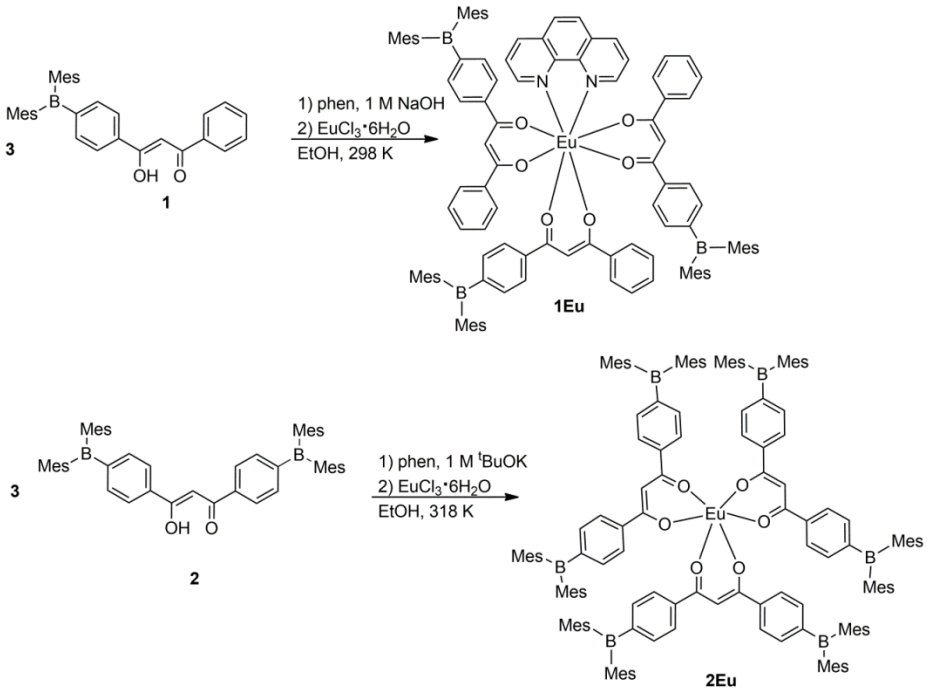

Scheme 3.3 Synthetic scheme for the complexes **1Eu** and **2Eu.**

3.3.1.2 Synthesis of 3Tb and 4Tb

The complexes **3Tb** and **4Tb** were identically synthesized, as seen in Scheme 3.4. Using ligand **3** or **4** from Chapter 2, TOPO, and $TbCl_3 \bullet 6H_2O$ and mixing in ethanol, a white precipitate immediately formed. The precipitate was collected, dissolved in CH_2Cl_2, and reprecipitated from ethanol. In order to sensitize the emission of Tb(III), the triplet state of the surrounding ligands needs to be ~3000 cm^{-1} above the $^5D_4$ state.[12] Therefore, chelating ligands such as 1,10-phenanthroline and 2,2'-bipyridine are unsuitable to be used as ancillary ligands.[13] In order to saturate the coordination sphere a large excess of TOPO was added in the synthesis of **3Tb** and **4Tb**. However, the characterization data revealed that TOPO was not present on either complex and the open coordination sites were occupied by water.

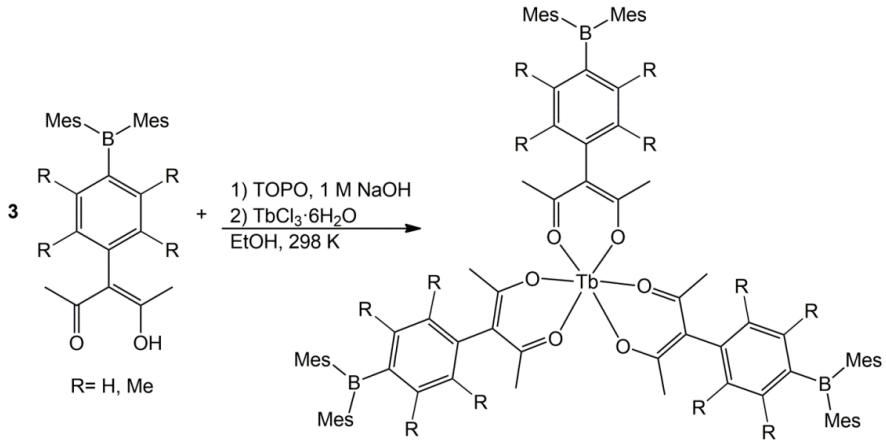

Scheme 3.4 Synthetic scheme for the complexes **3Tb** and **4Tb.**

3.3.2 Sensitization of Lanthanide Luminescence

Using the ligands from Chapter 2 of this thesis, complexes of europium and terbium were synthesized. In order to determine which compounds would be important to synthesize, the triplet state of each ligand was investigated by making a gadolinium complex. Gd(III) was used because it has a very high energy accepting state, hence cannot be sensitized by the same ligands that

would affect Eu(III) and Tb(III).[14] Due to the heavy atom effect and the paramagnetism of Gd(III), there is strong singlet-triplet state mixing which promotes the ligand's phosphorescence.[15] In order to measure the triplet state, the complexes were made similarly to the Eu(III) and Tb(III) complexes described in Section 3.2, however no ancillary ligand was added. This was to ensure that the phosphorescence was from the sensitizing ligands. The emission spectrum was then recorded at 77 K in CH_2Cl_2 using a time-resolved phosphorimeter and the T_1 energy was estimated using the edge of the emission spectrum (Figure 3.1). The triplet state energies of the Gd(III) complexes are summarized in Table 3.1.

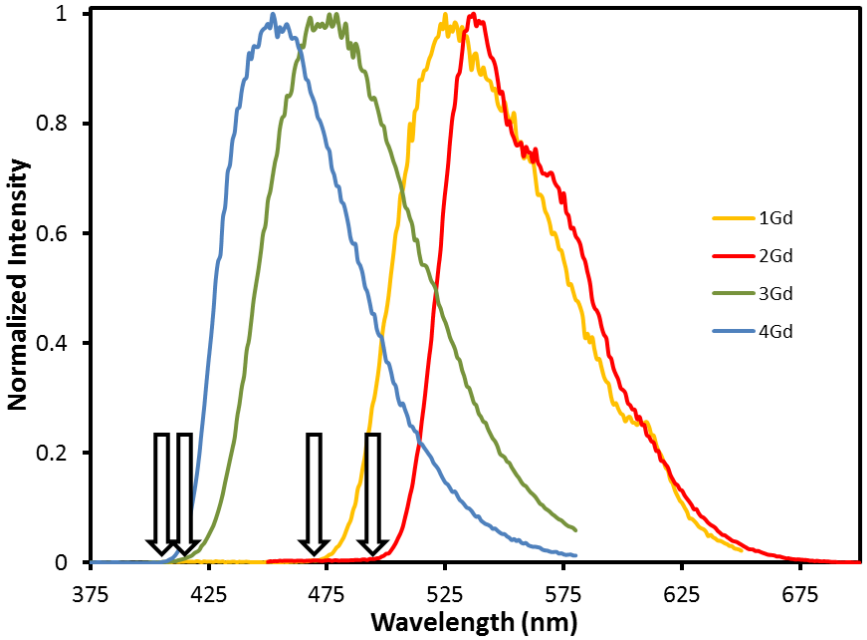

Figure 3.1 The emission spectra of the L_3Gd Complexes at 77 K in CH_2Cl_2 (λ_{ex}=360 nm for 1Gd, λ_{ex} = 397 nm for 2Gd, λ_{ex}=306 nm for 3Gd, λ_{ex}=310 nm for 4Gd)

Table 3.1 The triplet energy levels of the L_3Gd complexes.

Complex	**λ_{edge} (nm)/ (cm^{-1})**	**λ_{max} (nm)/(cm^{-1})**
1Gd	480/20800	525/19100
2Gd	505/19100	540/18500
3Gd	430/23300	470/21300
4Gd	410/24400	450/22200

These triplet energies agree with the TD-DFT calculated triplet energies in Chapter 2 with the exception that the experimental triplet energy for **3** is lower than that of **4**. This could be explained by examining the structure of **4**, which displays greater steric strain and is completely orthogonal with respect to the 1,3 diketonato backbone. These factors increase the energy of the triplet state. With this information, a comparison of these energy levels with the known energy levels of the Eu(III) and Tb(III) emissive states[15] can be made. A visualization of this can be found in Figure 3.2.

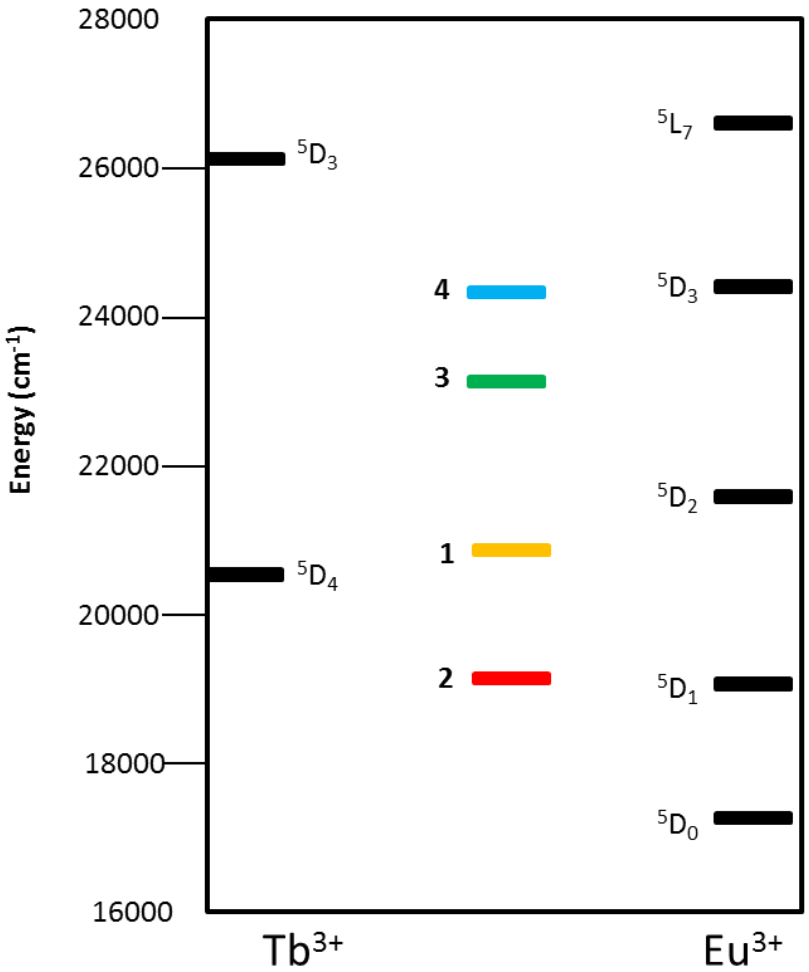

Figure 3.2 Energy level comparison of ligands' triplet state and Tb(III) or Eu(III) emissive/accepting state.

From this diagram, it is clear which ligand will sensitize which metal ion. **1** and **2** have triplet energies that are similar to or below that of the Tb(III) emissive state of $^5D_4$ (20500 cm^{-1})[15] making them unsuitable for terbium sensitization. In the case of Eu(III), however, the triplet states are above both the emissive state of $^5D_0$ (17250 cm^{-1}) and the accepting state of $^5D_1$ (19000 cm^{-1}). A study by Latva *et al*.[12] suggests that the optimum triplet state energy level for Eu(III) sensitization is ~19700 cm^{-1}, which is between the triplet states of ligands **1** and **2**. Therefore, despite the fact that the triplet energy of **1** and **2** is above the accepting energy level for Eu(III) sensitization, the luminescent quantum yields of their Eu(III) complexes are expected to be low. The triplet state energy of ligands **3** and **4** is higher than that of the $^5D_4$ of Tb(III), and therefore, they are expected to be able to sensitize Tb(III). In order to effectively sensitize Tb(III), however, the triplet state must be ~3000 cm^{-1} above the emissive state energy level.[12] This indicates that **4** is expected to have a higher sensitization effect than **3**. Both ligand **3** and **4**'s triplet states are above the Eu(III) $^5D_2$ state, and therefore are expected to be not very effective in sensitizing Eu(III) emission. Experimentally, it was observed that ligand **1** and **2** were effective at sensitizing only Eu(III) while **3** has only a very weak sensitization effect for Eu(III) sensitization effect. Both **3** and **4** were capable of sensitizing Tb(III) emission.

3.3.3 Absorption and Luminescent Properties

The photophysical properties of each complex were examined by UV-Vis and fluorescence /phosphorescence spectrometers. In each case, a solution of 1.0 x 10^{-5} M in THF was prepared in a quartz cuvette. The UV-visible spectrum and the emission spectrum of each complex were recorded. Also, a 20wt % doped PMMA film was prepared for each complex by spin-casting in order to measure the solid state emission. Figure 3.3 shows the normalized absorption, emission, and solid state emission for **1Eu.** The major absorption wavelength at 370 nm aligns with the absorption of the free ligand **1**, as shown in Chapter 2. In the solid state, the complex displays a bright red emission with $\Phi_{\mathbf{1Eu}}$= 0.13. The emission bands of **1Eu** at 579 nm, 587 nm, 612 nm, 645

nm correspond to the transitions $^5D_1 \rightarrow {}^7F_n$ where n= 0, 1, 2, and 3 respectively.[13] However, in solution, **1Eu** emits weakly (where $\Phi_{\mathbf{1Eu}}$= 0.01). This can be attributed to interactions with solvent molecules. Nonetheless, the energy transfer to the Eu(III) acceptor state seems to be efficient because the ligand emission at 420 nm is weak in solution and not detected in the solid state.

The absorption and emission spectra of **2Eu** are shown in Figure 3.4. Similarly to **1Eu**, the major absorption band of **2Eu** is from the ligand **2**. In THF, the emission is much weaker, $\Phi_{\mathbf{2Eu}} < 0.01$ and some ligand-based emission is present at 438 nm. The same is true for the solid state emission where $\Phi_{\mathbf{2Eu}}$ = 0.07. The presence of the ligand emission peak indicates that the energy transfer from ligand **2** to Eu(III) is inefficient.

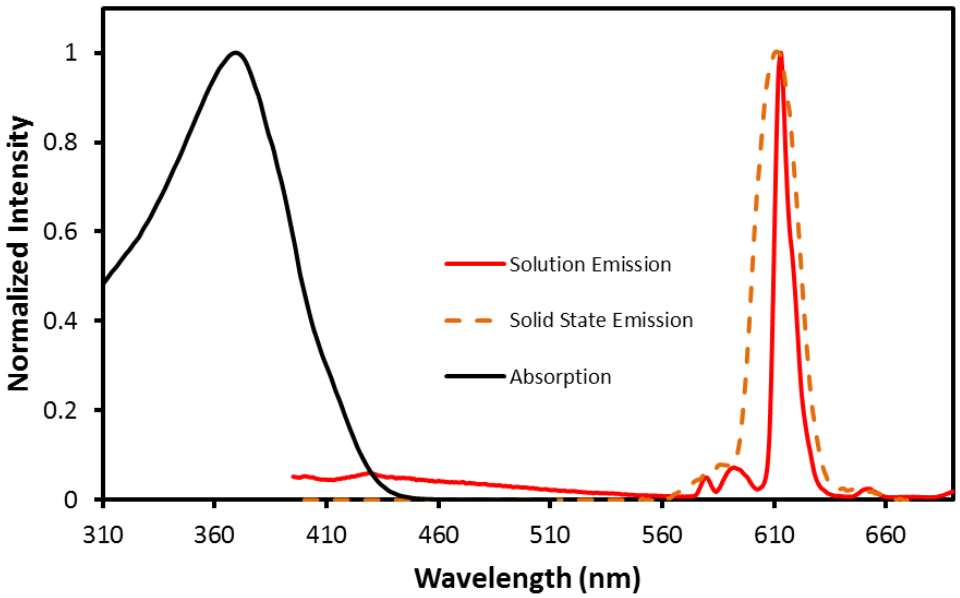

Figure 3.3 The normalized absorption and emission spectra for **1Eu** at 298 K in THF (λ_{ex} =360 nm).

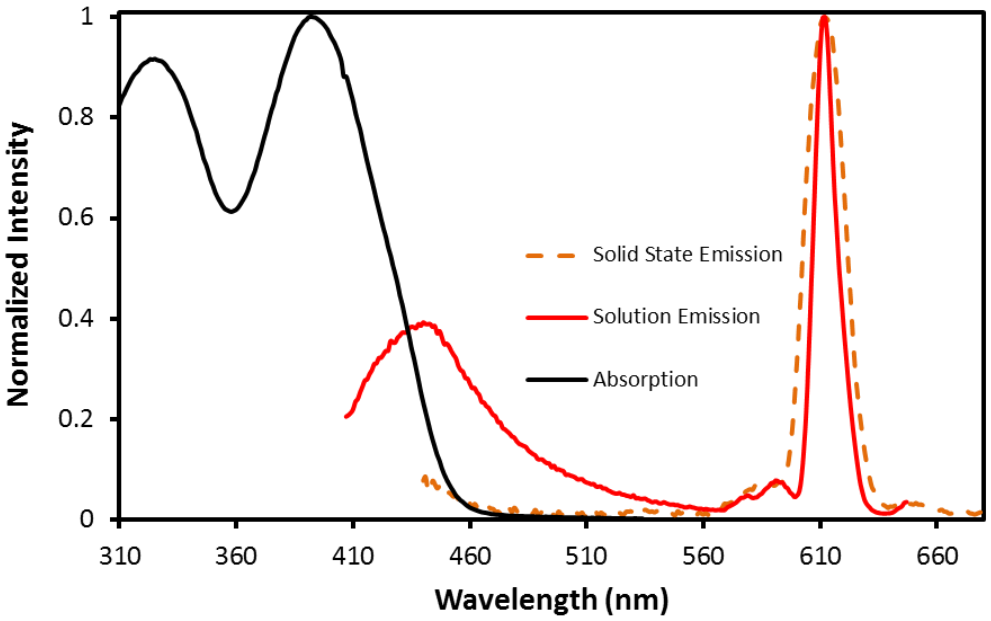

Figure 3.4 The normalized absorption and emission spectra of **2Eu** at 298 K in THF (λ_{ex} =397 nm).

While the complex **3Eu** was synthesized, it was not studied, or characterized, in detail due to the poor low emission intensity of the Eu(III) center (Figure 3.5). Most of the emission of **3Eu** is ligand-centered. This can be explained because the triplet state is more than 6000 cm^{-1} above the emissive state of Eu(III), which is well known to cause Φ_{Eu} to decrease.[12]

On the other hand, **3Tb** displayed a bright green terbium-based emission, although there was still a large amount of ligand character to the emission profile (Figure 3.6). Again, the absorption band can be attributed to the ligand's absorption. The quantum efficiency of 3Tb in THF was found to be $\Phi_{\mathbf{total}} = 0.16$ with $\Phi_{Tb} = 0.03$. This shows that the energy transfer from ligand to lanthanide in solution is poor in solution. However, in the solid state the emission of **3Tb** is much more efficient, with no ligand contribution to the emission, and a moderate quantum yield of $\Phi_{\mathbf{3Tb}} = 0.31$. The complex **4Eu** was synthesized but was found to have no Eu(III)-based emission, hence it was not further studied or characterized.

The complex **4Tb** was found to have an impressive bright green emission with only minor ligand contributions in the emission spectrum (Figure 3.7). The absorption is from the ligand **4**, but the emission is mostly Tb(III) based. In THF, the Tb(III) emission has a moderate efficiency with $\Phi_{total} = 0.17$ and $\Phi_{Tb} = 0.14$. There is no ligand contribution to the emission spectrum of **4Tb** in the solid state and the quantum yield is improved to $\Phi_{\mathbf{4Tb}} = 0.47$. This confirms that the energy transfer is much more efficient in this complex, as the ligand triplet state energy of **4** is higher than that of **3** in **3Tb.**

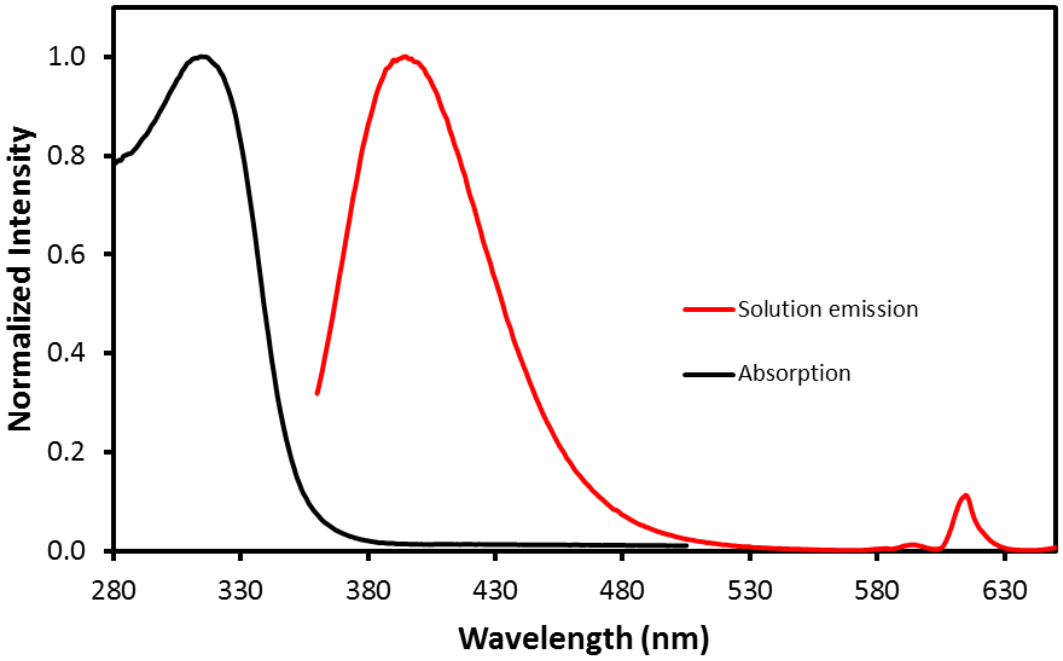

Figure 3.5 The normalized absorption and emission spectra of **3Eu** in THF at 298 K (λ_{ex} = 316 nm).

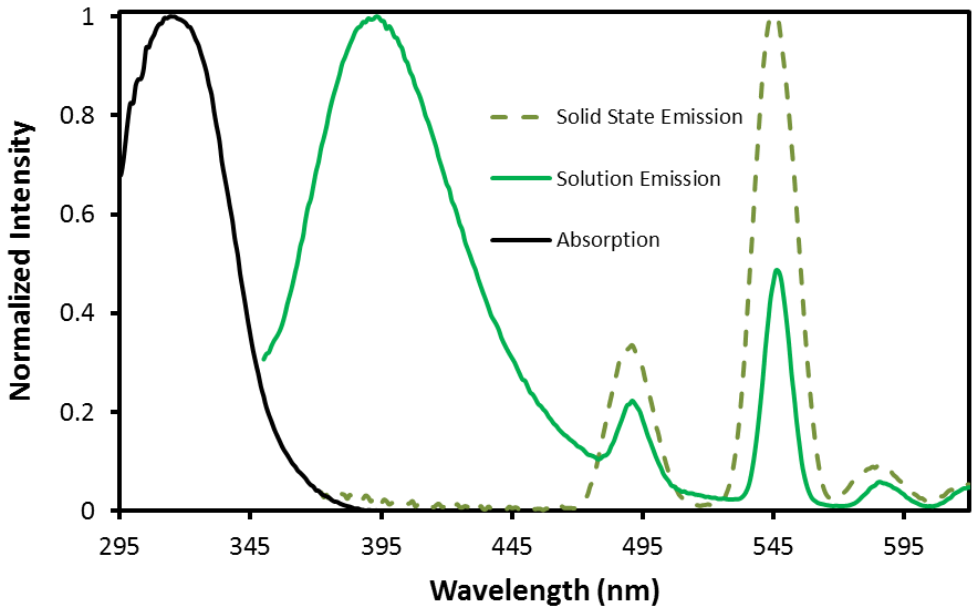

Figure 3.6 The normalized absorption and emission spectra of **3Tb** at 298 K in THF (λ_{ex} = 306 nm).

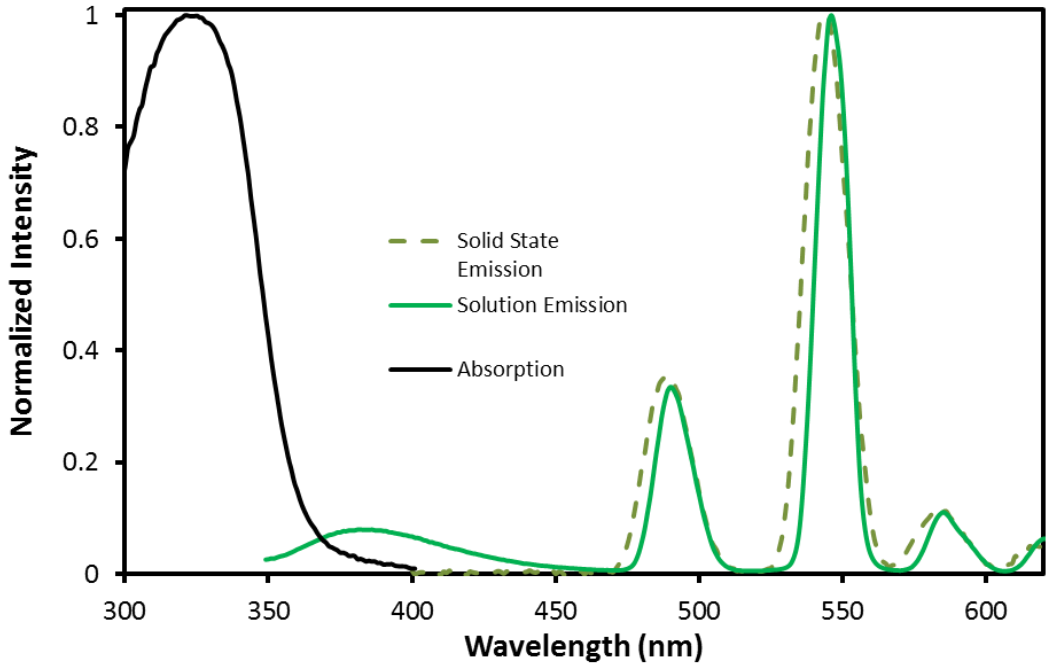

Figure 3.7 The normalized absorption and emission spectra of **4Tb** at 298 K in THF (λ_{ex} = 306 nm).

The low emission quantum efficiency of **3Tb** and **4Tb** in solution could be explained by the dynamic dissociation/association of the water and solvent molecules around the Tb(III) center. Photographs in Figure 3.8 show the emission color and the relative brightness of **1Eu**, **2Eu**, **3Tb** and **4Tb** in solution and solid state.

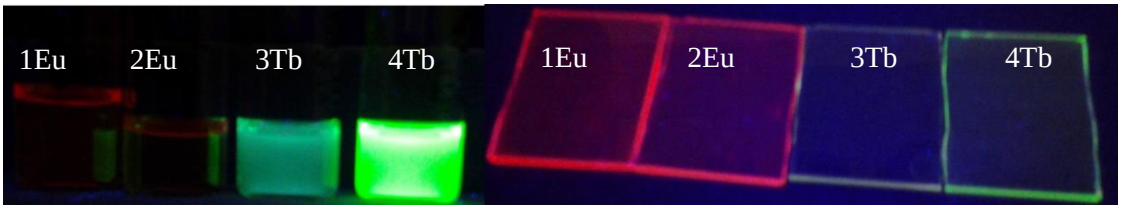

Figure 3.8 The emission colors of **1Eu**, **2Eu**, **3Tb**, and **4Tb** (~1.0 x 10^{-4} M) in THF and in 20% wt PMMA films.

The intra-ligand charge transfer involving the $BMes_2$ unit in **3** and **4** was found to play a key role in Tb(III) sensitization because a model *meso*-duryl-acac ligand, lacking the $BMes_2$ unit, was found to be ineffective in Tb(III) sensitization (Figure 3.9).

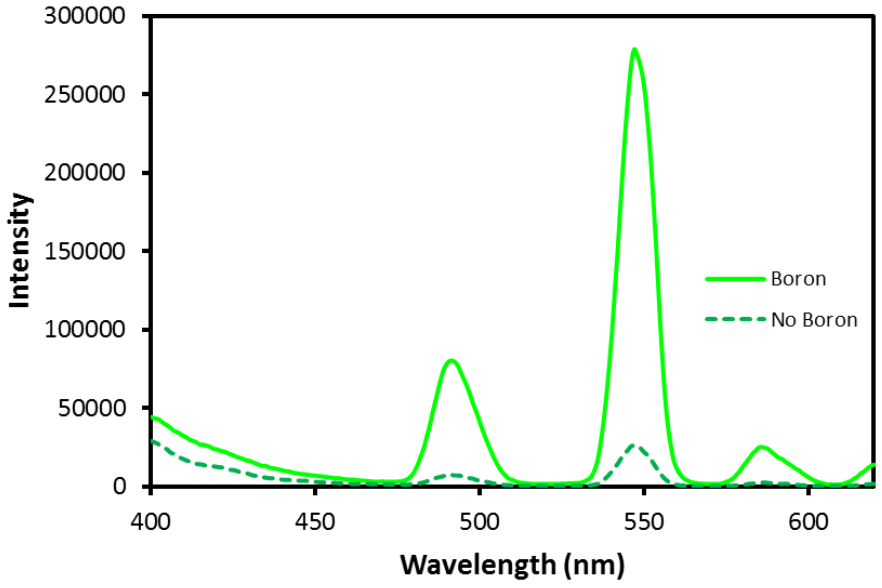

Figure 3.9 The emission spectra of **4Tb** and a model *meso*-duryl-acac Tb(III) complex (λ_{ex} = 323 nm, 298 K, THF).

3.3.4 Emission Lifetimes

One of the key features of lanthanide emission is their long excited state lifetimes. In order to determine the lifetimes of the complexes, they were dissolved in 2-Me-THF, cooled to 77 K, and their emission spectra were recorded. The decay lifetime of the lanthanide emission peak with the highest intensity was then determined using a fit curve that follows:

$$I(t) = I_0 e^{-\frac{t}{\tau}} \qquad \text{Equation 3.1}$$

Where I_0 is the intensity upon excitation, t is time, and τ is the lifetime. The lifetime was calculated using a macro on the Photon Technology International Phosphorescent lifetime spectrometer, Timemaster C-631F equipped with a xenon flash lamp and a digital emission photon multiplier tube for both excitation and emission.

The low temperature emission spectrum of **1Eu** contains no ligand fluorescence and has very little contributions from the $^5D_1 \rightarrow {}^7F_0$ and $^5D_1 \rightarrow {}^7F_3$ transitions, as shown in Figure 3.10. The decay lifetime was determined for the emission at 612 nm for **1Eu** and **2Eu**. The decay and fit curve is shown in Figure 3.11. Similarly, **2Eu** had minor contributions from the $^5D_1 \rightarrow {}^7F_0$, $^5D_1 \rightarrow {}^7F_1$, and $^5D_1 \rightarrow {}^7F_3$ transitions (Figure 3.12) and its decay and fit curve is shown in Figure 3.13. The low temperature emission spectrum of **3Tb** shows the major transitions $^5D_4 \rightarrow {}^7F_6$, $^5D_1 \rightarrow {}^7F_5$, and $^5D_1 \rightarrow {}^7F_4$ are present (Figure 3.14). The decay lifetime was determined for the emission peak at 547 nm (Figure 3.15). Finally, the low temperature emission spectrum of **4Tb** shows the transitions $^5D_4 \rightarrow {}^7F_6$, $^5D_1 \rightarrow {}^7F_5$, and $^5D_1 \rightarrow {}^7F_4$ with minor contributions from the $^5D_1 \rightarrow {}^7F_3$ (Figure 3.16). The decay lifetime was determined for the emission of 547 nm (Figure 3.17). All of the decay lifetimes are on the order of 0.1 ms, which is typical of lanthanide lifetimes.[13] All of the photophysical data are summarized in Table 3.2.

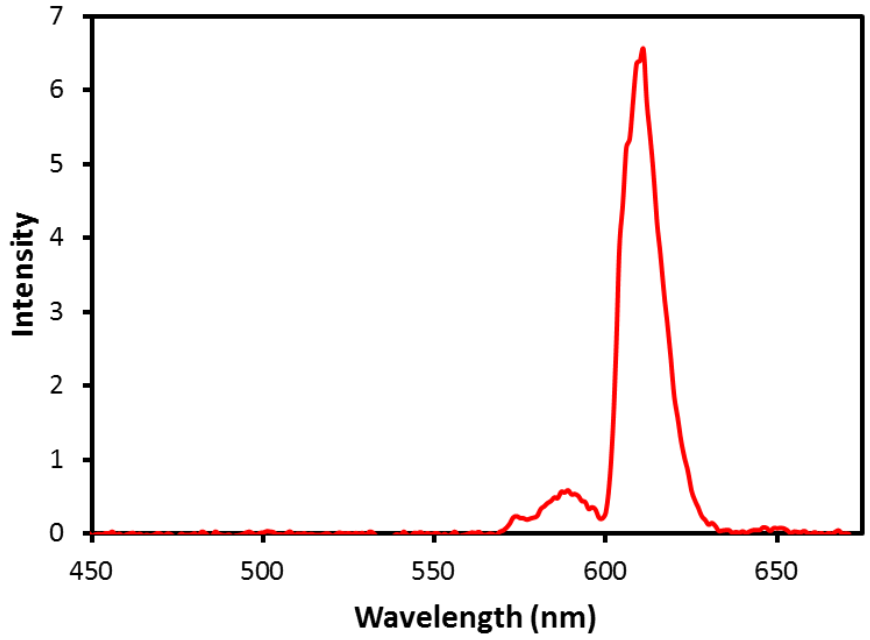

Figure 3.10 The emission spectrum of **1Eu** in 2-Me-THF at 77 K (λ_{ex}= 380 nm).

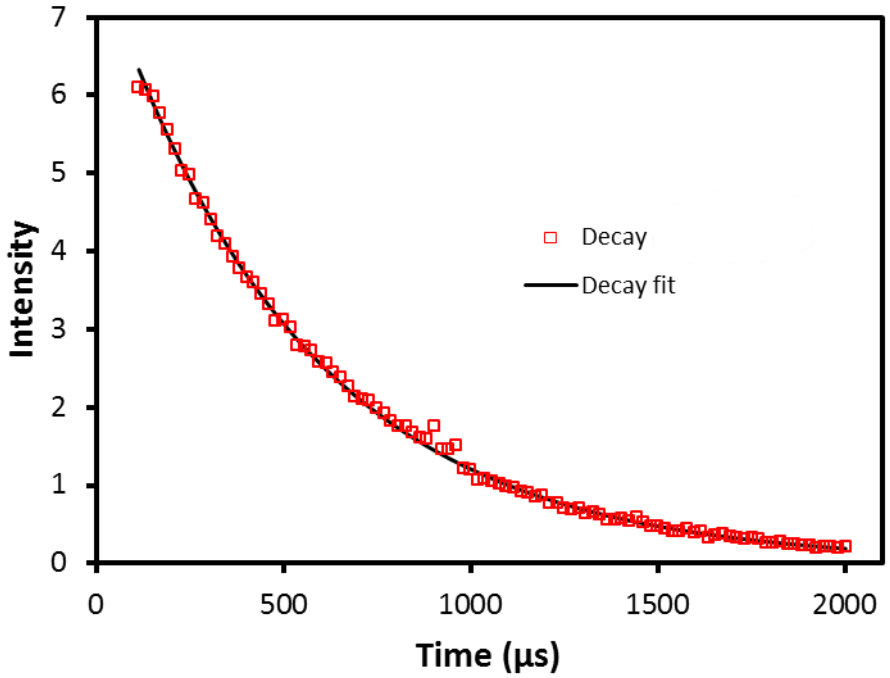

Figure 3.11 The emission decay curve of the 612 nm peak of **1Eu** in 2-Me-THF at 77 K and its fitting curve. The decay lifetime was determined to be 534 µs (λ_{ex} = 380 nm).

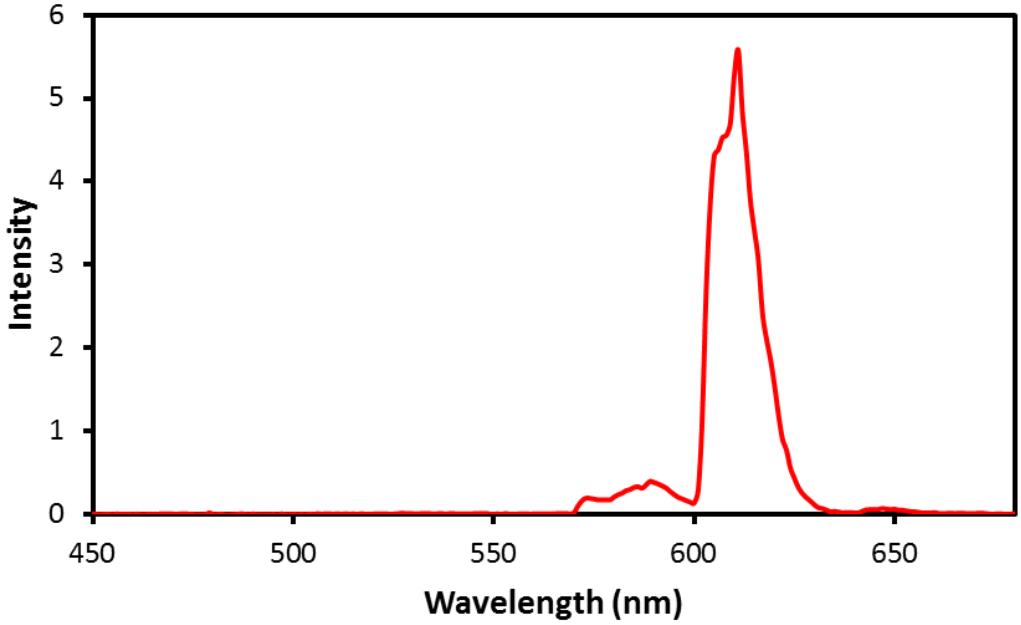

Figure 3.12 The emission spectrum of **2Eu** in 2-Me-THF at 77 K (λ_{ex}=397 nm).

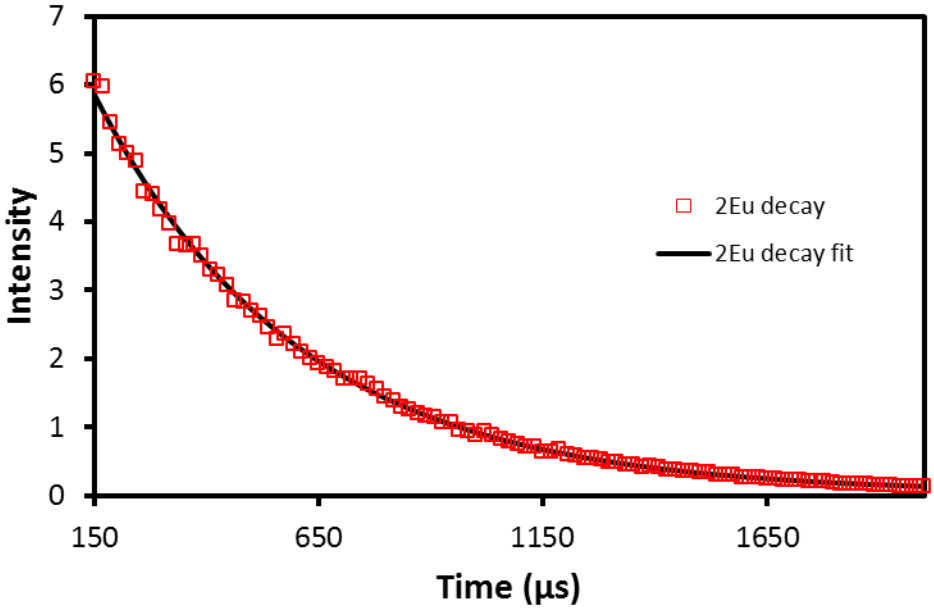

Figure 3.13 The emission decay diagram of **2Eu** in 2-Me-THF (λ_{ex}= 395 nm) and the fit curve at 77 K. The lifetime was determined to be 452 µs.

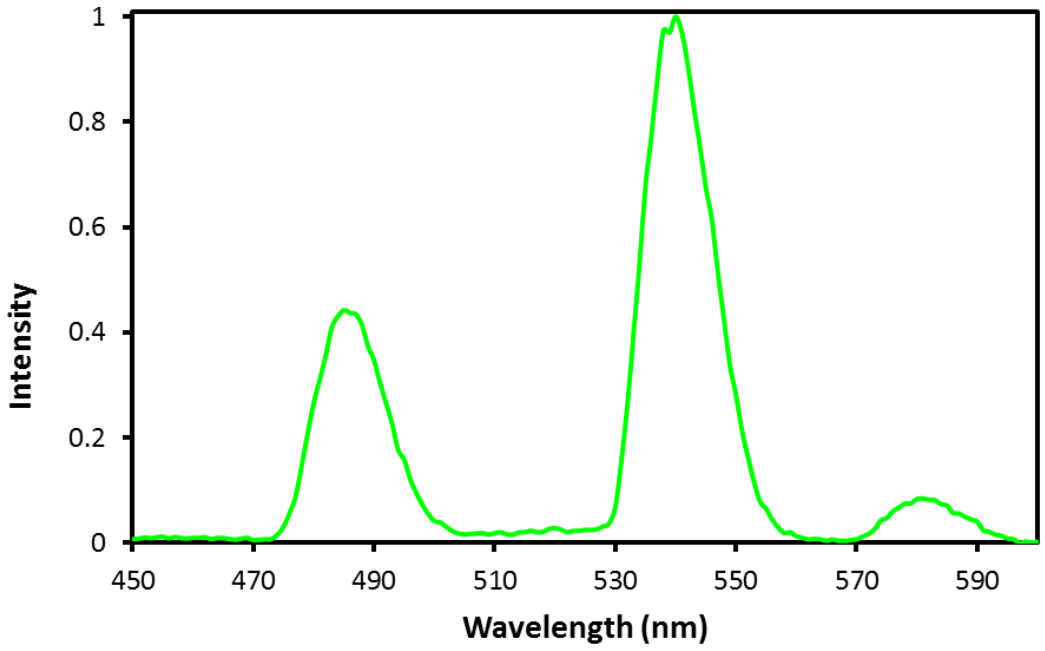

Figure 3.14 The emission spectrum of **3Tb** in 2-Me-THF at 77 K (λ_{ex}= 323 nm).

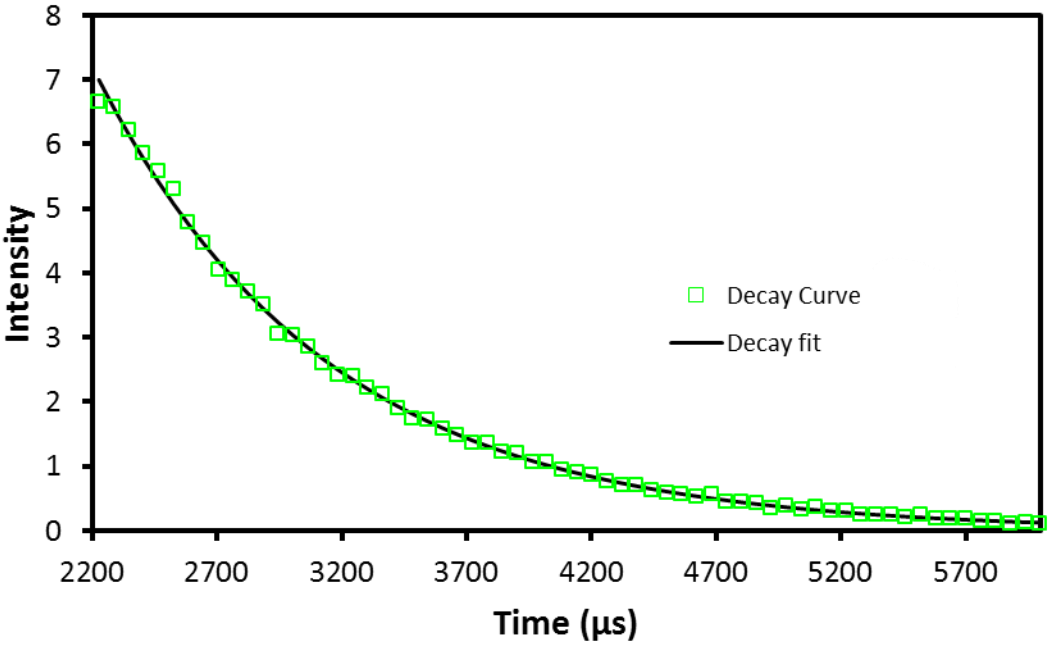

Figure 3.15 The emission decay diagram of the 547 nm peak (λ_{ex}= 323 nm) of **3Tb** in 2-Me-THF at 77 K and its fitting curve. The decay lifetime was determined to be 920 µs.

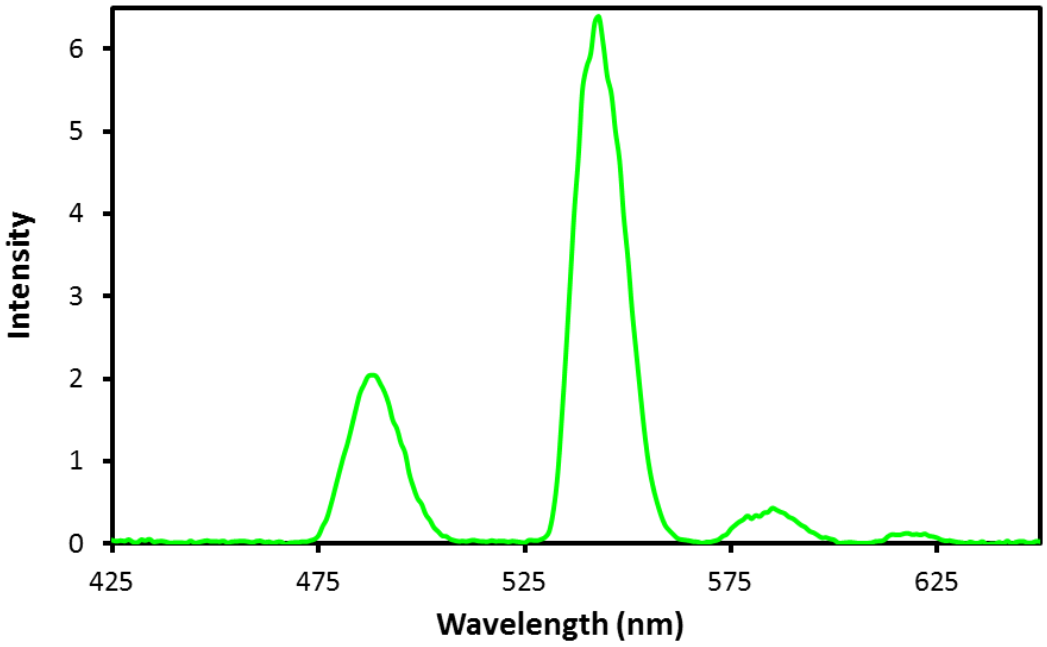

Figure 3.16 The emission spectrum of **4Tb** in 2-Me-THF at 77 K (λ_{ex}= 330 nm).

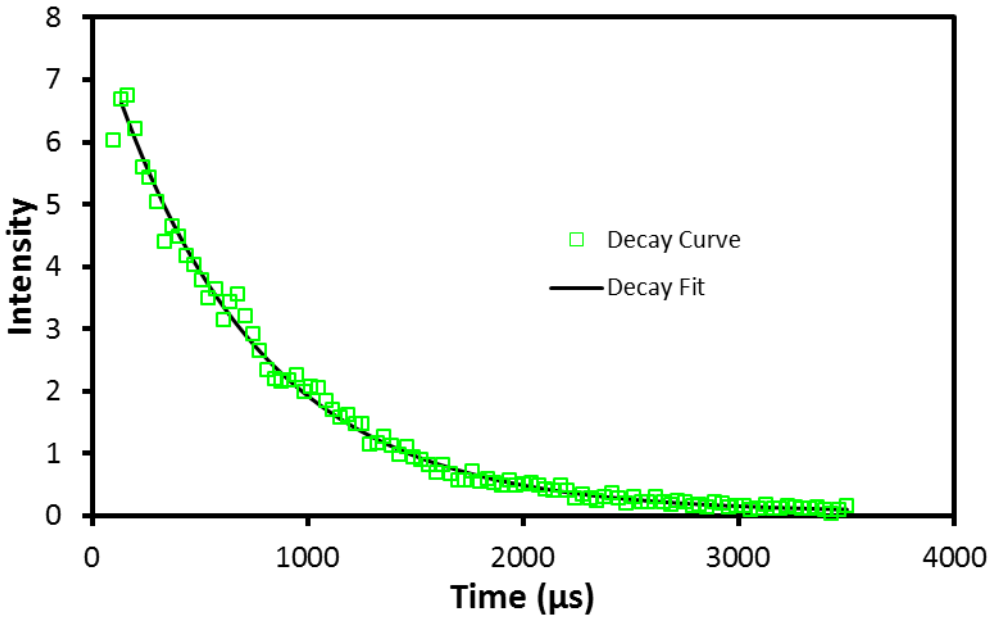

Figure 3.17 The emission decay diagram of the 547 nm peak of **4Tb** in 2-Me-THF at 77 K and its fitting curve. The decay lifetime was determined to be 688 µs (λ_{ex} = 330 nm).

Table 3.2 The photophysical properties of **1Eu**, **2Eu**, **3Tb**, and **4Tb**.

Compound	$\lambda_{ab,}$ (nm) (ε x 10^4 $M^{-1}cm^{-1}$)[a]	Emission Maxima (nm)	Φ_{Ln} [b] (Φ_{ss})[c]	Emission decay lifetime (μs) at 77 K
1Eu	370 (6.1)	425, 612	0.01 (0.13)	534
2Eu	325 (6.1) 390 (6.7)	440, 612	0.006 (0.07)	452
3Tb	316 (1.6)	393,488,546, 583	0.03 (0.31)	920
4Tb	323 (2.3)	489,546,583, 617	0.14 (0.47)	688

[a]Recorded in THF at 1.0 x 10^{-5} M
[b]Determined in THF vs cresyl violet in methanol (Φ = 0.54)[10]
[c]Determined using an integration sphere in a 20% w/w film in PMMA

3.3.5 Fluoride Sensing

In order to determine the fluoride sensing ability of the lanthanide complexes, a 3.0 mL portion of a 1.0 x 10^{-5} M solution in THF was added to a quartz cuvette and degassed. To this was added a solution of tetrabutylammonium fluoride (TBAF), such that 1 μL was 0.1 equivalents, and the absorption and emission spectral response was recorded. The complex's fluorescence response toward fluoride ions were examined in the same manner as described in Chapter 2 using their BF_2 complexes (Section 2.3). However, no attempt to measure the effect of fluoride on the triplet state was made in Chapter 2. To understand the impact of fluoride ions on the emission of lanthanide ions in complexes **1Eu**, **2Eu**, **3Tb** and **4Tb**, the gadolinium complexes were titrated with fluoride ions and the phosphorescence spectral change at 77 K was recorded and the data are shown in Figure 3.18 to Figure 3.21, respectively). As fluoride is added to the complex, the low temperature emission peak shifts to a shorter wavelength for **1Gd** and **2Gd** ($\Delta\lambda_{\mathbf{1Gd}}$ = 20 nm and $\Delta\lambda_{\mathbf{2Gd}}$ = 25 nm). This indicates that the triplet state energy increases as fluoride is added and could therefore cause an increase in sensitization of the Eu(III) complexes.

In the case of **3Gd**, when three equivalents of fluoride were added the edge of the band increased in energy, but a secondary, lower energy band was also observed. When an additional three

equivalents were added, this lower energy band increased in intensity (Figure 3.20). This indicates that as fluoride is added a lower energy triplet state is formed. This is predicted to have negative consequences on the sensitizing ability of the ligand to Tb(III) emission.

When three equivalents of fluoride anions are added to **4Gd**, the edge of the band ($\Delta\lambda_{\mathbf{4Gd}}$ = 10 nm) and the peak position red-shift to a lower energy (Figure 3.21). This trend continues with additional fluoride added. Similar to **3Gd**, this indicates that as fluoride is added, the Φ_{Tb} is expected to decrease.

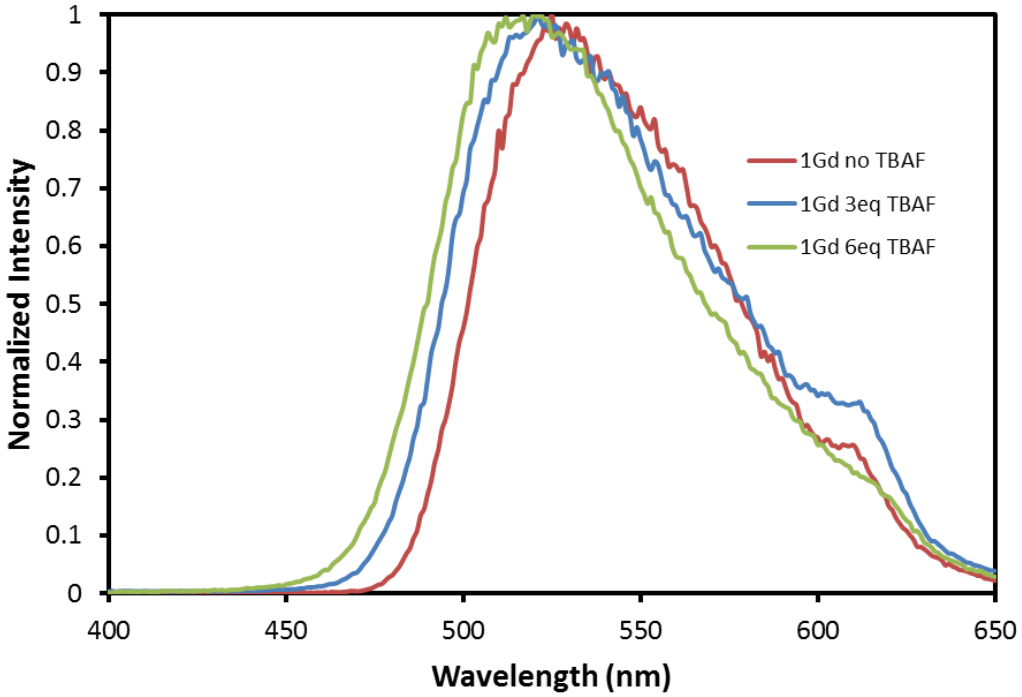

Figure 3.18 The emission spectra of 1Gd (λ_{ex} =357 nm) and its fluoride adduct in CH_2Cl_2 at 77 K.

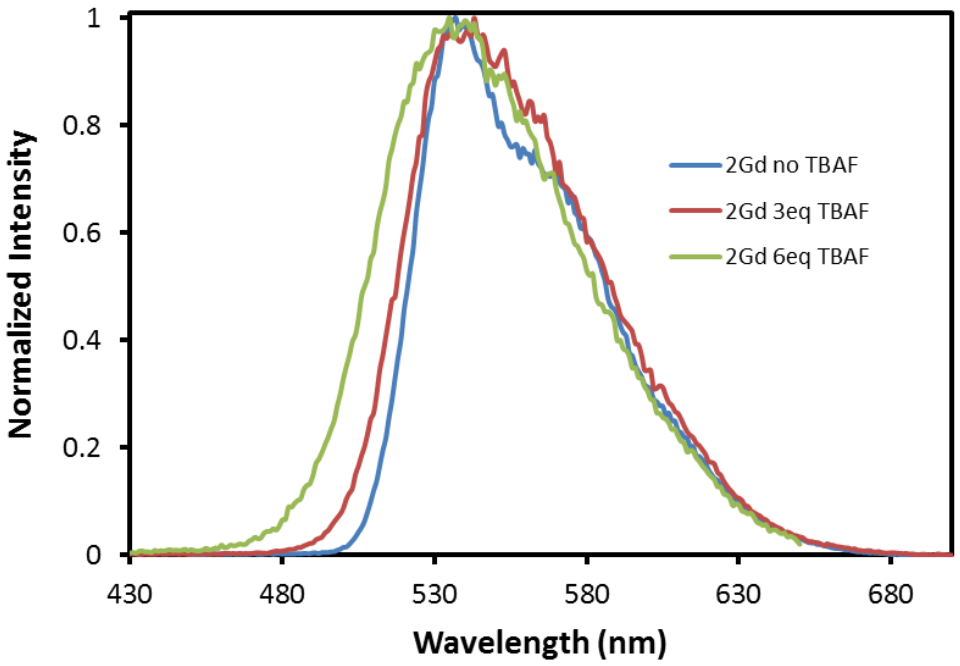

Figure 3.19 The emission spectra of **2Gd** and its fluoride adduct (λ_{ex} = 397 nm) in CH_2Cl_2 at 77 K.

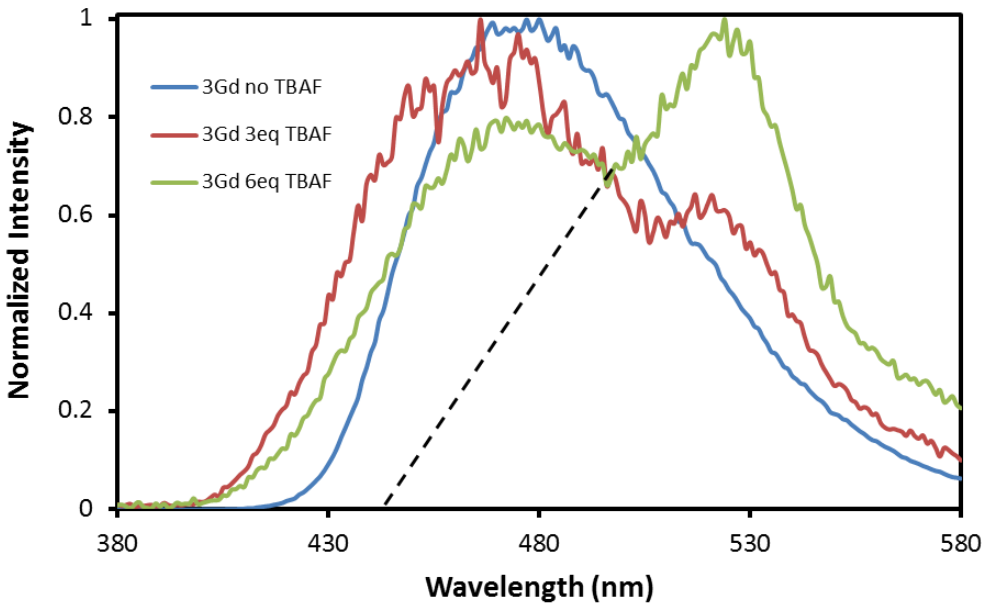

Figure 3.20 The emission spectra of **3Gd** and its fluoride adduct (λ_{ex}= 306 nm), in CH_2Cl_2 at 77 K. The dotted line represents the estimation of the band edge at ~445 nm.

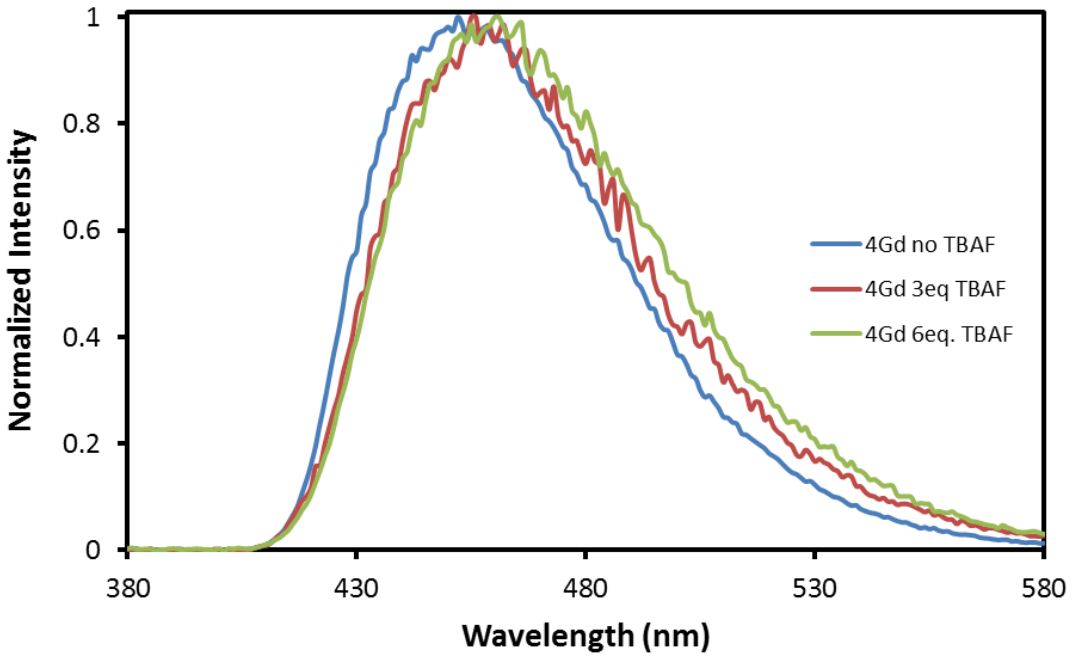

Figure 3.21 The emission spectra of **4Gd** and its fluoride adduct (λ_{ex} = 310 nm) in CH_2Cl_2 at 77K.

The change in triplet state energy after six equivalents of fluoride can be visualized in Figure 3.23. It shows that the energy of the triplet states of **1Gd** and **2Gd** increases with fluoride ions, which is expected to increase Φ_{Eu}, while that of **3Gd** and **4Gd** decreases with fluoride ions, which is expected to decrease Φ_{Tb}. The band edge of the lower energy band of **3Gd** was estimated.

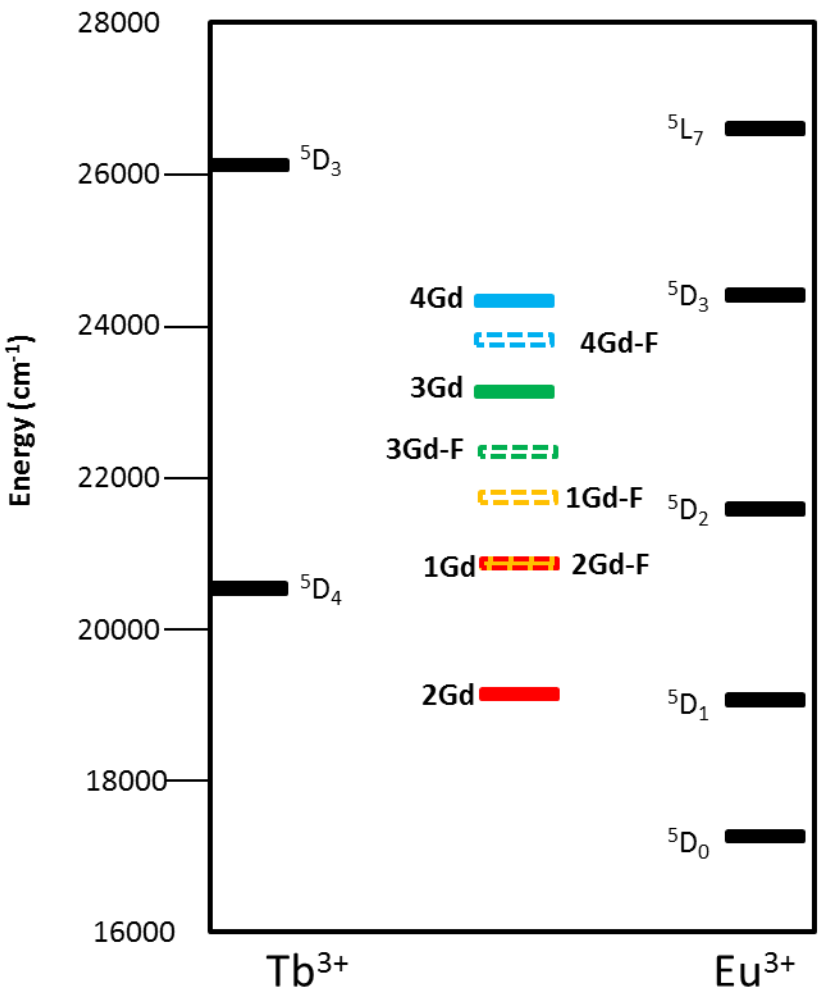

Figure 3.22 The change in triplet state energy upon the addition of TBAF to the ligands.

The titration of the lanthanide complexes by fluoride ions was monitored using UV-visible and fluorescence spectroscopy. The absorption changes of **1Eu** are visualized in Figure 3.23. As fluoride ions are added to the complex, the absorption wavelength blue-shifts towards a higher energy. This can be explained by the fact that the LUMO level (π^*) on the ligand has a significant contribution from the boron center. When F^- is added, it coordinates the boron and removes the boron contribution to the π^*, thus raising the LUMO and, therefore, the $S_0 \rightarrow S_1$ transition energy. The **1Eu** emission spectral change is shown in Figure 3.24. As expected from the **1Gd** titration, the addition of fluoride increases the emission intensity of Eu(III) in **1Eu** and the Φ_{Eu} changed to

0.1 (an increase of an order of magnitude). After the addition of ~ 5 eq. of TBAF, the absorption and emission changes could be reversed by adding water or methanol. However, the addition of a large excess of fluoride led to the dissociation of the diketonato ligand and the Eu(III) emission intensity suffered an irreversible decrease.

A similar trend was observed for **2Eu**. As fluoride is added to the solution, the absorption band blue-shifts (Figure 3.25). After 2 eq. of TBAF are added to the solution, there is a small shift in the absorption wavelengths and no change in the emission spectrum (Figure 3.26). This can be attributed to the interaction with fluoride with the associated water molecules with the complex. Further addition of TBAF causes a further blue-shift in the absorption spectrum and a great intensity increase of the Eu(III) emission. The quantum efficiency of the **2Eu** complex increases by an order of magnitude upon the binding of fluoride to the boron center because of the increased triplet energy. However, as also seen in the case of **1Eu**, addition of a large excess of fluoride leads to an irreversible quenching of the Eu(III) emission because of the dissociation of the ligands.

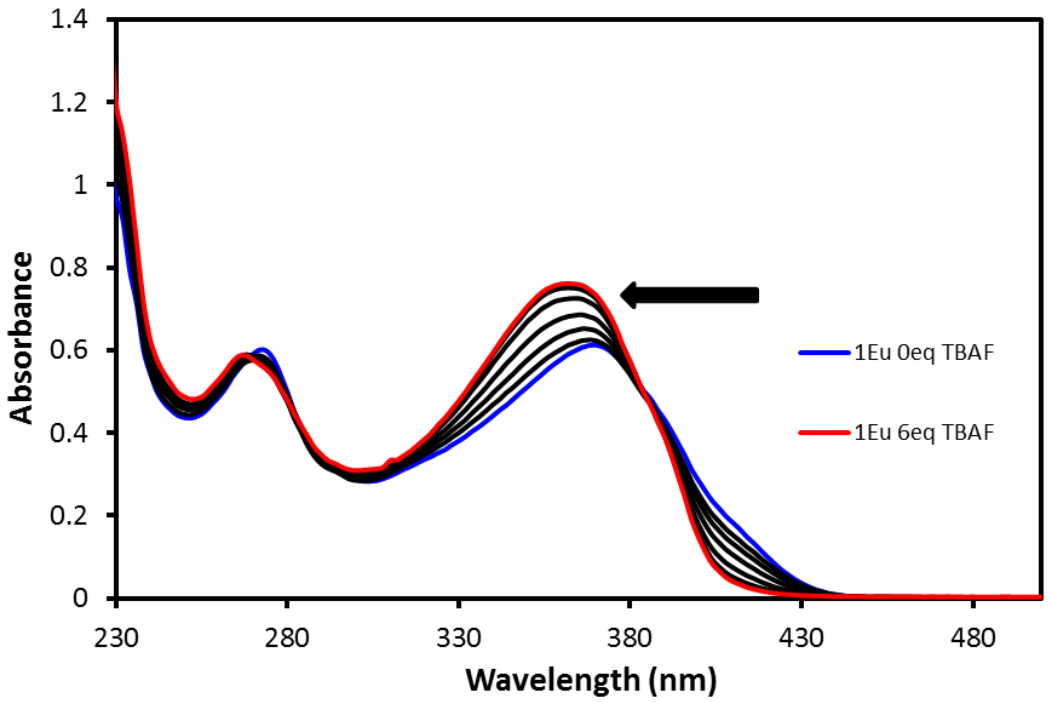

Figure 3.23 The absorption spectral change as fluoride is added to **1Eu** at 298 K in THF.

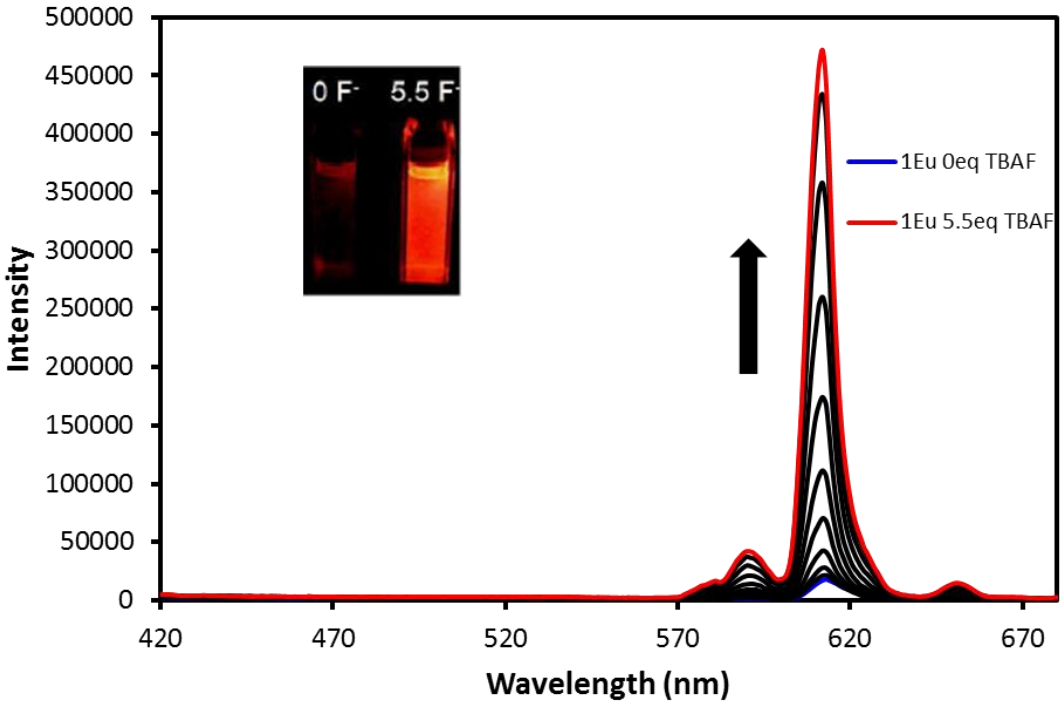

Figure 3.24 The emission spectral change of **1Eu** upon addition of at 298 K in THF (λ_{ex} = 370 nm).

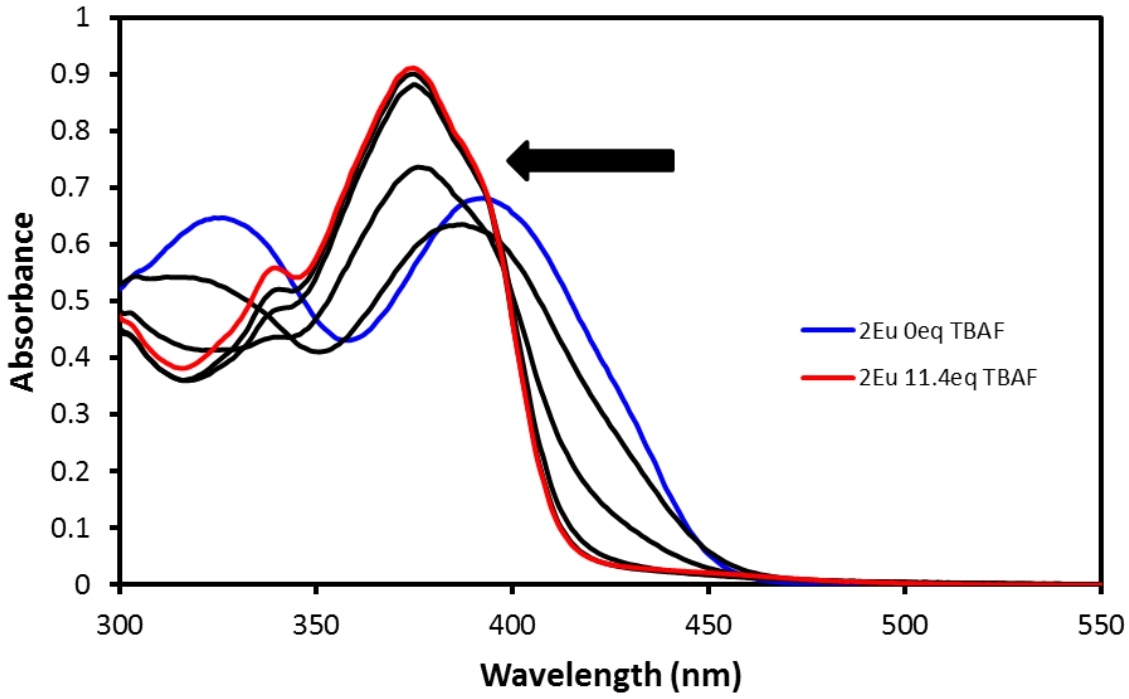

Figure 3.25 The absorption spectral change of **2Eu** upon the addition of TBAF at 298 K in THF.

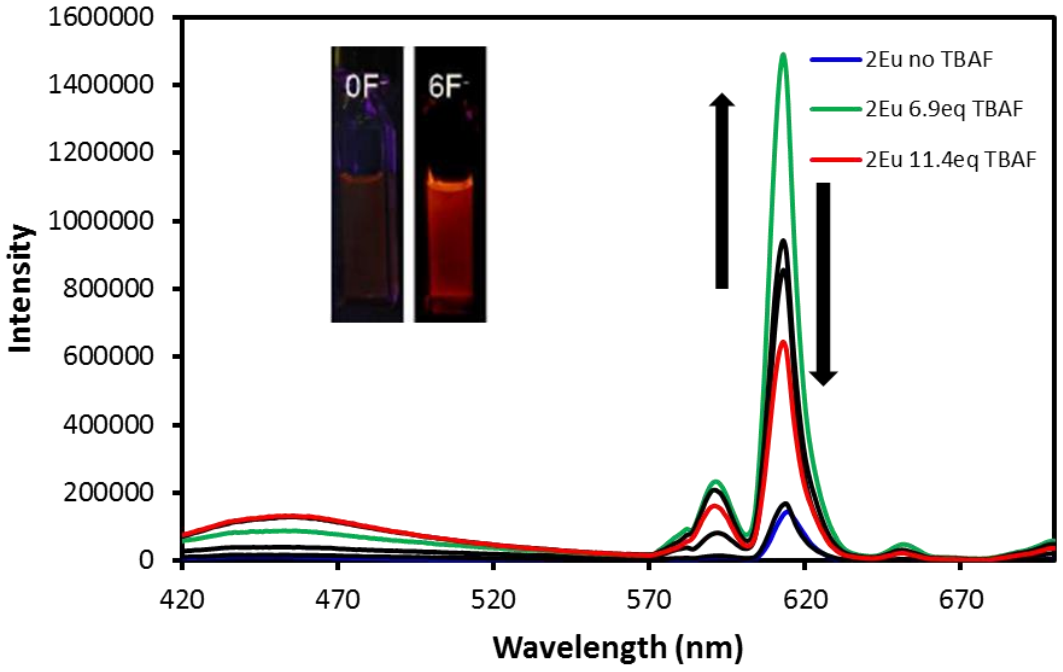

Figure 3.26 The emission spectral change of **2Eu** upon addition of TBAF at 298 K (λ_{ex} = 397 nm) in THF.

The addition of fluoride to **3Tb** has an opposite effect, compared to the Eu(III) compounds. When TBAF is added to the solution, the absorption maxima shifts to a lower energy (Figure 3.27). This is in agreement with the titration of **3Gd** by TBAF where the triplet state energy decreases with addition of fluoride. As the triplet state of the ligands is decreased, the ability of the ligand to sensitize decreases even further. This causes the energy transfer between the ligand and the metal to become less efficient, which decreases the metal-centered emission and increases the ligand-centered emission (Figure 3.28), which is indeed the case for **3Tb**.

The absorption titration of **4Tb** shows an increase in the initial absorption band, as well as a lower energy band that increases (Figure 3.29). The lower energy band can be attributed to the $BMes_2$(duryl)F → diketonato charge transfer transition. In this ligand, the boron has no contribution to the LUMO level and thus, the fluoride binding does not alter the LUMO; instead it destabilizes the HOMO, leading to a decrease in the $S_o \rightarrow S_1$ transition energy. The emission spectrum of the titration of **4Tb** (Figure 3.30) shows a gradual quenching of the Tb(III) emission as fluoride was added. The ligand centered emission increases until ~5eq of TBAF are added—this is consistent with the titration of **4-BF_2**, supporting that the fluoride is binding to the boron center. The absorption and emission spectral changes could not be reversed with the addition of water. This suggests that the addition of fluoride is causing an irreversible dissociation of **4** on **4Tb**. Therefore, the quenching of the Tb(III) emission can be attributed to both the decrease in triplet state energy and the dissociation of the ligand. The unsaturated coordination sites of **4Tb** are most likely responsible for the facile dissociation of the ligands in the presence of fluoride.

The binding constants of these complexes were not calculated due to the complex nature of the 3:1 binding and the dissociation of ligands upon addition of excess fluoride.

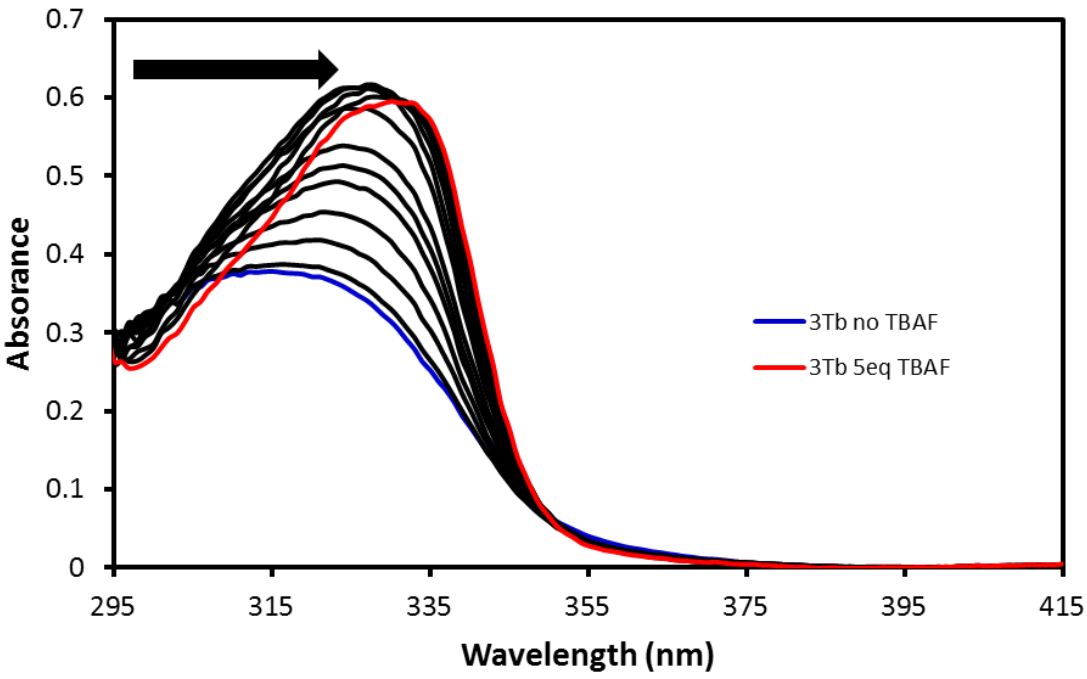

Figure 3.27 The absorption spectral change of **3Tb** with TBAF at 298 K in THF.

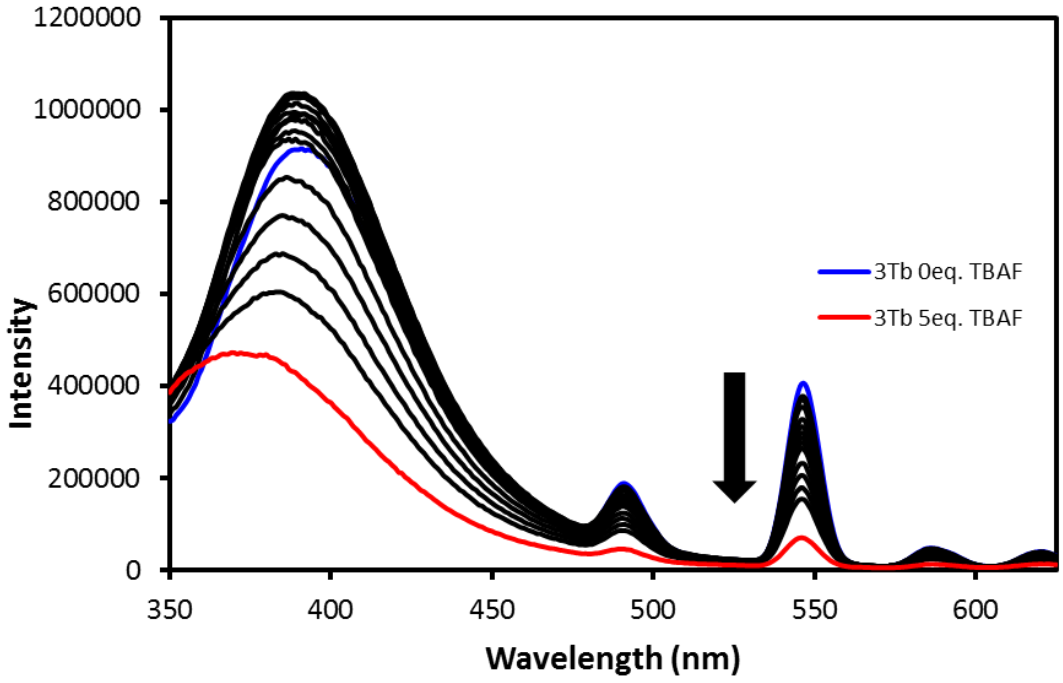

Figure 3.28 The emission spectral change of **3Tb** upon addition of TBAF (298 K, THF, λ_{ex} = 320 nm).

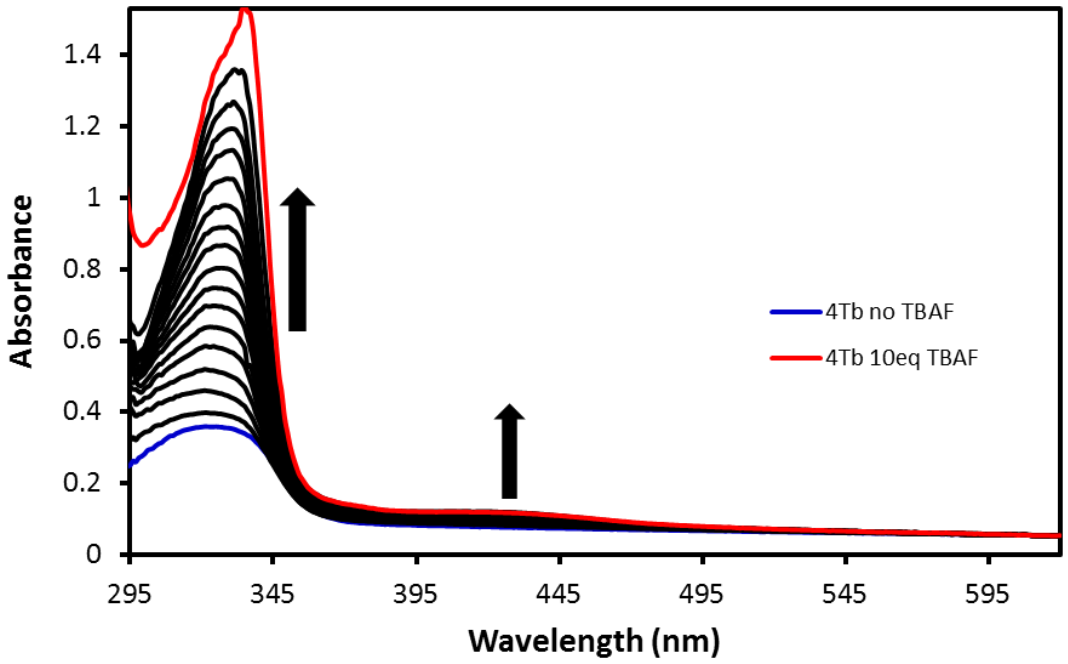

Figure 3.29 The absorption spectral change of **4Tb** upon addition of TBAF (298 K, THF).

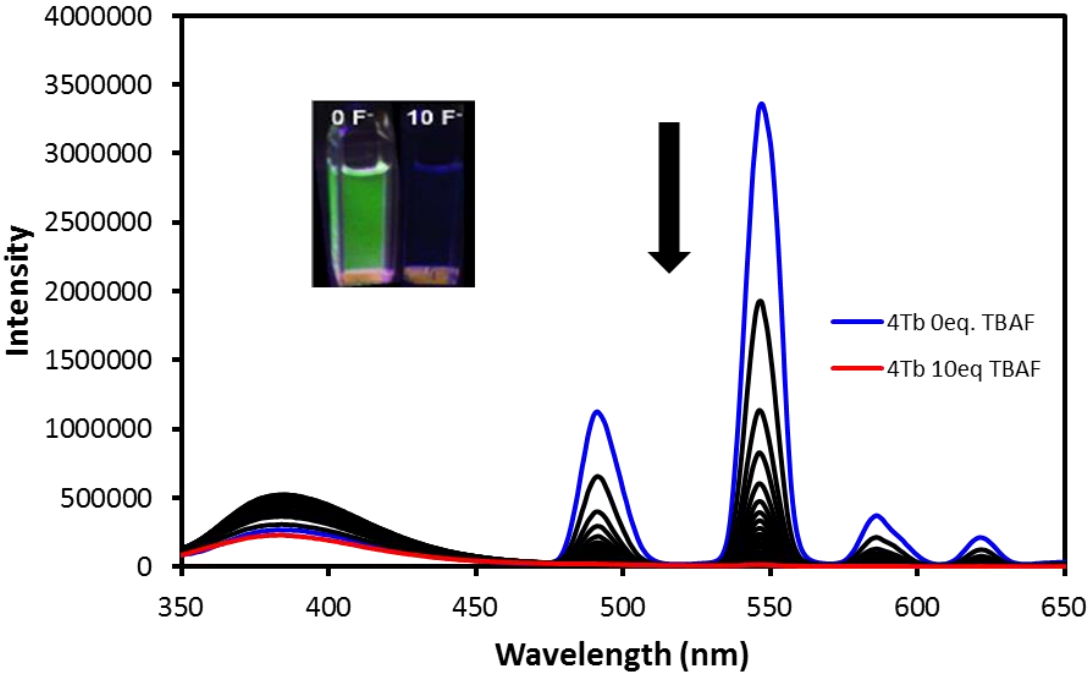

Figure 3.30 The emission spectral change of **4Tb** upon addition of TBAF (298 K, THF (λ_{ex} = 330 nm).

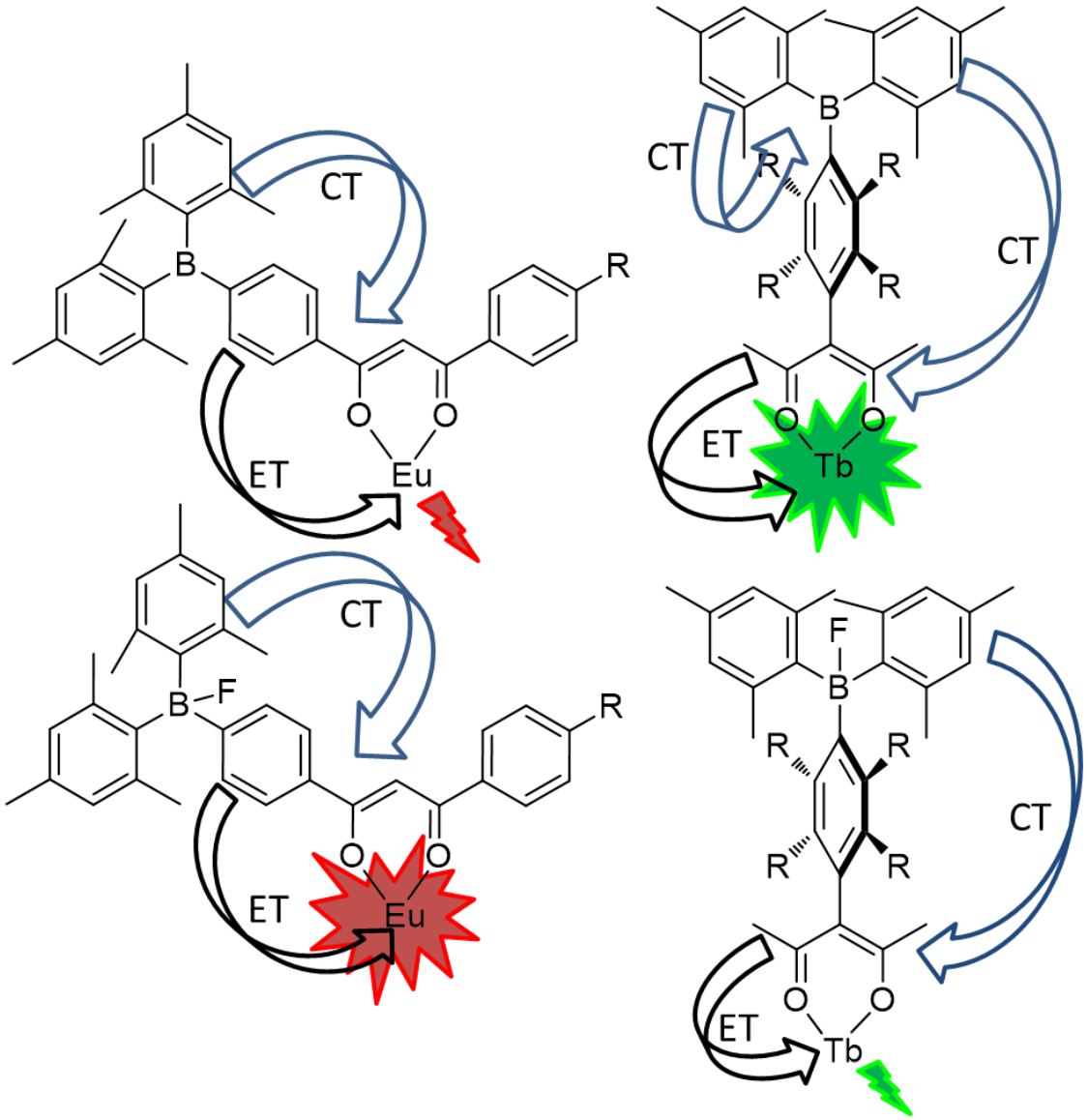

Figure 3.31 The effect of fluoride on lanthanide emission.

The impact of the fluoride ion on lanthanide emission is illustrated in Figure 3.31. For the conjugated ligands **1** and **2**, the addition of fluoride removes the boron contribution from the LUMO, causing an increase of the triplet energy, making these ligands to be more effective in sensitizing Eu(III) emission. For the orthogonal ligands **3** and **4**, the addition of fluoride ions affects mainly the HOMO level, causing a significant decrease of the CT transition energy and the triplet energy, which leads to the decrease of the Tb(III) emission sensitization.

3.4 Conclusions

To conclude, the four ligands synthesized in Chapter 2 were studied for their ability to sensitize lanthanide emission. First, they were reacted to synthesize a gadolinium complex in order to determine their triplet states. It was determined that the orthogonally twisted ligands, **3** and **4**, have a high triplet state energy, and the coplanar ligands, **1** and **2**, have a low triplet state energy. This information led to the hypothesis that **1** and **2** would be useful for Eu(III) sensitization and **3** and **4** would be useful for Tb(III) sensitization.

Based on this information, four lanthanide complexes were synthesized and their photophysical properties were investigated. All four complexes displayed typical lanthanide properties: large Stoke's shifts, long excited state lifetimes, and typical emission wavelengths. In the case of **3Tb**, the triplet state energy level of the ligand was not high enough for an efficient energy transfer to Tb(III), leading to a large contribution from the ligand's fluorescence in the emission spectrum.

The four lanthanide complexes were also investigated as fluoride sensors. First the L_3Gd complexes were titrated to determine the effect of TBAF on the triplet state of the ligand. It was found that **1Gd** and **2Gd** experience an increase in the triplet state energy, while **3Gd** and **4Gd** experience a decrease in the triplet state energy.

When titrated by TBAF, **1Eu** and **2Eu**, showed a blue-shift in the absorption wavelength and an increase in emission intensity until ~6 eq. of TBAF was added. Then, the emission was irreversibly quenched. Meanwhile, **3Tb** displayed an increase in absorptivity of the complex but a decrease in emission intensity. **4Tb** showed a new and lower energy absorption band that increases in intensity with TBAF, which was attributed to the $BMes_2(duryl)F \rightarrow$ diketonato charge transfer. The distinct response of **1Eu**, **2Eu**, **3Tb** and **4Tb** toward fluoride ions is caused by the distinct change of the ligands in these complexes upon binding with fluoride ions.

3.5 References

The work contained in this chapter has been published as:
Smith, L.F.; Park, H-J.; Blight, B.A.; Wang, S. *Inorg Chem.* **2014**, *53*, 8036.

(1) Bunzli, J-C.; Piguet, C. *Chem. Soc. Rev.* **2005,** 1048.

(2) Van Eldik, R.; Stochel, G. *Advances in Inorganic Chemistry: Inorganic Photochemistry*; Elsevier: San Diego, **2011**; Collect. Vol. No. 63, pp10-45.

(3) Kaltsoyannis, N.; Scott, P. *The f elements*; Oxford University Press Inc.; New York, **1999**

(4) (a) Bhaumik, M.L.; Fletcher, P.C.; Nugent, L.J. ; Lee, S.M.; Higa, S.; Telk, C.L.; Weinberg, M. *J. Phys. Chem.*, **1964**, *68*, 1490. (b) Wolff, N.E.; Pressley, R.J. *Appl. Phys. Lett.***1963**, *2*, 152. (c)Binnemans, K. *Chem. Rev.* **2009**, *109*, 4283.

(5) (a) Butler, S.J.; Parker, D. *Chem. Soc. Rev.* **2013,** *42*, 1652.(b) Pal, R.; Parker, D.; Costello, L.C. *Org. Biomol. Chem.*, **2009,** *7*, 1525. (c) Parker, D.; Senanayake, P. K.; Williams, J.A.G. *J. Chem Soc. Perkin Trans. 2* **1998,** *10*, 2129.

(6) (a) Bunzli, J-C. G.; Eliseeva, S.V. *Chem. Sci.* **2013**, *4*, 1939. (b) Reardon, D. F. US Pat., 2008305243 A1 20081211, **2008**.

(7) Kido, J. *Chem. Rev.* **2002,** *102*, 2357.

(8) (a) Thibon, A.; Pierre, V.C. *Anal. Bioanal. Chem.* **2009,** *394*, 109. (b) Frias, J.C.; Booba, G.; Cann, M.J.; Hutchinson, C.J.; Parker, D. *Org. Biomol. Chem.* **2003,** *1*, 905.

(9) Varlan, M.; Blight, B.A.; Wang, S. *Chem. Commun*, **2012,** *48*, 12059.

(10) Brouwer, A.M. *Pure Appl. Chem.*, **2011,** *83*, 2213

(11) Melby, L.R.; Rose, N.J.; Abramson, E.; Caris, J.C. *J. Am. Chem. Soc.*, **1964,** *86*, 5517.

(12) Latva, M.; Takalo, H.; Mukkala, V-M.; Matachescu, C.; Rodriguez-Ubis, J.C.; Kankare, J. *J. Lumin.* **1997,** *75*, 149.

(13) Shi, J.; Hou, Y.; Chu, W.; Shi, X.; Gu. H.; Wang, B.; Sun, Z. *Inorg. Chem.* **2013,** *52*, 5013.

(14) Strasser, A.; Vogler, A. *Inorg. Chim. Acta*, **2004,** *357*, 2345.

(15) (a) Dawson,W.R.; Kropp, J.L.; Windsor, M. W. *J. Chem. Phys*., **1966**, *45*, 2410. (b) Carnall, W.T.; Goodman, G.L.; Rajnak, K.; Rana, R.S. *J. Chem. Phys.*, **1989,** *90*, 3443.

Chapter 4

Summary and Outlook

4.1 Summary and Conclusions

This work began with the investigation of the impact of a triarylboron moiety on the photophysical properties of β-diketone ligands. Acetylacetone and dibenzoylmethane were chosen as classical frameworks from which the impact of the position of the triarylboron functionalization on the photophysical properties could be studied. To this achieve this, four triarylboron β-diketone ligands were synthesized. Two of the ligands incorporated a triarylboron on the 1 or 1 and 3 positions and were synthesized *via* Claisen condensation. The other two ligands incorporated a triarylboron on the α-carbon and were synthesized through reaction with a phosphole. These ligands differed by their aryl-link to the aceteylacetone backbone where one was linked through a phenyl moiety and one was linked through a duryl moiety.

In Chapter 2, these ligands were further reacted to synthesize difluoroboron chelate compounds. These complexes were characterized with NMR spectroscopy and EA. The structures of the chelates were investigated by computational and crystallographic analysis. **1-BF_2** and **2-BF_2** are coplanar with respect to the β-diketonate backbone, which extends their conjugation while **3-BF_2** and **4-BF_2**, are orthogonally twisted from the β-diketonate backbone, which disrupts the conjugation. The absorption and emission of each complex was also studied and it was found that **1-BF_2** and **2-BF_2** spectra were more red-shifted and they had higher quantum yields than **3-BF_2** and **4-BF_2**. An interesting aspect of the emission of **1-BF_2** and **2-BF_2** is their concentration dependent excimer emission that can lead to a white emission color. The complexes were titrated with fluoride and the changes in absorption and emission were followed with UV-visible and fluorescence spectroscopy. The binding constants were estimated with a non-linear regression

model using the absorption titration data. All of the binding constant estimates were found to be typical of a moderately protected triarylboron.

Chapter 3 describes the synthesis of the same ligands with Eu(III) or Tb(III) in order to sensitize their emission and the characterization of each compound. Gd(III) complexes were made to study the triplet state of each ligand, as well as how the triplet state changes with addition of fluoride. The position of the triarylboron moiety on each ligand affected the triplet energy level and, therefore, could selectively sensitize Ln(III) ions. Ligands **1** and **2** were appropriate for Eu(III) sensitization while ligands **3** and **4** were appropriate for Tb(III) sensitization. **1Eu**, **2Eu**, **3Tb**, and **4Tb** displayed typical lanthanide photophysical properties: long excited state lifetimes, large Stoke's shifts, excitation wavelengths relating the ligands, and typical emission wavelengths. The complexes were titrated with TBAF and the changes in absorption and emission were followed with UV-visible and fluorescence spectroscopy. When fluoride was added to the Ln(III) complexes, it caused the Eu(III) complexes to increase their quantum yield by an order of magnitude. However, the Tb(III) complexes had their emission quenched. This is because the triplet state of **1** and **2** increased with addition of fluoride, but the triplet state of **3** and **4** decreases. In each case, after a large excess of fluoride was added, the complexes decomposed and all luminescence was quenched.

This research has established that the position of a triarylboron moiety can affect the electronic and photophysical properties of β-diketone ligands. These ligands contribute to an ever-expanding library of β-diketone ligands. They are useful luminescent materials when in a chelate complex with difluoroboron or for lanthanide sensitization. They have potential applications for fluoride sensing because fluoride changes the ability of ligands to sensitize lanthanide ions: either by increasing in ligands **1** and **2**, or decreasing in ligands **3** and **4**.

4.2 Future Directions

Future studies should consider continuing to expand the triarylboron β-diketone library. This can be achieved by introducing new functional groups onto the unfunctionalized phenyl ring in ligand **1** (Figure 4.1). The charge transfer to the boron should be further enhanced by incorporating an electron-donating group. It would be interesting to study the effect of this group on the triplet state and the efficiency of charge transfer to a lanthanide.

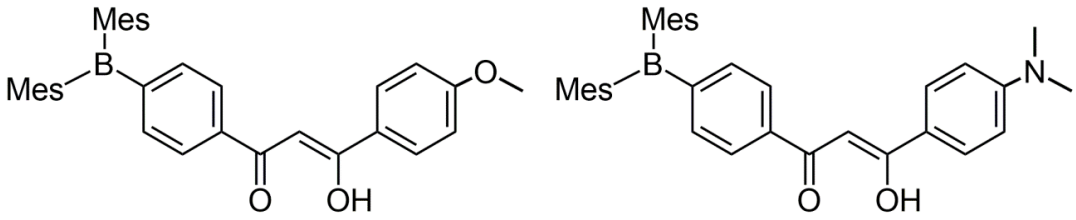

Figure 4.1 Suggested additions to the triarylboron functionalized β-diketone library.

Another intriguing future project would be to functionalize a cyclen ligand with a triarylboron (Figure 4.2). These ligands on lanthanides would be nonadentate and would remove the need for ancillary ligands with appropriate energy levels. The lanthanide complex would have a formal anionic charge and, thus, would be more water soluble. This would make it more appropriate for fluoride sensing in aqueous media.

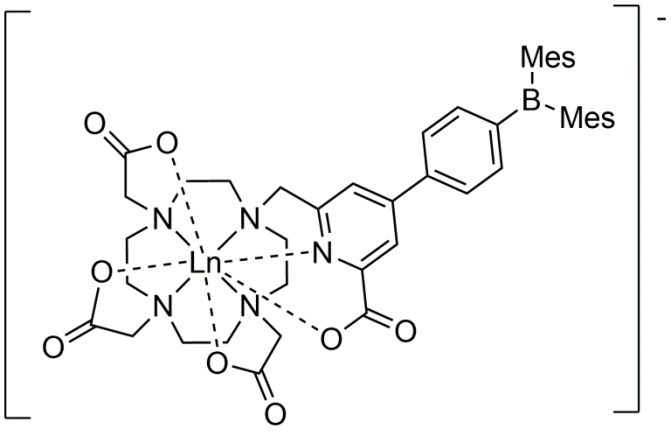

Figure 4.2 Triarylboron functionalized cyclen for enhancing lanthanide fluoride sensing.